Master Thesis

Designing for Post-Processing: A Case Study of a 3D Printed Surgical Instrument

Mathijs Bruins

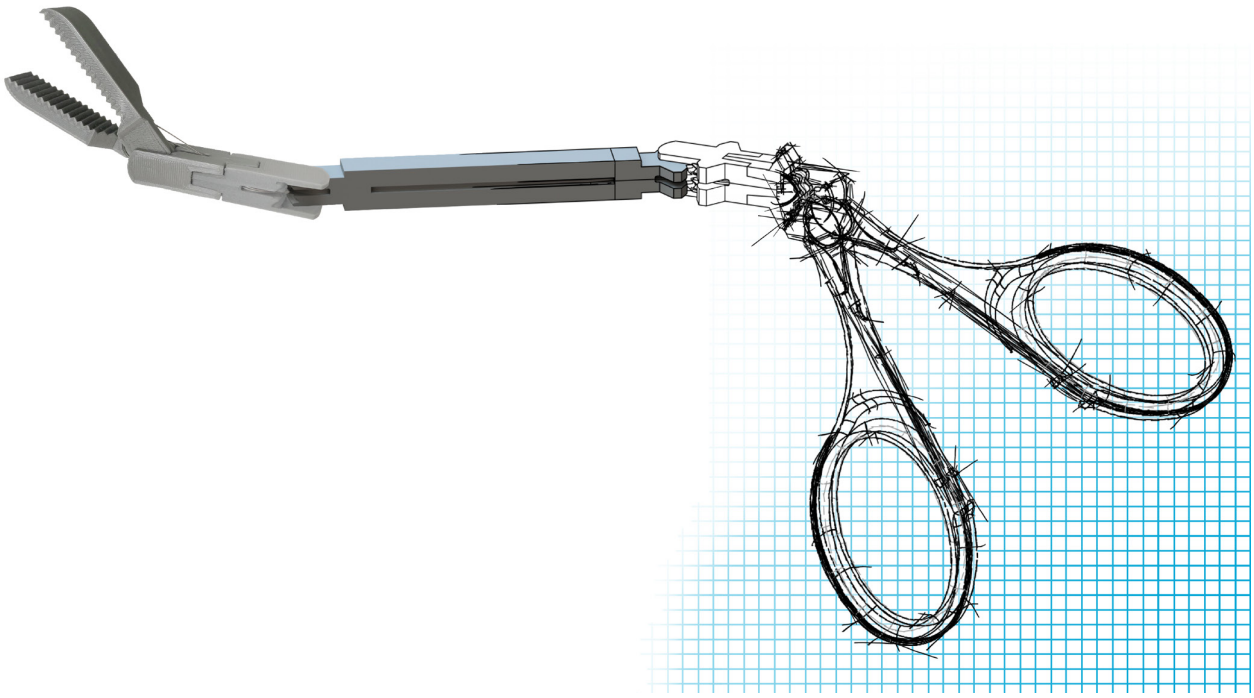

TU Delft

Department of BioMechancial Engineering

Student Number 4572130

February 11th 2021

Thesis Committee

Ir. K. Lussenburg, Supervisor

Prof. Dr. Ir. P. Breedveld

Dr. J. Zhou

Abstract

In this report a design is proposed for a laparoscopic gripper that can be manufactured with metal 3D printing and polished with mass finishing. The design is a continuation of the development of a laparoscopic gripper that can be 3D printed in plastic. Laparoscopic grippers 3D printed solely out of metal have not yet been presented. Laparoscopic instruments are limited in width to 5 mm, which is bordering the manufacturing limits of selective laser melting 3D printing. The use of 3D printing for medical instruments has the potential to customise instruments specific to patient, procedure, and surgeon.

Metal 3D printing can produce complex parts, albeit with a high surface roughness. Post-processing is required to reduce the surface roughness. Mass finishing techniques are a group of mechanical polishing techniques, of which centrifugal disc finishing was selected due to its capability to process parts in bulk without requiring workpiece fixation.

To synthesise a suitable design, the processes of printing and polishing were analysed to formulate design guidelines. The analyses were part literature study, part experimental study. The experimental study had the aim to quantify and supplement the guidelines found in handbooks and articles. Using a novel visualisation technique, the polishing of different geometries could be distilled into quantitative design considerations. Here, a marking lacquer was applied to the surface of workpieces, which remained on unpolished surfaces. In this experiment a number of features were used, which corresponded to aspects that had potential to be used in the design. The use of channels was deemed unviable for polishing at the scale of laparoscopic instruments, which required the removal of these from the design. Mass finishing polishing removed the coarse surface structure present on metal produced with 3D printing, and brought surfaces of the test pieces to 0.05 mm below their desired width.

Application of the design guidelines to the laparoscopic instrument was focused on making printing and polishing compatible joints. The laparoscopic gripper has two degrees of freedom for increased manoeuvrability. The features that comprise the joint are protrusions and cut-outs, sinusoidal gear arches, and actuation cable guides. Each of these features were dimensioned with values from the guidelines. The joint design required a number of components to be split so polishing access could be guaranteed, specifically for the cable guides. This had the added benefit of having each part be orientated during printing individually. The final design is based on application of the relevant design guidelines, and has been validated using scale models for mechanical stability.

Contents

List of Abbreviations

AM	Additive Manufacturing
CAD	Computer Aided Design
CDF	Centrifugal Disc Finishing
DMLS	Direct Metal Laser Sintering
DOF	Degrees of Freedom
EBM	Electron Beam Melting
FDM	Fused Deposition Modelling
MFT	Mass Finishing Technique
MIS	Minimally Invasive Surgery
PBF	Powder Bed Fusion
SILS	Single Incision Laparoscopic Surgery
SLM	Selective Laser Melting
SLS	Selective Laser Sintering

1 Introduction

1.1 Background Laparoscopy

Laparoscopic surgery is a type of Minimally Invasive Surgery (MIS) in which laparoscopic instruments are used to perform operations in the abdominal cavity of a patient. With laparoscopic surgery the abdominal wall of the patient is opened with a few small incisions. Through these incisions tools are inserted to perform the desired operation. Figure 1.1 shows a schematic illustration of the laparoscopic procedure.

The alternative to MIS is open surgery, which is associated with higher risk of infections, scarring, and longer recovery times [1]. For routine surgical procedures MIS is preferred for these reasons, and an increasing number of procedures is performed in a minimally invasive fashion. The incisions made to access the abdominal cavity are fitted with air-tight ports, called trocars. Inserted through these ports are at least one form of optic instrument and one or more manipulating instruments. The abdominal cavity is expanded with CO_2. The expansion of the abdominal cavity provides the surgeon with the necessary space to maneuver the instruments.

As laparoscopic surgery becomes more routine, a shift towards single incision laparoscopic surgery (SILS) is noticed. SILS is a laparoscopic procedure in which the camera and the required manipulators are inserted through one incision. Recently, the use of laparoscopy robots continues to expand the procedures possible and the number of surgeons capable of performing the complex procedures [2].

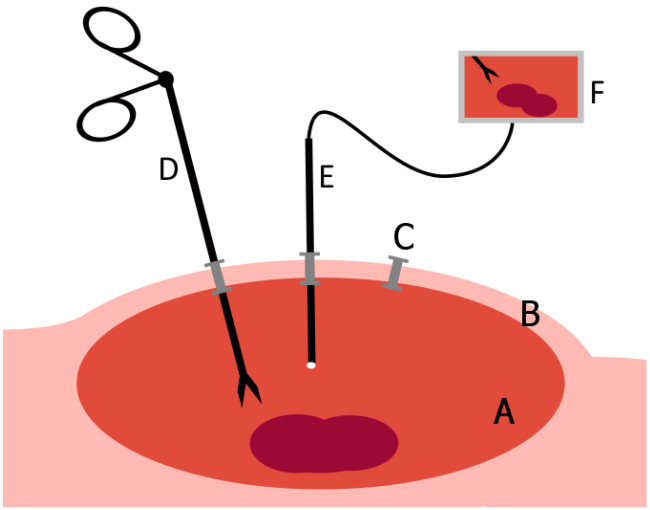

Figure 1.1: Schematic depiction of laparoscopy with A) abdominal cavity B) abdominal wall C) trocar D) laparoscopic gripper E) laparoscopic camera or laparoscope F) monitor.

1.2 Laparoscopic Instruments

The laparoscopic instruments are inserted through the trocar placed in the abdominal wall. A smaller trocar requires a smaller incision in the abdominal wall, which decreases trauma and recovery time. Typical trocar sizes are 10 - 12 mm, 10 mm and 5 mm [3]. For the aforementioned reasons, many of the standard surgical tools used in laparoscopy have a width of 5 mm.

Laparoscopic instruments consist of three components: the handle, the shaft, and the tip. The tip is where any surgical end-effector is placed, which can be an actuated gripper or cutter, or a unactuated probe or knife. The shaft connects the tip to the handle, through the abdominal wall. A surgeon uses the handle to control the instrument, which can include a number of actions. Laparoscopic instruments have four Degrees Of Freedom (DOF) to move the tip, and often an additional DOF for the actuation of the end-effector, for grasping or cutting for example. The instrument is restricted by the trocar, which is acting as a fulcrum. Laparoscopic instruments can translate axially, but cannot translate in both radial directions due to this constraint. Figure 1.2 illustrates the DOF of a rigid instrument, in this case a gripper.

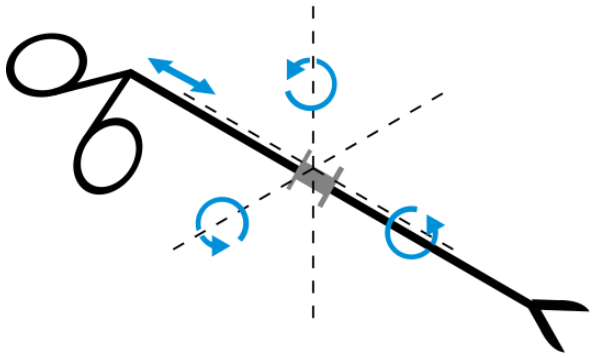

Figure 1.2: Degrees of freedom of a laparoscopic instrument during a procedure. Three rotational degrees of freedom around the trocar and one axial translation constitute the four degrees of freedom this instrument possess to orient the tip, and are depicted by the blue arrows.

In addition to rigid laparoscopic instruments, steerable instruments have been developed so the tip can be steered and re-oriented inside the body. Steerable instruments have one or more hinge points or sections about which they can rotate the tip with respect to the shaft, see Figure 1.3. These hinge locations can allow rotation in one or two directions, depending on the joint type, granting one or two additional DOF. This additional maneuverability of the tip aids surgeons in approaching their target tissue from an appropriate direction. Currently, steerable laparoscopic instruments are manufactured with conventional machining to create the intricate components of which they consist [4].

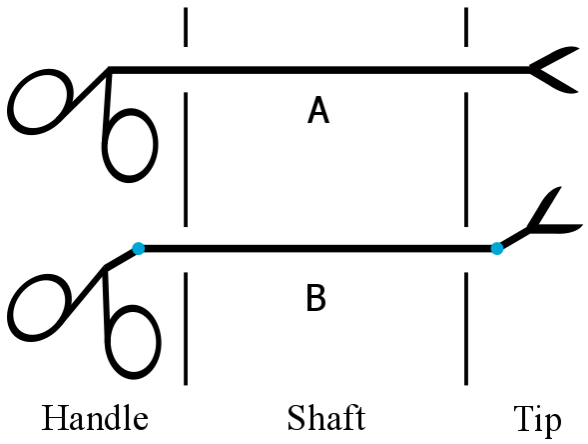

Figure 1.3: Schematic illustration of A) a rigid laparoscopic instrument and B) a steerable laparoscopic instrument. Steerable laparoscopic instruments have one or more directions in which the tip can orient itself with respect to the shaft.

1.3 3D Printing

3D printing, or Additive Manufacturing (AM), is a group of production methods that build a part, often layer by layer, by fusing material together directly from a computer model [5]. This approach differs from the more conventional, subtractive manufacturing, in which material is removed. With subtractive manufacturing, addition of geometrical features increases production time, as for instance an extra hole has to be drilled or a convex surface milled. However, for AM the manufacturing time is proportional to the outside dimensions of the part. This means that a part with a high shape complexity takes as long to print, as a part with a low shape complexity, of the same size. The phrase 'complexity is free' is often used to describe this effect [6].

To go from a CAD model to a part with AM, only one intermediate step is required. This intermediate step is using CAM software, often referred to as slicer software, to translate the 3D model to a set of commands for the 3D printing machine to follow. The ease with which 3D printing can produce geometrically complex parts, combined with the small number of steps required with which a design can go to manufacturing, have made it a preferred choice for the production of prototypes and scale models. However, over the recent years, 3D printing has grown out of this niche and is starting to become adopted among many different industries on a functional level. In particular healthcare was one of the early adopters of 3D printing for functional components [7]. The use of 3D printing ranges from patient specific prostheses, printing of organs (bio-printing), dosage specific drugs, and specialty instruments [8]. The application of 3D printing for specialty instruments has had several reasons. The use of cheap, disposable tools, that are made when required, can be used by low income countries, field hospitals or space missions [8]. On the other hand, the high shape complexity has the potential to develop novel tools, or customisable instruments for specific procedures, patients, or surgeons.

Culmone *et al.* [9], presented a state of the art of 3D printing in medical instruments. They discussed a number of MIS tools, ranging from steerable needles to laparo- and endoscopic instruments, in addition to other other medical instruments. Among all of the presented instruments, 86 % were made from polymers and 11 % from metals, and metal 3D printed laparoscopic instruments were absent [9].

The abundance of polymeric parts is a result of 3D printing techniques often able to be applied to polymers [10]. This in turn is attributed to the lower fusion temperature of polymers compared to metals. AM technologies often depend on fusing material to previous layers, making polymers more versatile in 3D printing use. However, there are inherent drawbacks of using polymeric medical instruments [9]. The mechanical properties of many of the polymers used in 3D printing are relatively low. The three biggest groups of polymeric material reported in 3D printed medical instruments were ABS (26 %), resins (19 %) and PA (18 %) [9]. These materials all have an elasticity modulus of around 2.3 GPa [11, 12]. This is two orders of magnitude lower than that of steel, which has an elasticity modulus of 210 GPa. For thin parts with a high aspect ratio (i.e. slender), like the shaft of a laparoscopic instrument, the material choice dictates the stiffness of the instrument. High stiffness instruments are desirable because this increases the accuracy of the force feedback for the surgeon.

Aside from the mechanical properties, the sterilisation of polymeric parts is harder to achieve [9]. The most common sterilisation method, the autoclave, uses heat and pressure. However, only a limited number of 3D printable plastics are able to withstand the heat and pressure. This is a result from both the low mechanical properties and melting point.

3D printing of metals relevant for producing laparoscopic instruments, such as stainless steel and titanium alloys, can be achieved by several printing techniques [13], which are all considered Powder Bed Fusion (PBF) techniques. PBF is a group of techniques in which a layer of powder is selectively fused to the previous layer by an energy beam. By building up the desired work piece in a layered fashion, a 3D object is constructed (Figure 1.4).

One significant drawback of PBF techniques is that they leave the part with a high surface roughness. Figure 1.5 is a photo of parts produced by PBF without post processing. Friction and wear are dependent on surface roughness, and a rough surface will increase both. While some degree of friction is inevitable and perhaps desir-

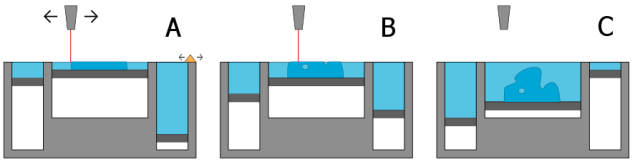

Figure 1.4: Schematic overview over the powder bed fusion process. A) an energy beam, laser or electron, fuses material to a base plate. A reservoir of powder is spread by a spreader to deposit the next layer. B) this continues as layers begin to form the object and C) the process stops when the final layer has been fused. The product is then removed from the base plate and ready for post-processing.

able, wear is undesirable, as it breaks particles off the surface. This is particularly pronounced during the initial use of a product, as the running-in of components see the highest wear rate [14]. Many medical instruments are single-use, resulting in them only experiencing initial use, and therefore shed the most particles if produced with a rough surface.

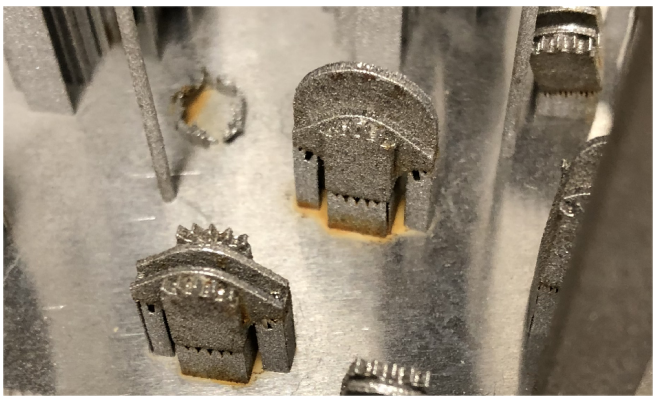

Figure 1.5: Close up of small (5 mm) parts produced with powder bed fusion in SS 316-L. The surface roughness is visible by eye.

1.4 Design Objective

Currently used steerable laparoscopic instruments are all made using conventional manufacturing. Designing 3D printed, metal laparoscopic gripper would be bringing the advantages of 3D printing to MIS. The advantages include the possibility to design surgeon, patient, or procedure specific components. Before these perks can be investigated, a working base instrument must be developed. This requires a design in which the disadvantages of 3D printing, specifically PBF, are mitigated. The main disadvantage of using PBF is the poor surface quality, requiring post-processing to reduce the surface roughness. PBF allows to produce components with a high shape complexity and with minimal manual intervention. Additional surface roughness reducing steps should be accommodating of both these advantages, to not undo the complexity of 3D printed geometry. Therefore, the polishing post-processing step must alter the geometry of any product predictably and reliably. Conversely, the geometry of the product must also allow for the polishing to occur sufficiently. The primary objective is to generate a design for a laparoscopic gripper that is manufacturable in metal using 3D printing. This will be achieved by formulating and validating the design considerations that originate from combining metal PBF with a post-processing step in order to facilitate the production of fine medical instrumentation.

1.5 Report Structure

This research starts with investigating the manufacturing processes of metal 3D printing and surface polishing in Chapter 2. This investigation will result in a number of design requirements for each of the associated manufacturing methods.

As a starting point for the development of a 3D printed, metal laparoscopic gripper, a design developed within the Bio-Inspired Design Group (BITE) of the Delft University of Technology will be used [4, 15–18]. They have previously been successful in designing and manufacturing a steerable, 3D printed laparoscopic gripper out of polymer, named the DragonFlex, see Figure 1.6. This instrument is analysed in Chapter 3, as to understand the working principles of the instrument.

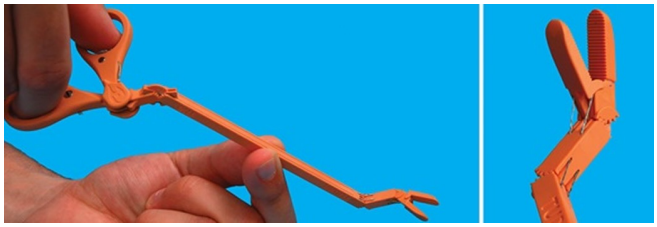

Figure 1.6: Image of the DragonFlex II laparoscopic gripper, taken from [4]. Left a picture of scale, the shaft and tip have a 5 x 5 mm^2 cross-section to comply with standard trocar sizes. Right is a close-up of the two additional degrees of freedom hinges and the tip.

In Chapter 4 the design requirements of manufacturing are incorporated into the design requirements of the instrument. Here, also a systematic design approach is used to generate a concept design for a metal 3D printed laparoscopic instrument.

This is then followed by Chapter 5, in which an experiment aimed at understanding the influence of geometry on the polishing process, and vice versa. This understanding is applied in Chapter 6 to quantify and finalise design. The report concludes with Chapter 7 & 8, which are the discussion and conclusion, respectively.

2 Production method

2.1 Powder Bed Fusion

2.1.1 Process description

Powder bed fusion is a group of techniques with a comparable working principle that can effectively make parts ranging from 1 to 500 mm [10]. PBF uses an energy beam to fuse powder particles together to create a part. A layer of powder is fused onto a previous layer, each layer adding a sliver of local cross section to the work piece. In Figure 1.4 this is illustrated. Currently, PBF is the only 3D printing technique used to make medical instruments that can produce full metal parts [9].

Within PBF several techniques exist, primarily differentiated on the energy intensity and energy type used [10]. Electron Beam Melting (EBM) and Selective Laser Melting (SLM) use different energy types to achieve full melt. This process is different from Selective Laser Sintering (SLS) or Direct Metal Laser Sintering (DMLS), which sinter material together. Sintering, as opposed to melting, does not liquefy the material, but rather makes the particles fuse at the contact points with other particles. Sintering requires a lower temperature for the material to fuse together, than required for full melting. The size of the fused area is dependent on time, temperature, and pressure. There are advantages and disadvantages to sintering and melting. Because less heat is required for sintering, heat induced warpage and energy spot diameter are lower, which results in better spatial resolution. The disadvantage of sintering is that the material is only partially fused together, resulting in diminished mechanical properties compared to the solid material. To combat this, sintered parts can be infused with a lower melt point metal, to create a fully dense product [10]. However, the infused material will still not have the same material properties as the base metal.

In this project the choice for SLM 3D printing was made as this was the method available.

2.1.2 Surface roughness

Surface roughness is an inherent process limitation of which the effects can only be minimised [10]. The extent of these factors can be controlled and channeled with design and process. Surface roughness is a result of powder size and the layered nature of PBF. Powder does not stack in flat planes, resulting an innate roughness due to powder stacking. The surface roughness left by the PBF process is very high, and according to Gibson *et al.* [10] it ranges from 10 μm to 100 μm, depending on the chosen surface roughness quantity. Multiple surface roughness units exist, and they are used depending on what aspect of the surface roughness is described. According to Townsend *et al.*[19] the arithmetical mean deviation of the surface, the Ra value, is the most adopted in roughness quantification in metal AM. The Ra value is measured by tracing a needle over a surface and taking the average of the absolute value of the height deviations with the mean height. Analysing fifteen articles [20–35] on metal AM found a slightly lower but comparable average surface roughness (Ra value) of 9.6 ± 5.8 μm.

Surface roughness depends on surface orientation [10]. Klingaa *et al.* [36] investigated the relation between the direction of the normal vector of a surface and its roughness. Overhanging surfaces with respect to the building directions have the worst surface quality. Areas without a supporting layer underneath do not have the same heat sink that supported area does. This means that unsupported area will stay above the fusion temperature for longer, spreading more heat, causing more particles to adhere. Surfaces facing in the 'up' direction ($\pm$ 90° from the normal vector of the base plate) have a surface roughness (Ra) an order of magnitude or more lower than surfaces facing 'down', 7 μm and 75 μm, respectively [36].

Aside from particle packing, the layered nature has another implication for the surface roughness. Each shape has to be approximated by layers, which results in a discrepancy between the desired shape and printed shape. This discrepancy is called the staircase effect, and it is illustrated in Figure 2.1. The staircase effect is most pronounced in surfaces non-parallel and non-orthogonal to the building direction.

The building orientation dictates which faces experience the staircase effect, and can be used to change the location or direction of the effect. For example, if the 'steps' of the staircase effect run parallel to the direction of a sliding surface the negative effect is far less than if the steps would run perpendicular to the sliding direction.

The high surface roughness of 3D printed metal also makes it have a low fatigue strength without proper surface treatment like shot-peening or milling [20, 24, 32, 37]. The valleys in the surface act as stress concentrators which cause local stress peaks. Repeated large deflections for 3D printed metal is likely to result in premature fatigue failure.

2.1.3 Minimum feature size

The smallest volume that can be individually made using PBF is expressed as the minimum feature size. Minimum feature size is a machine property, limited by two factors: the melt pool size and layer height. Both these aspects cannot be infinitesimally small. These two aspects together limit the smallest possible size a feature can be. The layer height for PBF ranges between 0.02 mm to 0.15 mm [10]. The melt pool size is depending

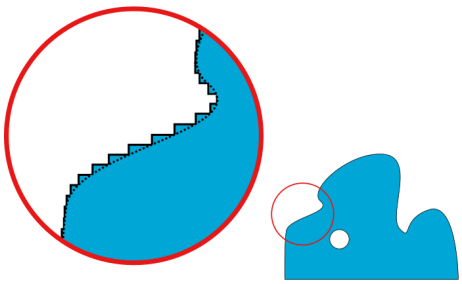

Figure 2.1: Schematic illustration of the staircase effect. Within the encircled close-up the uninterrupted line represents the actual part contour, while the dotted line represents the desired contour.

on the energy beam intensity and duration, however, 0.5 mm wall thickness is a general lower limit [38].

The spatial resolution is also not equal in-plane and out-of-plane. The spatial resolution out-of-plane is a result of the minimum layer height, whereas in-plane the resolution is defined by a minimum feature size or thickness. This means that a smooth perimeter can be achieved in-plane but not out-of-plane.

2.1.4 Support material

Support structures are required to produce parts out of metal with SLM, and has to be removed after printing [39]. Support material is needed for overhanging structures, anchoring to the base plate, and as a heat sink.

With SLM only short unsupported layer distances are possible, only about one time the layer thickness [10, 40]. When the unsupported layer length increases, the risk of manufacturing faults also increases. For overhanging surfaces with an angle less than 45° to the base plate, support material is needed. In Figure 2.2 different orientations are shown and it can be observed the likeliness of a part being produced adequately decreases as the overhanging angle get smaller than 45°. Geometries where this is necessary are for example the roof of a large hole or protruding elements parallel to the base plate. Small overhangs are possible, but the unsupported distance is depending on the specific machine and process. Using fillets or chamfers reduces the amount of support needed for overhanging surfaces. As the print orientation dictates which surfaces are considered overhanging, defining a printing orientation prior to designing is advisable.

Support material can also be used to absorb and diffuse the heat used to fuse the powder away quicker. This reduces the melt pool size, increasing the resolution of the print. The thermal conductivity of loose powder is lower than that of fused material, and the powder may work as an insulator. The necessity for and location of thermal support are a matter of experience by the operator or designer [40]. Thermal support is dependent on the part itself, but also the surrounding parts during printing.

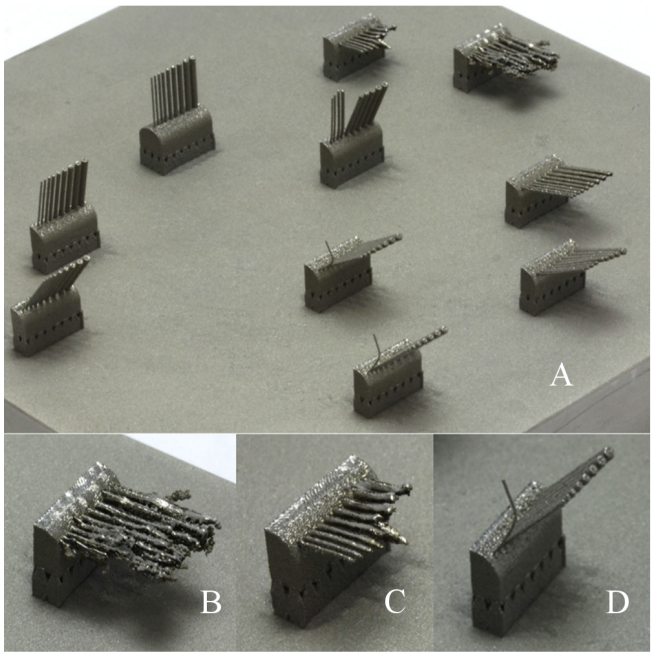

Figure 2.2: Example structures to assess the manufacturability of overhanging geometries. Each structure has a different overhang angle and different sized struts. A) shows a collection of different angles used. B) is a close-up of horizontal long pillars. C) is a close-up of horizontal short pillars. D) is a close-up of pillars on a 45° angle. The longer the unsupported length, the worse the printing quality becomes. Taken from [40].

Finally, support material is used to maintain part alignment. For example to prevent movement of the part while spreading of the next layer of powder, or to decrease warpage by bracing the part.

Support material is sacrificial and needs to be removed after printing. The support material removal is manual process. The location at which the support material determines which removal method can be used and how effectively. For curved surfaces, and especially concave surfaces, and recessed faces, support removal can become a challenge. With SLM the support material is the same as for the part, which makes metal supports tough to remove. Hard to remove support structures potentially leave marks on the surface, and often only manual inspection and finishing will completely remove them. Support material marks and high surface roughness can be minimised by making smart design choices, and part build direction reorientation.

Flat surfaces or even vertices are preferred as this reduces the complexity of support removal. In these cases removal can be done with relative ease using sawing, milling or wire discharge machining [10]. Curved, and especially double curved surfaces increase the difficulty of removal as wire erosion or band saws can only remove material in a line. This would then require milling or

clipping to remove supports. Placing support material on a surface where it is hard to remove and if the surface quality of that surface is of importance should be avoided.

2.1.5 Warpage

The building orientation influences several aspects of production. Most 3D printing techniques, including PBF, are anisotropic because of a difference between intra and inter layer fusion. The fusion between layers is less than the fusion within a layer, which can cause delamination. Delamination can be problematic for part layers with a large surface area, where thermal warpage is most pronounced. Angling a workpiece can reduce the cross sectional area, and therefore the chance of delamination and warpage. Alternatively, creating hollow or strutted volumes is a good way to decrease cross sectional surface area. It should be noted that enclosed voids are undesirable, as this leaves the excess powder trapped in the part.

Surfaces parallel to the building plate experience an effect that creates unwanted dimensional inaccuracies. To ensure a smooth, continuous outer perimeter, the energy beam fuses the material with an outside perimeter pass. This outside pass partially overlaps with the hatching pattern (i.e. the filling path of the energy beam) used for the material inside of the perimeter. This overlap results in an increased local layer height around the perimeter. It is unclear whether increases linearly with the number of layers following the same perimeter, but manufacturers advice including an angle of a few degrees to nullify this effect (email correspondence).

2.2 Material

Three alloys currently used for medicals instruments can also be 3D printed [9]. These three alloys are titanium (Ti), stainless steel (SS), and cobalt-chromium (Co-Cr) based alloys. All of these materials are used, in 3D printed form, in medical items like implants and non-medical items. Any of these materials could be used to produced laparoscopic instruments with. The usage of stainless steel was most prevalent among these three for usage in medical instruments according to Culmone *et al.*[9]. All three alloys can be produced with PBF, and changing the material between these three has limited effect on the production.

2.3 Post-processing

2.3.1 Overview

Post-processing of metal parts typically includes removal of support structures and a heat treatment. The steps used during post-processing heat treatment depend on the alloy, but aim to achieve a similar goal. In general the heat treatments are used to normalise the stresses in the material induced by the repeated rapid heating and cooling, and for some materials an additional re-hardening cycle is applied. The support material is removed mechanically. In the case of 3D-printing metal parts, post-processing will also include some type of surface treatment to lower the surface roughness.

There are numerous ways to decrease surface roughness, but not all methods are equally suited for all additively manufactured parts. The surface roughness can be lowered by use of mechanical, electrical or physical processes. Many of the techniques found in literature that are applied to 3D printed metal parts require the parts to be affixed and processed individually. While this is not necessarily a problem, there are a few techniques that do not require individual processing and indexing. Applied to AM produced metal parts the found techniques were mechanical, chemical, and electro-chemical polishing.

2.3.2 Mass Finishing Technique process

Mass Finishing Techniques (MFT), i.e. surface finishing techniques that can process a larger number of parts simultaneously. MFT is a group of mechanical surface and edge finishing and deburring operations [41]. Generally speaking, with MFT an abrasive medium, consisting of ceramic, plastic or metal particles, is run past, over, or through one or more work pieces, Figure 2.3. Free flowing or fixtureless MFT is a sub group in which the workpieces and media tumble, vibrate, or flow together [42]. These techniques are one of few that can work on all surfaces in one sitting, assuming the media can access each surface. This is not the case with most other techniques, where the work piece has to be fixated on at least two different surfaces to polish the whole item. Additionally, many of the MFT are unaffected by batch quantity, meaning that one cycle can process many items, even different items, at once. MFT and metal AM have the potential to work complimentary, because both techniques are free from the need of having flat, straight, or circular geometries which many other techniques do prefer. The MFT available at Dienst Elektro-Mechanische Ontwikkeling (DEMO), the contractor who makes test set-ups and prototypes for the Delft University of Technology, is Centrifugal Disc Finishing (CDF).

2.3.3 Abrasives

To speed up the process and preserve the lifetime of the abrasives, oftentimes coarse to progressively finer abrasives are used. With MFT parts of many different materials can be polished, although not in the same batch. Ceramic abrasives are used for harder metals like steel

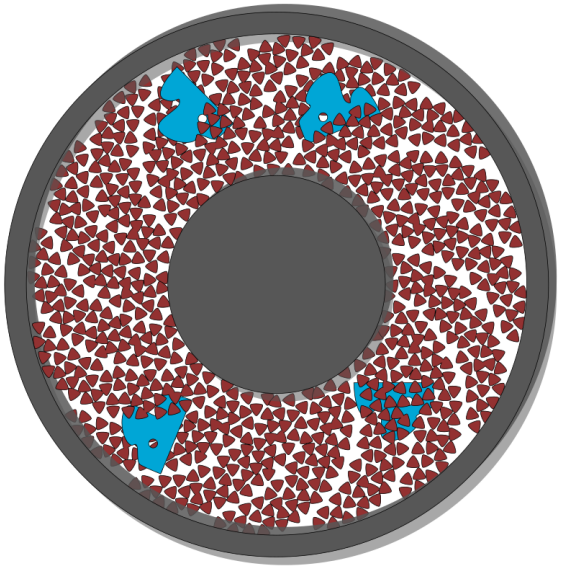

Figure 2.3: Schematic illustration of a general mass finishing polishing process. A moving bulk of polishing media (red) in which multiple workpieces (blue) are processed simultaneously. The polishing media and workpieces can be moved by vibration or rotation.

and titanium. These abrasives can be formed in many different shapes and sizes. Common shapes include cylinders with a circular, ellipse, triangle, tri-star base, but also cones and tetrahedrons [43]. Sizes for ceramic abrasives range from 1 mm to 15 mm [43].

2.3.4 Polishing access

In order for MFT to be effective, the polishing media has to be able to access the to be polished surfaces. This means that the smallest available abrasive has to fit inside recessed or internal features for them to be polished. Depending on the media's shape, this could mean more than one time the diameter of the abrasive, as jamming of abrasives is common for small holes [44]. For MFT, internal radii have to be equal or bigger than the peak radius of the media to be accessed properly [41]. Any inside radius smaller than this peak radius is unpolishable.

As explained, MFT effectiveness is a result of the polishing media's capability to access the local surfaces. However, not all surfaces have to obtain the same surface roughness. In fact, some surfaces can be left unpolished to increase design effectiveness. The necessity of (fully) polishing a specific surface should be analysed before making design adaptations. For example, a higher surface roughness increases the strength of interference fits, which is a suitable method for joining components that have to be permanently connected [45]. The same extends to other fits dependent (in part) on friction. The surfaces that do have to receive proper polishing are rolling and sliding surfaces, as these experience wear and possible particle detachment.

2.3.5 Material removal

The parts are taken to final dimension with the post-processing technique, which is important for parts that have to fit or mesh into each other. The exact amount of material that is removed is a depending on process parameters like duration and intensity (speed), but also on the polishing media's age [44]. With time, the polishing media can dull which increases its smallest radii and lowers its cutting ability. The rate at which material is removed is depending on many factors and can best be experimentally quantified [41].

The material removal rate is likely to be heterogeneous, as more accessible surfaces will experience more abrasion. More accessible surfaces include outside corners, but also free standing pillars. Less accessible surfaces can include trenches and inside corners.

2.3.6 Surface roughness reduction

MFT can be used to achieve a few goals: it can be used to deburr edges, give edges a radius, reduce surface roughness, or increase a surface' reflectivity. Often, more than one of these aspects is affected, depending on the material of the work piece and abrasives. Zooming in on the surface roughness, the final surface roughness is a result of the initial surface roughness and the MFT process. A surface roughness measurement on 3D printed stainless steel polished with CDF at DEMO showed a surface roughness reduction of around 35 % (Appendix A). Two test pieces, each with four differently angled surfaces was measured before and after polishing. The average surface roughness across the different surfaces and angles went from $9.2 \pm 1.7 \mu m$ to $6.3 \pm 1.5\ \mu m$. The polishing in this case was done with two steps of 1.5 hours, using medium and fine abrasives as described later in Section 5.3.

2.4 Production Guidelines

2.4.1 Selective Laser Melting

To ensure a 3D printed part that is as close as possible to the desired shape, a number of design guidelines can be formulated. Many of the production hardships of SLM are related to the part orientation during printing, and many ways of mediating these hardships can be applied for a specific building direction.

- Choose a building direction prior to designing.

- Avoid overhanging surfaces with an angle lower than 45° relative to the base plate.
- Avoid requiring support on recessed and curved surfaces, and if possible have all the support on flat surfaces or vertices.
- Avoid cross-sections with a dimension larger than the building height of the part.
- Prevent perimeter-line height increase by avoiding faces parallel to the building plate.
- Do not use features smaller than 0.5 mm.

2.4.2 Centrifugal Disc Finishing

The use of CDF adds additional constraints to the design. The choice and state of the abrasive media is the biggest factor in what can and cannot be polished. Unfortunately, many of the guidelines found in literature are qualitative in nature, and have to be quantified experimentally.

- Identify surfaces that require polishing.
- Ensure media access by limiting recessed features.
- The smallest internal radius should be larger than the smallest external radius of the polishing media.
- Take into account the loss of feature definition.

Media access, smallest internal radius, and loss of feature definition are qualitative guidelines. To quantify these guidelines a practical method was formulated in Chapter 5.

3 Design Analysis of the DragonFlex

3.1 Overview

The DragonFlex is a steerable gripper for general laparoscopic surgery [4, 15–18]. This instrument was designed with the aim to create a high stiffness, high endurance instrument. The design of the DragonFlex consists of eleven components, of which some are joined together to create seven bodies (Figure 3.1).

The design of the DragonFlex is a result of a number of design objectives aside from fulfilling the laparoscopic gripper function [16]:

- The DragonFlex is designed to be fully mechanically actuated in two perpendicular directions for ± 90°.
- The instrument has to have a high stiffness, which can be an issue for laparoscopic grippers, since 5 mm is the smallest standard trocar size [3].
- The actuation cable curvature has to be as low as possible, as this improves the lifespan of the actuation cables. Short cable lifespan is an issue for high stiffness laparoscopic grippers.
- To be compliant with laparoscopic standards, the design has a cross section no wider than 5 mm from the tip up to the beginning of the handle (components 1 to 6 in Figure 3.1).

The next sections (Section 3.2, 3.3, and 3.4) analyse and discuss the design objectives in more detail. In Section 3.5 the design of the joints used to facilitate the design objectives is dissected. To conclude, this joint design is viewed through the lens of the desired production techniques in Section 3.6.

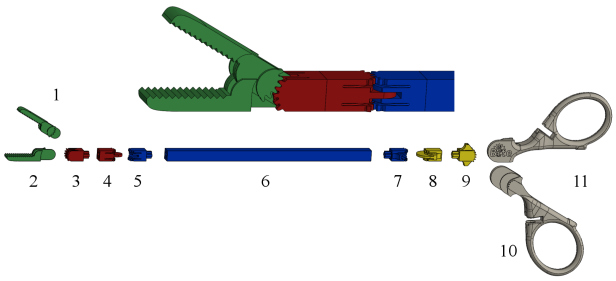

Figure 3.1: Exploded view of the DragonFlex' components. Green elements (1 & 2) form the gripper. The elements 1 to 5 together are considered the tip of the instrument. Component 6 is the shaft and is press fit to components 5 & 7. Components 3 & 4, and 8 & 9 are press fit together, too. The components 7 to 11 form the handle, and actuate and control the tip. The grey components (10 & 11) are finger holds for the operator. The top image is an unexploded close up of the tip.

3.2 Actuation & Control

An unsteerable laparoscopic instrument has five DOF: four rigid body movements constrained by the trocar, and one gripper actuation DOF. The DragonFlex has two more DOF, which allow the gripper to have additional orientational freedom. The DOF that pertain to the actuation and orientation of the gripper will be referred to as internal DOF, and similarly rotation and translation of the entire instrument will be referred to as external DOF. Figure 3.2 illustrates the direction of rotation and position of these additional DOF, and what should be noted is that the gripper actuation DOF and one steering DOF coincide at one location at the distal joint. This means that rather than two individual rotational DOF and an individual DOF for actuation, the DragonFlex has three rotational DOF, of which two together result in an actuation freedom.

The DragonFlex is set up as a master-slave system. The position of the handle (master) is transferred to the gripper (slave) using cables. The internal DOF are limited to $\pm$ 90° by physical stops at the master side. Each of the three internal DOF has two bodies associated with it, forming master-slave pairs. One pair are the centre bodies on each side of the shaft, and these are ensured to always be parallel to each other. The other two pairs are formed by one of the gripper elements with one of the handle elements. The handle and gripper elements are paired diagonally, meaning element 1 with 10, and element 2 with 11 as shown in Figure 3.1. The way the system operates is the direction or angle the master-side makes to the hinge, is equal to the angle the slave-side makes away from the hinge. With this type of control, the user experiences no mirroring or amplification of movement. Additionally, because of the high stiffness design objective and the physical connection via cables, the user also experiences accurate force feedback. Without force feedback the surgeon would have to rely on visual information from the laparoscope only. The position of the DragonFlex is transmitted from the handle to the gripper using cables.

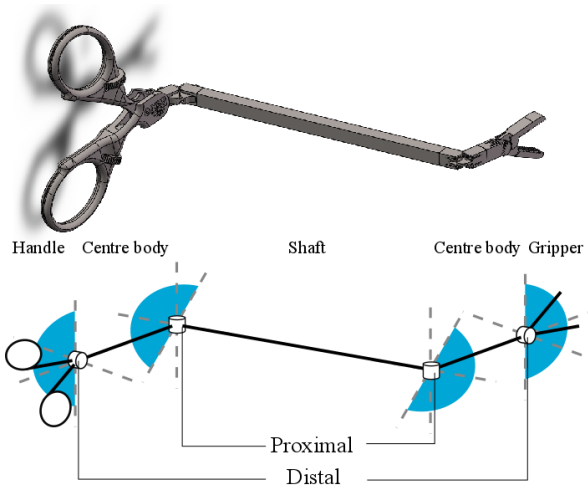

Figure 3.2: CAD model of the DragonFlex (top) and a schematic depiction of the hinging directions of the joints (bottom). The DragonFlex gains its additional degrees of freedom from two joints, which are mirrored along the shaft. The proximal joints allow for one degree of freedom bending. The distal joints allow two DOF, one for each gripper half.

3.3 Stiffness

Stiffness in laparoscopic instruments is the relation between the total error in position caused by an external force, and the force required to create that error. In other words, how much force at the end effector is needed to create a deflection. In particular a force perpendicular to the shaft direction is problematic, because laparoscopic instruments behave similar to a cantilever. So when a laparoscopic gripper is used to manipulate tissue, the force can cause unwanted deflection. Deflection is undesired for two reasons: for one, it is an error between input and output, complicating control, and secondly, it stores elastic energy in the instrument. Energy stored in the instrument is additional work which the surgeon has to both generate and release.

The total stiffness of a system is dependent on the stiffness of its components and how they are structured. In the case of steerable laparoscopic instruments the total stiffness is primarily comprised by stiffness of the shaft and hinge(s), which are working in series. The stiffness of a system of components in series is always lower than the stiffness of its lowest component. Therefore no low stiffness elements can be used to create a high stiffness instrument.

Underactuation lowers the stiffness of a laparoscopic instrument, and is a common approach to creating range of motion. Jelinek *et al.* classified joints used in steerable MIS instruments found that many of the hinging principles used rely on underactuation. An underactuated system is a system with more DOF than actuators. This can come in the form of multiple hinges in series or a flexible section. To control multiple small DOF (joints) with one actuator, a path of least resistance has to be imposed on the system. This usually has the form of a compliant components, but can also use the stiffness of the actuation cables. It is this additional compliancy that drastically reduces stiffness at the end effector.

The DragonFlex does not use multiple joints in series to achieve a DOF, but rather uses one hinge per internal DOF. This is not unique to the DragonFlex, as more laparoscopic systems use fully actuated hinge designs. Most noteworthy is the EndoWrist by Intuitive Surgical Inc., Sunnyvale, CA, USA, which is a system used in the da Vinci surgical robot [46, 47]. The DragonFlex'

design was in part an answer to one of the EndoWrist's endurance related drawbacks, while maintaining a high stiffness system [16].

3.4 Endurance

Actuation cable longevity was one of the additional design objectives for the original DragonFlex. As explained previously in Section 3.3, a single, full range of motion joint increases the stiffness of the system, however, it also increases the curvature actuation cables have to endure. This is because the arc length of the section of cable that curves becomes shorter with a single hinge point, while the same range of motion has to be achieved. The lifespan of cables depends on the curvature and frequency of bending as well as the thickness of the cables. The frequency of bending cannot be limited without diminishing the value of the instrument for the application, and the thickness of the cables also has a lower limit. This leaves the curvature as the only design parameter which can be tuned.

The simplest cable path would be using a cylinder to wrap the cables around between two bodies, leaving a single point of rotation. This is how the EndoWrist (Figure 3.3) is designed, and this approach is effective. However, the curvature of bending is relatively high, and results in a limited number of ten procedures that can be performed with one set of cables [46]. The bending radius (inverse of curvature) of the cable for this system is 0.5 times width of the instrument.

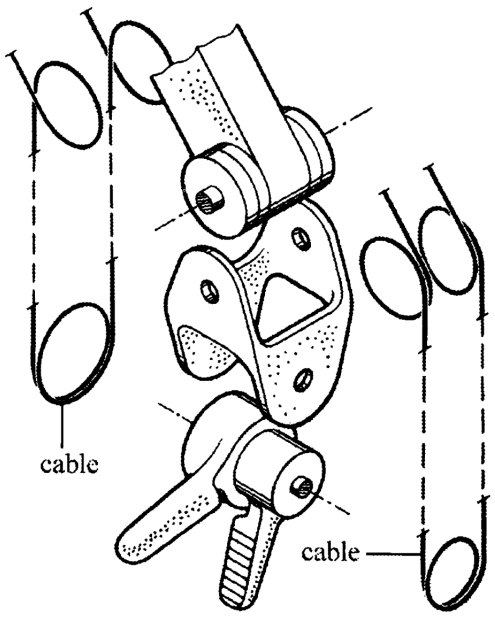

Figure 3.3: Simplified exploded view of the EndoWrist, taken from [48].

The DragonFlex design decreased the maximum curvature by allowing the cables to cut the corners in bending. This approach is illustrated in Figure 3.4, where the cable paths are depicted for different rotation angles. The final bending radius was increased to 0.8 times the instrument width.

For the cables to be able to cut the corners, a continuously changing pivot point is needed. A fixed pivot point would cause the joint to become unstable near the end of the range of motion. This is achieved by a rolling contact point.

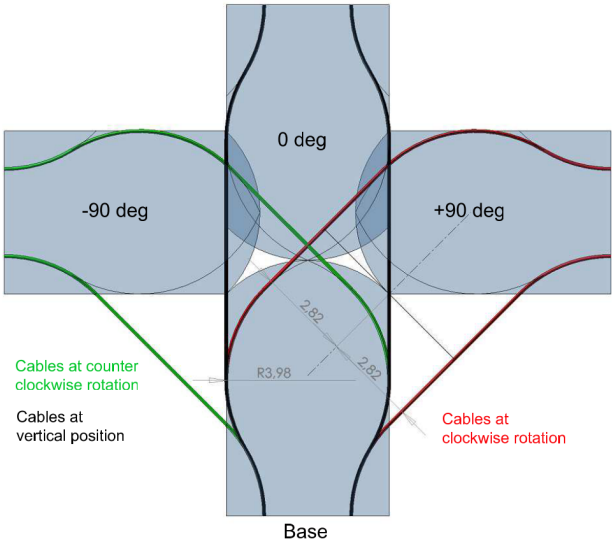

Figure 3.4: Schematic view of cable path throughout the range of motion of a DragonFlex joint, taken from [16]

3.5 Joint Constraints

Four joint locations are present in the DragonFlex, consisting of two pairs, as discussed in Section 3.2. To analyse how the joints currently function, the joints will be referred to as proximal and distal, in relation to their position relative to the shaft. In particular the gripper side will be analysed, as the handle is both a copy and does not have a space limitation like the gripper does.

That the proximal and distal joints are different is a result of the number of bodies and constraints they control. The proximal, full width joint consists of seven functional regions or layers. The distal joint consists of four functional layers, and one layer which is not functional for the working of the joint. In Figure 3.5 the functional layers are illustrated in an exploded view:

1. Spur gear arcs: constraining translation in X-direction
2. Cable path guides: actuation and Z-direction separation

3. Rolling contact surface: guiding the motion and Z-direction constraint

4. Protrusion/cut-out: constraining Y-direction translation, and X and Z rotation

In the proximal joint, a number of layers are redundant. Multiple layers prevent the rotations around Y- and Z-axes. Both the the protrusion/cut-out layer, and the cable path and rolling surface layers prevent rotation around the Y-axis. Likewise, the protrusion/cut-out layer, and the gear arcs constrain the rotation around the Z-axis. Although not necessarily problematic, using more than the required number of geometries to constrain a joint indicates a simpler joint could be constructed.

Analysing the distal joint shows it is a split version of the proximal joint. In what is the mid-plane in the proximal joint, the functional layers are split. This leaves a total of eight functional layers for the whole joint, four for each gripper. In Figure 3.5 an exploded view of five layers is shown, in which the last layer is redundant for the working of the joint. Figure 3.6 illustrates the two joints schematically. This schematic representation will be used to explore and investigate concepts later on.

In the distal joints there are no over constraints, as every possible relative motion between two bodies is controlled. The choice to use similar joints for the proximal and distal joints is intuitive. The distal joint is the more complex joint, and a design that works in that case also works mirrored or full width.

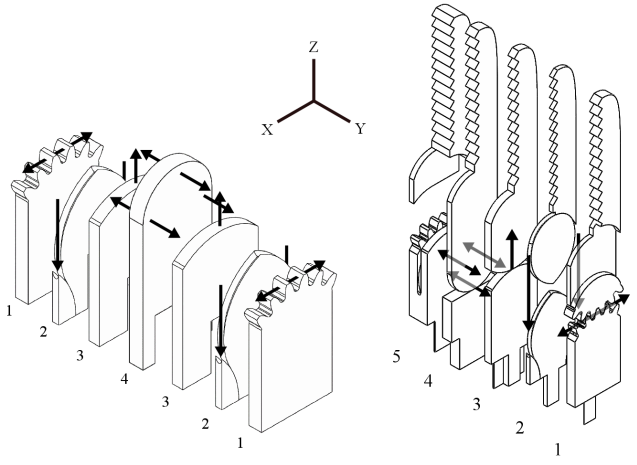

Figure 3.5: Exploded view of the two joint types in the DragonFlex. The arrows indicate reaction forces which occur when external forces are applied to the counterpart of this joint. Left: Exploded view of proximal joint's components, without the opposing body. Right: Exploded view of distal joint's components, with one opposing body.

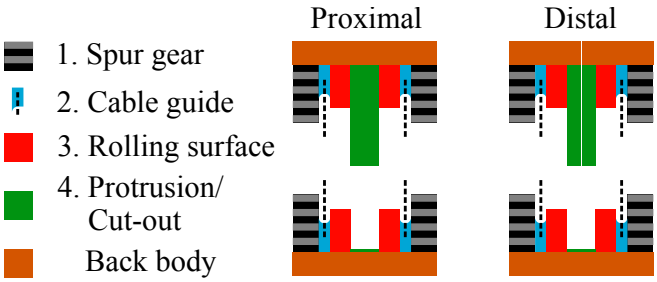

Figure 3.6: Schematic representation of the layers that comprise the dragon flex joints. The image illustrate the similarity between the two joints.

3.6 Production Technique Incompatible Joint Features

The design of the DragonFlex has a number of geometries which are difficult to produce with either PBF or MFT. Printing of the original design parts had shown that SLM cannot consistently produce the cable paths. The cable paths are intended to be circular holes following a curved path. The small diameter of this hole (0.4 mm) proved problematic for loose powder removal, and for geometrical resolution of PBF. A few of the holes were even fused shut completely. The layered nature of PBF resulted in non-circular holes, making threading of the cables through the holes not possible at instances. For this reason, when 3D printing circular holes, Gatto *et al.* suggest undersizing the hole by 0.6 mm, and drilling the hole to final diameter [49]. This is clearly not feasible with this hole diameter. Next to that, the cable paths curving in two directions makes opening up the hole after printing a difficult task altogether.

The design also contains many slender plates to create the protrusion/cut-out layers, and occasionally these slender objects would be warped by thermal stress, as is visible in Figure 3.7. Warpage of a part is hard to predict as it does not just depend on the part itself, but also on the surrounding parts during build [42]. Increasing the thickness of these plates would reduce the effect of warping, but the current design does not leave space for this.

Support material removal is a possible point of concern for many designs produced with PBF, as well for the DragonFlex. In Figure 3.8 the amount of support material that is needed to produce handle components of the DragonFlex. Due to the complexity of this support material, all of it had to be removed by hand. Support material cannot be avoided, but clever design choices can minimise the amount of manual labour involved with support removal.

To reduce the surface roughness with MFT, the polishing media has to sufficiently access the surfaces, as explained in chapter 2.3. The DragonFlex design does

not take this into account, as stereolithography leaves the parts with an excellent surface quality. In particular the cable paths, gear teeth, and the cut-out in the centre are hard to polish or unpolishable. The blue lines in Figure 3.7 are designed to be parallel with a distance of 2 mm apart, which is smaller than the smallest available abrasive medium and is therefore unpolishable.

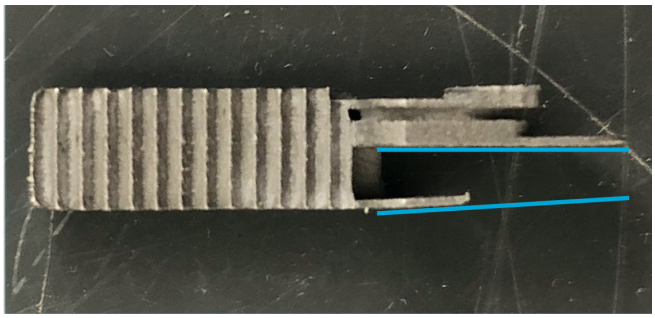

Figure 3.7: One of the gripper jaws produced in SS 316-L with Selective Laser Melting. Thermal stresses caused the 0.5 mm thick plate right above the lower blue line to curve inwards.

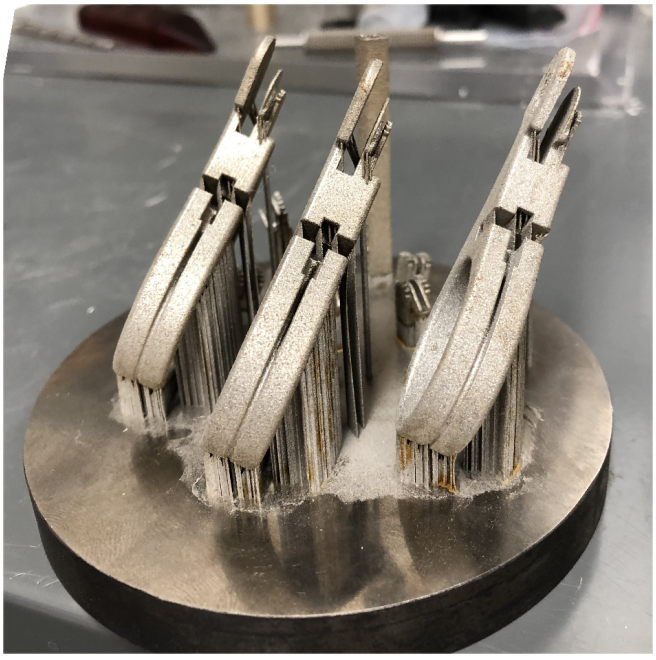

Figure 3.8: Handle components of the original DragonFlex design produced in SS 316-L with Selective Laser Melting. The components are still affixed to the build plate, and the amount of scaffolding to support the part during build is significant.

4 Concept Design

4.1 Programme of Requirements

The programme of requirements is a set of targets that encompasses the design problem that has to be solved [50]. The requirements are separated further into hard requirements and wishes. Hard requirements have to be met in order for a concept to be viable. Wishes are additional to the hard requirements, and can be a reason to choose one concept over the other.

The design for a metal 3D printed laparoscopic gripper will be based on the design of the DragonFlex [16]. A number of requirements of that design will be absorbed into the programme of requirements, listed below as requirements R1 to R5. R5 in the original design was a range of motion of ±90°, however, 60° is the market standard and will be used as a minimum.

Hard requirements

R1 The tip of the instrument up to the end of the shaft has to fit through a 5 mm trocar [16].

R2 The instrument should be mechanically actuated by cables[16].

R3 The instrument should be fully actuated as opposed to underactuated to ensure a high stiffness [16].

R4 The instrument should have at least two DOF working in two planes perpendicular to each other [16].

R5 The instrument should have a minimum range of motion of 60 degrees in both directions (± 60°) [51].

R6 The instrument should have an actuated gripper.

R7 The minimum cable bending radius of 4 mm should be respected where the cable experiences bending that changes throughout use.

R8 The instrument has to be fully 3D printable, in metal, using SLM, with the exception of any cables.

R9 SLM, support material removal, heat treatment, and MFT are the only necessary manufacturing steps to produce the instrument.

R10 All surfaces which experience contact with another surface have to be polished using MFT, including surfaces that would contact bodies other than the instrument.

Wishes

W1 The design consists the same number (11) components as the DragonFlex, or fewer.

W2 Support material should only be needed at flat surfaces or edges.

4.2 Joint Type Selection

A classification of joints used in laparoscopic instruments that have a range of motion in two perpendicular directions is shown in Figure 4.1 [52]. The current design employs a layer of rolling friction joint and a layer of rolling toothed joint, among a protrusion/cut-out layer and cable guide layers as discussed in Chapter 3.5. These two joint types as presented in Figure 4.1 provide DOF in two rotational directions and constrain one. However, some of these joints do not constrain all translational DOF. In fact, only the rolling belted and bending flexure joint are fully constrained. Unfortunately, these two joints are problematic to execute in metal, as they rely on high ductility of the material or result in a low stiffness system, as Chapter 3.3 explains. 3D printed metal is notorious for having a low fatigue strength [20, 24, 32, 37], which is why a flexure joint hard to produce reliably.

A rolling joint is used in the DragonFlex to limit the maximum cable curvature. Pessers [16] showed that this is the only type of joint that can be used which abides requirements R1, R5 and R7.

If the joint type has to be of the rolling joint variety, and belted joints are unviable to 3D printed, that leaves the rolling friction and the rolling toothed joint according to Figure 4.1. Theoretically, the rolling friction joint should provide all the necessary constraints using friction. However, this would require pretension throughout the whole range of motion and relying solely on friction to constrain the DOF is problematic when bodily fluids can act as lubricants. In addition to uncertainty in the coefficient of friction, any loss of pretension throughout the range of motion will cause the joint to fail. Considering these factors, rolling toothed joints are the most viable option. As the rolling toothed joint is not constrained in all the desired directions, additional constraining features must be added.

4.3 Joint Components Designed for 3D printing & Polishing

4.3.1 Gears & rolling surfaces

Toothed joints rely on shape enclosed force transfer, as opposed to friction (rolling friction joint) or material (rolling belted joint) for force transfer. In Figure 4.1 only one type of toothed joint is illustrated, an involute spur gear, also illustrated in Figure 4.2 (A). The involute function is optimal for gear teeth, as it minimises the sliding component throughout the motion of gears turning, which reduces friction. Unfortunately, this tooth design is hard to polish as discussed in Chapter 3.6.

A tooth profile that is better accessible by a polishing medium is required. Minimising friction is not of great importance for finite angle gears. A sinusoidal gear (Figure 4.2 (B)) profile does not have sharp inside corners, and is therefore a good candidate for a polishable gear. The sinusoidal function can be adjusted to the size of the polishing media available by changing the frequency and amplitude.

The shallow teeth angle of sinusoidal teeth are better at accepting radial loading than the involute teeth, which means they can fulfill the function of gear arch as well as rolling surface, as described in Chapter 3.5. Absorbing two functions into one geometry requires fewer features in the joint. This is highly desirable as instrument width is a hard constraint (R1).

For a smooth trajectory, a gear tooth must be engaged with other teeth at both sides. A sinusoidal spur gear does not have its teeth engaged at both sides throughout the range of motion. With this being the case, the gears will jump from one constraint position to the next, creating a rocky motion. Fortunately, this can be remedied by constructing helical gears instead of straight spur gears. Figure 4.3 (A) and (B) show spur and helical gear profiles. By placing the gear teeth on an angle, multiple teeth are engaged at once, which will smoothen the motion.

Related and a descendant of the helical gears are the herringbone profile gears. Herringbone gears are two helical gears with opposing angles placed on the same axis. In this manner the gear can absorb axial loading, effectively constraining this direction. Figure 4.3 (C) illustrates a herringbone profile. This gear profile is more complex, but does constrain more directions than a spur or helical gear.

4.3.2 Cable guides

Small holes or tunnels are a challenge to correctly 3D print, due to the risk of fusion, and in addition cannot be polished. A solution for this is opening the tunnels into channels along the surface. This means the cable guides have to be placed on an exterior surface of the joint.

Cables are only experiencing tensile forces, and therefore only require support at the inside of a bend. Cable support on any side other than the inside bend is not required (Figure 4.4). This can be used to increase the polishing medias access to the cable guide surfaces.

The cable guides have to be accommodates on the outside of the part, to allow proper polishing access. This means either that the cable guides are placed on the exterior of the instrument (Figure 4.5 A), or additional 'outside surfaces' are created (Figure 4.5 B). Creating additional outside surfaces requires splitting the part.

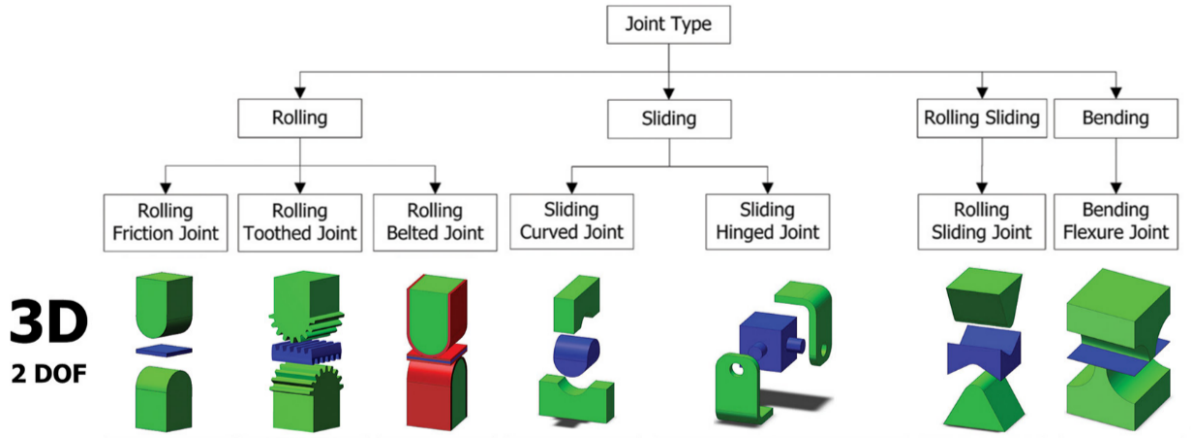

Figure 4.1: Classification of rolling joints that can provide rotation in two perpendicular directions (R4). Adapted from [52]

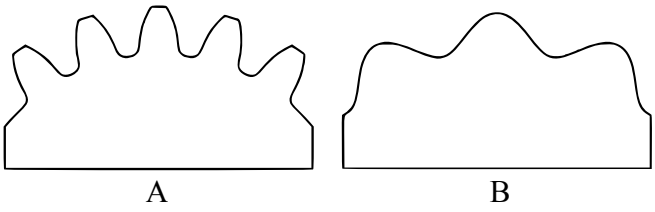

Figure 4.2: Illustration of A) involute gear teeth and B) sinusoidal gear teeth. The polishability of the sinusoidal teeth is a lot higher.

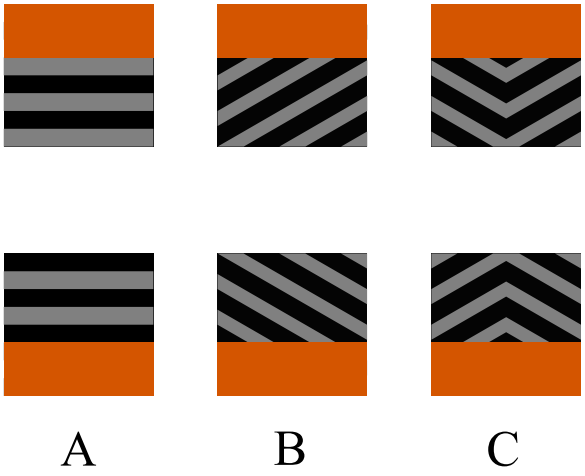

Figure 4.3: Schematic illustration of different tooth profiles. A) spur tooth profile, B) helical tooth profile, and C) herring bone tooth profile. The gears are viewed parallel to the rolling axis. The grey and black lines illustrate the tooth faces of the gear.

4.3.3 Protrusions & cut-outs

Protrusions and cut-outs are able to constrain three directions at once, making them a very useful feature. Unfortunately, the inside surfaces of cut-outs are hard to polish. The reason for this is that the smallest available media is around 2.8 mm across. As stated in requirements R1, the thickness of the instrument cannot exceed 5 mm, thus keeping a clearance of at least 2.8 mm will utilise much of the available feature space in the joint.

The issue with protrusions and cut-outs is comparable to that of the cable guides. In fact, approaching cut-outs from the same angle reveals that when placed on the outside of a part, the polishing access is created (Figure 4.6 A). Likewise to the cable guides, splitting the whole joint body in half can allow the protrusion and a narrow cut-out to be in the centre line of the joint (Figure 4.6 B).

4.4 Joint Concepts

4.4.1 Proximal joint

The proximal joint is the simpler joint of the two, and will be used as a start for reinventing a joint suitable for SLM and MFT. As found in the analysis of the original design, the proximal joint is overconstrained and does not need all the constraining features. Combining the gear arch and the rolling surface frees up joint space, which improves printability and polishability.

Unfortunately, polishable cable guides and cut-outs compete with each other for space on the outside of the part. Only when splitting the joint length-wise would there be the required 'outside surface' for both cable guides and cut-outs in the same joint.

For the proximal joint there are four options; having the cable guides on the centre line or on the exterior of the joint, and whether or not to use protrusions and cut-outs. Whether protrusions and cut-outs are required is a matter of stability; adding this feature would constrain the joint in all directions except along the instrument axis without the cables. Omitting protrusions and cut-outs relies on the cables to constrain rotation perpendicular to the DOF, as well as rotation along the

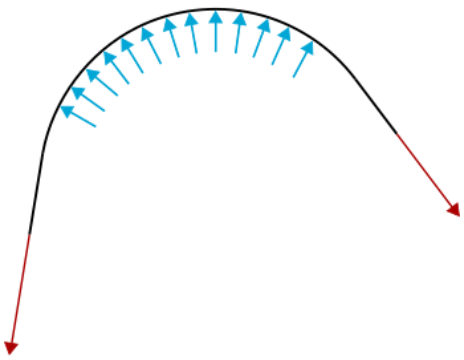

Figure 4.4: Illustration of the reaction forces (blue) that occur when a cable (black) is put under tensile load (red) around a surface. Note that the reaction forces are only on the inside of the bend, the rest of the cable can be left unsupported. If the cable only needs to curve in one direction, support only needs to be present at the blue arrows.

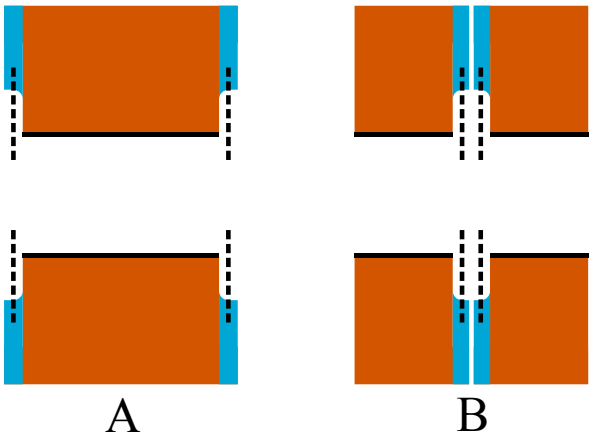

Figure 4.5: Schematic depiction of polishable cable guides. In this figure blue are cable guides, orange are the other features and base, and black is the contact area that the two halves are engaged on. Both parts have the hard to polish areas on the outside of each part. In (B) the both sides of the joint consist of two parts.

instrument. If the a joint has the mechanical stability required, not including the protrusions and cut-outs is favoured because this simplifies the joint structure.

These four options are schematically presented in Figure 4.7. All four concepts use helical gears, either oriented as herring bone gears or not, to ensure a smooth range of motion. In the case of the proximal joint, any joint split required to accommodate polishable cable guides or cut-outs will have to be joined together during assembly.

4.4.2 Distal joint

The distal joint can be approached in a similar fashion to the proximal joint. Different from the proximal joint however, is that only three options remain (Figure 4.8). Where the centre body held together P1, this is not the

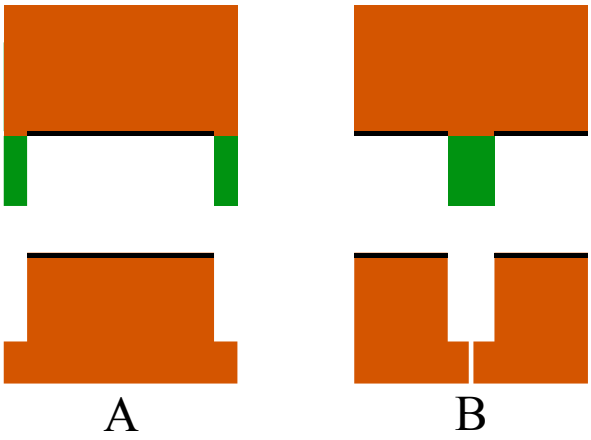

Figure 4.6: Schematic depiction of polishable protrusions & cut-outs. In this figure green are protrusions, orange are the other features and base, and black is the contact area that the two halves are engaged on. Both parts have the hard to polish areas on the outside of each part. In (B) the bottom joint half with the cut-out consists of two parts.

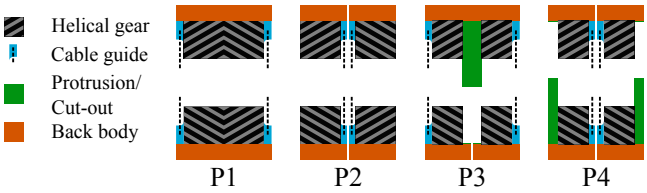

Figure 4.7: Schematic depiction of the four possible concepts for the proximal joint when using herring bone gears to constrain (P1 & P2), and when using protrusions and cut-outs with helical gears to constrain (P3 & P4) the motion. Note that different joint splits are necessary to make these concepts work. P1 does not require any split, P2 & P4 require a split on both sides to accommodate polishable cable guides, and P3 requires a one-sided split to accommodate a polishable cut-out.

case for the grippers, as these need to remain separate. This required separation will cause the cables to pull the grippers apart, rendering this option unviable for the distal joint. If the cables are placed on the exterior of the joint, a protrusion and cut-out are needed to maintain gripper alignment. Cables placed on the interior of the joint will not have this problem, as the cables in tension will help the grippers stabilise each other.

The distal joint concepts only function in the orientation presented in Figure 4.8. On the side of the centre body the back body is joined during assembly.

4.4.3 Joint selection

There is no requirement to use the same arrangement of joint features in the proximal and distal joints, so these two groups can be assessed separately. To validate the mechanical stability of these concepts, they were 3D printed at a 3:1 scale in PLA using Fused Deposition Modelling (FDM). In particular the effectiveness of

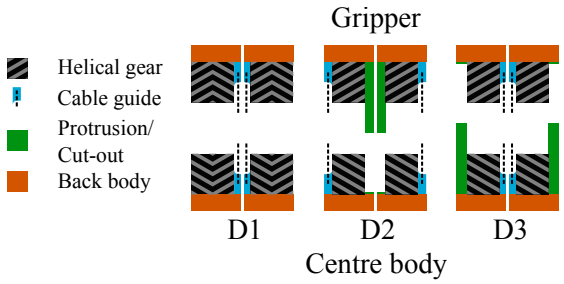

Figure 4.8: Schematic depiction of the three possible concepts for the distal joint with polishable cable guides and cut-outs. D1 uses a herring bone gears to constrain the joint. D2 & D3 use helical gears with protrusions and cut-outs to constrain the joint.

the cable guides and gears had to be investigated. The effectiveness of the protrusion and cut-out was already validated in the original DragonFlex design. The scaled proximal (Figure 4.9) and distal joints (Figure 4.10) were assembled and wire cable was used for actuation and retention.

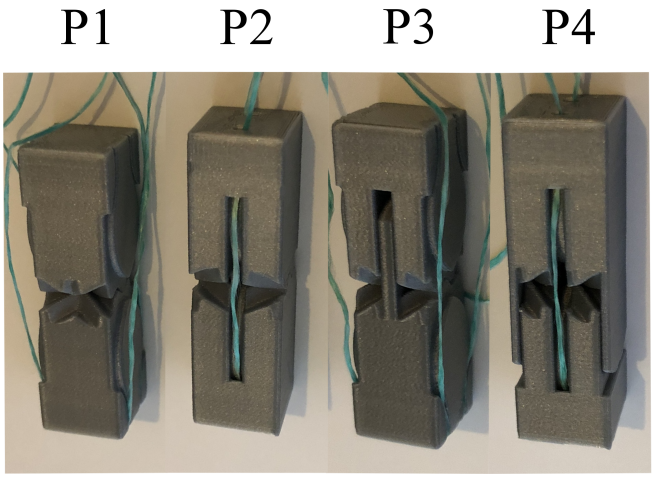

Figure 4.9: Photos of the scale models of the distal joint concepts printed in PLA on a 3:1 scale using Fused Deposition Modelling.

By evaluating the prototypes of the concept joints, the following aspects were discovered:

- Exterior cable guides (P1, P3 & D2) are problematic as their cable retention was lacking throughout the range of motion. Deeper cable guides could be a solution, but this likely makes the polishability of the parts go down. This is due to a section of cable guide in the joint that needs to enclose the cable on both directions. Deepening the cable guides would likely make this section unpolishable.
- The axial torsional stiffness (rotation along the length of the instrument) of joints without protrusions (P1, P2 & D1) is low. Steeper gear teeth will likely increase the stiffness, but the sinusoidal gears were designed to have shallow teeth, to improve polishability.
- For distal concepts D1 & D3 the interior cable guides limit the opening of the gripper to around 60°. Increasing this angle makes the gripper bodies come loose and the joint fails. However, this is within the requirements.

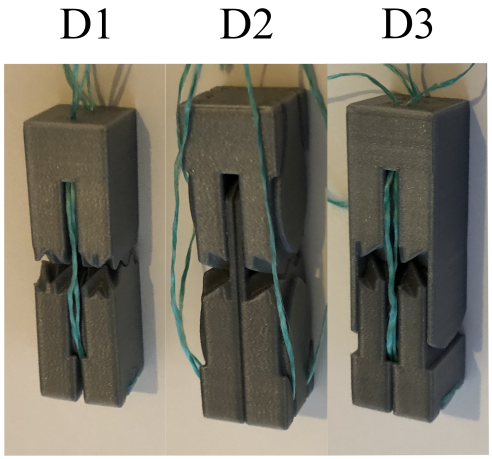

Figure 4.10: Photos of the scale models of the distal joint concepts printed in PLA on a 3:1 scale using Fused Deposition Modelling.

Of the four proximal concepts and the three distal concepts, proximal concept P4 and distal concept D3 are the most mechanically stable throughout the range of motion. These two joint configurations have been selected as the base for the design.

4.5 Centre Body Design

The selection of concepts P4 & D3 requires a centre body that accommodates a centre split on both joint sides, while maintaining rigidity in the assembled state. Figure 4.11 illustrates three options for the centre body composition.

Of the three options, C1 uses the fewest components which is a preferable according to wish W1. As with the joint concepts, this was printed in 3:1 scale using FDM (Figure 4.12). With the scale model it was discovered that this approach used very tight tolerances. It was found that with approach C1, any misalignment will either present itself by twisting the centre body, or not fitting together due to overconstraining. This can be avoided by proper dimensional control during production, but is an omen for poorly fitting parts when applied to metal 3D printing. C2 had comparable problems, although this time caused by one rigid backbone component to which the additional components had to adapt.

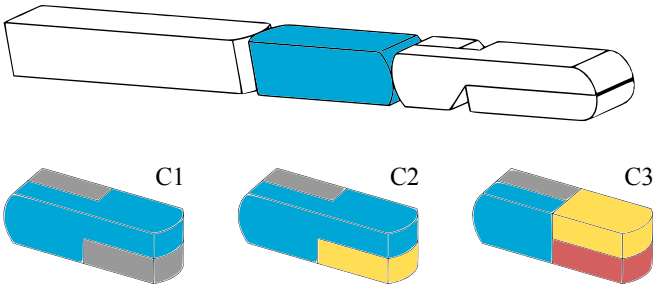

Figure 4.11: Schematic overview of three options to construct the centre body with a joint split on both joints. The colours (grey, blue, yellow, and red) of the different options indicate different components. The centre body can be comprised of two (C1), or three (C2) or four (C3) components. Going beyond four components will likely not have any advantage over having four components.

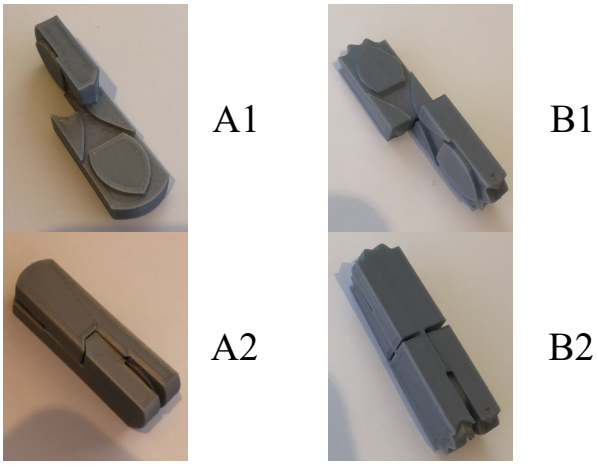

Figure 4.12: Two approach to combining two components into one part as per C1. A1&2 are the same solution, and B1&2 are the same. In A) the two parts slide onto each other from the top direction. In B) the parts click together using a flexure and are kept together by a socket and a ball.

While the twisting of the centre body can be avoided by tolerancing the parts to fit, a simpler and more robust solution can be achieved using C3. In option C3 the parts can have a clearance in the axial direction (Figure 4.14) Whether the centre body is slightly longer or shorter is inconsequential to the functioning of the design. This design option puts less strain on the tolerances of the production process and by extension makes the design more appropriate for SLM and MFT.

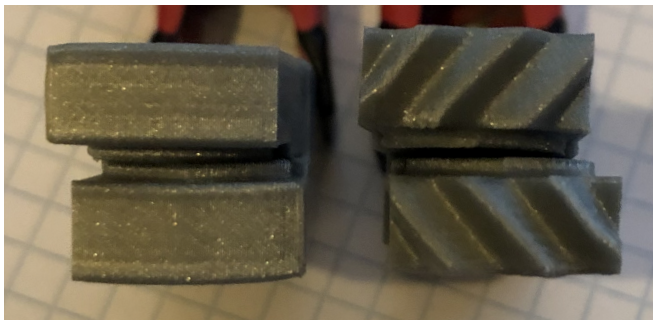

Figure 4.13: The two approaches to C1 both showed a big misalignment after assembly. Both parts were sanded to final dimension on the mating faces.

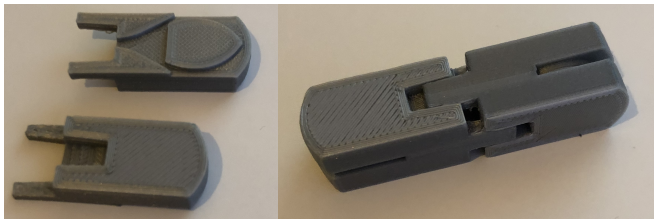

Figure 4.14: Centre body split according to C3. Four equal components assembled together make the part. The right side shows the extension in the axial direction.

5 Experimental Observations on Polishing

5.1 Goals

5.1.1 Effect of the geometry on polishing

Many papers discussing MFT and its effects on 3D printed metal focus on the surface roughness values that can be achieved. These papers generally use simple geometries like plates or cubes to examine one of their faces. However, this does not help in the evaluation of what constitutes a well-designed part for MFT. In an attempt to quantify the reported and expected effects of MFT on parts, a number of features relevant to the design discussed in Chapter 4 were absorbed into a 3D printed test piece. These features and their functions are discussed one by one in Section 5.2.4, to answer the question of what is the geometry specific polishing accessibility when designing for MFT.

The approach to determine a whether a part is well-designed for MFT is two pronged. On one side there is how the geometry of the part affects the efficiency MFT, and on the other side there is how MFT affects the geometry of the part. To investigate how the geometry of the part affects the MFT, a method is used to visualise how well polishing media can access certain geometries. This is done using a marking lacquer that shows where the polishing media chipped away at the lacquer.

5.1.2 Effect of polishing on geometry

The effect of MFT on the geometry is observed through dimensional measurements of the part and features. Comparing how different features compare to one another under different MFT conditions gives insight on how different polishing steps affect the part geometrically. What level of feature definition loss can be expected with MFT?

The polishing test consist of four groups of three test pieces. Each group receives a different MFT polishing sequence. The MFT steps range from coarse, to medium, to fine. The test pieces that receive a different treatment will be compared to investigate the effect of the different available abrasives. In particular the edge radius, corner radius, material removal rate and rate distribution are relevant.

5.2 Hypotheses

5.2.1 Edge rounding

Sharp outside edges of a part will be rounded by MFT. The final radius of outside edge after MFT is a measure of how much feature definition is lost. The quantification of the corner rounding will help decide which of the abrasive media is suited to use on small features.

The test pieces will be subjected to three polishing steps, each with a different level of abrasive media coarseness. With the four groups of test pieces receiving different MFT treatments, it is expected that coarser media will round the edges most. Medium and fine media are hypothesised to not have a significant effect on the edge rounding after the coarse media. However, if the coarse step is skipped and just the medium and fine steps are used, then the medium and fine steps will be relatively more aggressive compared to when these are following the coarse step.

The edge rounding will be observed on the edge marked red in Figure 5.1.

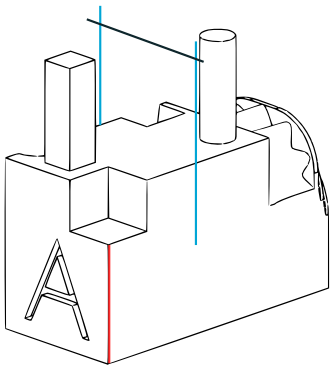

Figure 5.1: Test piece with the measurement locations of the edge rounding (red edge) and the base width (blue and black lines).

5.2.2 Material removal

MFT will remove material from the top of surfaces. The amount will depend on the type of abrasive media used, and the polishing duration. Measuring the width of the test piece base (Figure 5.1) before and after polishing steps will quantify how much material is removed. The amount of material removal is required to make an accurate prediction of final part dimensions. In addition to knowing how much is removed during MFT, it is necessary to know what the starting dimension is directly from the printing. The 3D printing dimensional error and the MFT material removal will contribute together to the final part dimension.

It is expected that the coarser abrasive will remove more material, and subsequent media will have a smaller effect. However, if the effect of medium abrasive will have more effect if the coarse media polishing step is skipped. This evaluation metric will both to gauge the necessity of a coarse first polishing step, and quantify the absolute material removal of two parallel faces.

5.2.3 Material removal distribution

It is likely that more material will be removed from the tip of protruding elements than from the base. To investigate how much more this is, extending pillars (red) have been added to the test piece. Comparing the pre and post MFT dimensions of the base and the tip of these pillars will tell how much more the ends will be abraded (Figure 5.2).

As MFT takes the parts to final dimension, the difference in material removal rate could be of importance for the fit of parts. In particular the use of prongs in the centre body connection. These prongs rely on a taper, and when the taper angle is altered too much during polishing these might no longer fit.

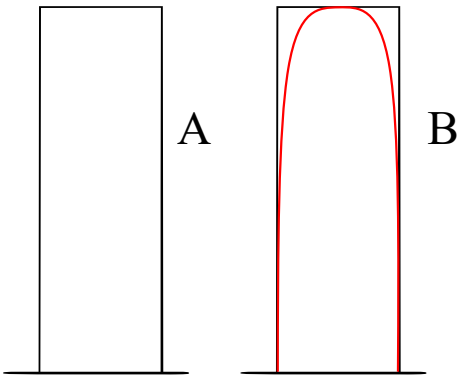

Figure 5.2: Illustration of the extending pillar with A) as printed, and B) hypothesised after polishing.

5.2.4 Surface access

To evaluate the ability of media to access recessed or concave surfaces the features marked yellow, orange, and grey in Figure 5.3 were added. These features are (partially) hard to reach, and will show where the accessibility limits of MFT are. These features were designed with the aim to observe how the polishing efficacy changes with different abrasive media.

The blue and pink marked features also investigate the polishability of geometries, but rather than exploring the limits of MFT, these features will be used to validate specific designs. Whether an area can be polished is not just a matter of finding an abrasive medium that can reach the area, it must also be probable that the abrasive medium comes in contact with the area often.

Recessed corner
With the recessed corner (yellow) the minimum inside radius for polishable inside edges and inside corners should be made visible. We hypothesise that a region non-polished will remain close to the edge, and a slightly larger area close to the corner. Figure 5.4 illustrates the expected polishing pattern.

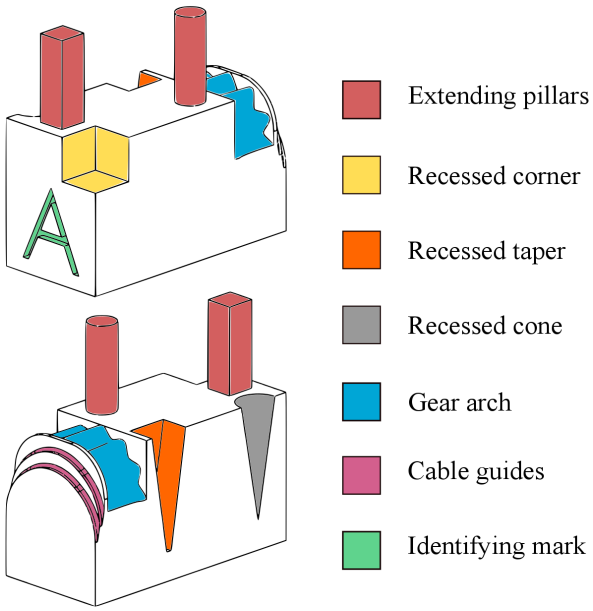

Figure 5.3: Illustration of the test piece used to investigate the effect and accessibility of mass finishing polishing. The colours mark different features used.

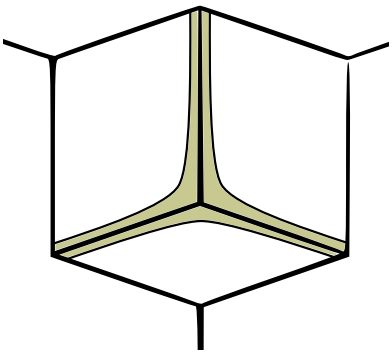

Figure 5.4: The expected polishing pattern for the recessed corner feature. Marked in olive green is the expected unpolished region. The width of of the unpolished section is to be determined after the experiment.

Recessed taper
The recessed taper (orange) feature is designed to evaluate a polishable channel for the available MFT media. The top of the taper is wider (3 mm) than the smallest available abrasive (2.8 mm) and tapers down to 0.5 mm. Expected is that the wide end of the taper walls is polishable, but towards the narrower side the walls remain unpolished (Figure 5.5).

Recessed cone

The recessed cone (grey) is, like the recessed taper, aimed at observing the effect of a channel on the polishability. We hypothesise that at the wide end, the smallest media can polish the entire cone, but this decreases towards the small end (Figure 5.5). Additionally, the area closest to the edge is expected to be the hardest to polish at smaller diameters.

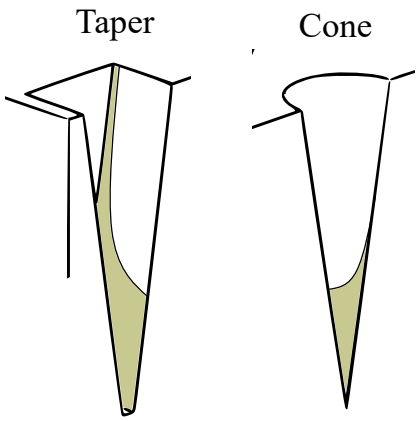

Figure 5.5: The expected polishing pattern for the recessed taper and recessed cone features. Marked in olive green is the expected unpolished region. For the taper the unpolished sections are expected to be most pronounced in the inside corner of the taper. For the recessed cone the area just underneath the top edge is expected to be the hardest to polish.

Cable guides
The cable guides (pink) feature have the function to validate a design choice of using 0.2 mm as the cable guide radius. This size stems from the original DragonFlex design. The feature will be assessed on two aspects The polishability of the internal radius is the first aspect in assessing the functionality of this cable guide after MFT (Figure 5.6). The second is how much material will be removed from the retaining edge, as this might cause the cable to slide off the edge.

Gear arch
The gear arch (blue) feature is, like the cable guides, added to validate a design. In this case the sinusoidal gear design, aimed to replace the rolling surface and spur gear arches. The gear profile is asymmetrical, with on the side closest to the recessed taper the sinusoidal function has an amplitude of 0.3 mm, which increases to 0.5 mm at the cable guide side.

5.3 Method

5.3.1 Equipment

3D Printing
The services of Materialise NV (Belgium) were employed

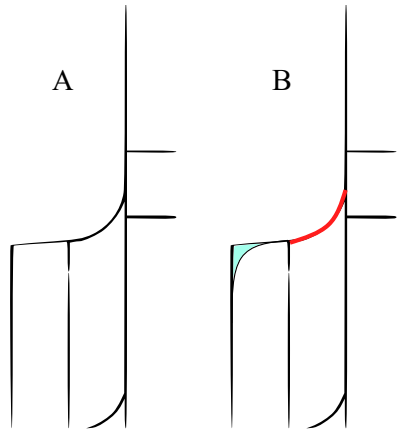

Figure 5.6: Side view of the cable guides. A) is the cable guide as drawn. B) has areas marked that are of interest after polishing. Light blue marks the material that is likely to be removed during polishing, and red marks the surface of which it is uncertain whether it can be polished.

in the 3D printing of the test pieces. Twelve test pieces were ordered, each marked with a letter, ranging from A to L. The parts were ordered using their Performance grade stainless steel. The SLM printer used was the EOS M280, using stainless steel 318L. Parts were removed using wire electrical discharge machining and received a relaxation heat treatment to reduce internal stresses, but no other surface roughness treatment. The technical drawings of the test pieces are included in Appendix XXX.

Polishing machine
The CDF polishing machine used was a CF 1x18 B produced by OTEC (Germany).

Polishing media
The polishing media used was DZS 6/6, KM 10, PM 10, ZSP 3/5, and DZP 3/3 (Figure 5.7), with liquid compound SC 5 and SC 15, all by OTEC (Germany). DZS 6/6, ZSP 3/5, and DZP 3/3 are ceramic bonded abrasive media, while KM 10 and PM 10 are plastic bonded. The manufacturer classifies the DZS 6/6 media as intense grinding and coarse finish, the KM 10 and PM 10 media are used for fine grinding to polishing, and the ZSP 3/5 and DZP 3/3 are both used for polishing.

Measurements
Dimensions have been measured using a Mitutoyo Digimatic micrometer IP65 0 - 25 mm (Japan) for height, width and length measurements of the test piece base, and using Ironside calipers to measure the base and tip width of the extending pillars. Photos were taken with a Nikon D850, and a Dino-Lite 3.0 Digital Microscope. The colouring material used was Traceelac marking

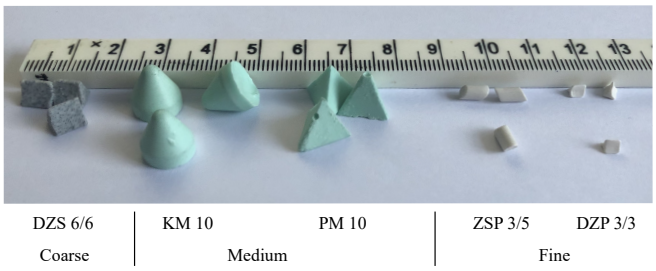

Figure 5.7: Photo of the abrasive media used, with a yard stick for scale. The media is grouped into three groups. DZS 6/6, ZSP 3/5, and DZP 3/3 are ceramic bonded abrasive media, while KM 10 and PM 10 are plastic bonded.

spray by Griffon (Bolton Adhesives, The Netherlands).

5.3.2 Experiment set-up

The approach of this experiment consisted of the following steps.

1. Taking measurements of the width of the base of the test pieces, and the base and tip of the extending pillars.
2. Taking photos of features.
3. Applying marking lacquer in thin, consistent layers until fully coated.
4. Follow polishing steps as laid out in Table 5.1, with the polishing steps as described in Table 5.2. These steps were chosen as they estimated a previously executed polishing test done by Summa Surface, a retailer of mass finishing technology machines.
5. Repeat measurements and photos.

Table 5.1: Table showing the mass finishing polishing steps each group of test pieces receives.

Step	Group 1	Group 2	Group 3	Group 4
Coarse				
Medium				
Fine				

5.4 Results

5.4.1 Overview

In Figure 5.8 photos are presented of the test pieces before and after polishing, one of each polishing group. The photos referenced in this section can be found full scale in Appendix D.

Table 5.2: Table showing the abrasive media and duration of the different mass finishing polishing steps.

Step	Media	Compound	Duration
Coarse	DZS 6/6	SC 15	120 minutes
Medium	KM 10 PM 10	SC 15	120 minutes
Fine	ZSP 3/5 DZP 3/3	SC 5	120 minutes

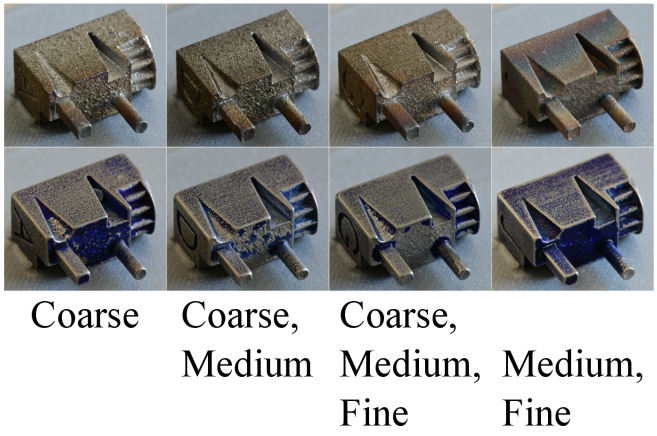

Figure 5.8: Photos of the test pieces before and after polishing, taken with a Nikon D850 digital camera. Each of the four photos is one of a different group.

5.4.2 Edge rounding

The quantification of the corner rounding was done by comparing the radii of the same edge of each test piece. The chosen edge was the vertical edge at the corner of the test piece, at the side of the recessed corner. The values are tabulated in Table 5.3, and the values prior to polishing are tabulated in Table 5.4. It should be noted that the measurements of the edge radii prior to polishing was distorted due to the particles that were partially fused all around the work pieces.

Table 5.3: Edge radii after polishing. Measured using the DinoXscope three point radius feature. The groups are tagged with a C for Coarse, M for Medium, and F for Fine.

Group	Values [mm]			Average [mm]	Deviation [mm]
1 C	0.24	0.22	0.23	0.23	0.0082
2 C-M	0.23	0.25	0.24	0.24	0.0082
3 C-M-F	0.23	0.27	0.22	0.24	0.0182
4 M-F	0.16	0.21	0.22	0.20	0.0242

Table 5.4: Edge radii prior to polishing. Measured using the DinoXscope three point radius feature.

Edge radius [mm]		
0.17	0.17	0.19
0.15	0.15	0.12
0.13	0.10	0.14
0.10	0.20	0.19

5.4.3 Material removal

Measuring the width of the base of the test piece before and after the polishing steps yielded the results presented in Figure 5.9 and Figure 5.10. The values were gathered by measuring the width of the base of the test piece before and after the polishing steps with a micrometer. The average width of the base of the test piece before polishing is 8.17 ± 0.05 mm.

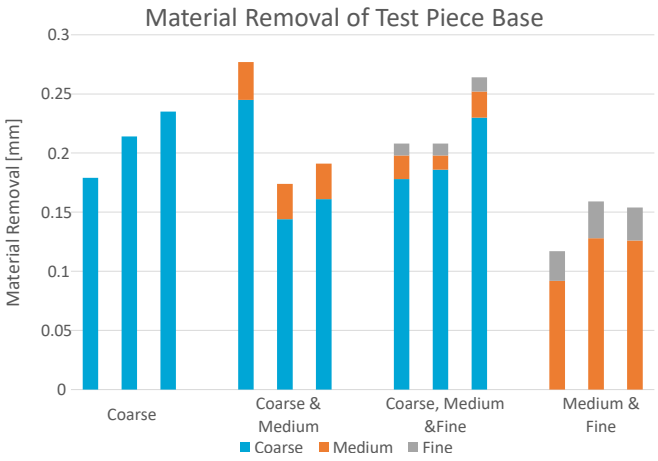

Figure 5.9: Graph of the material removal done by the mass finishing polishing steps. The test pieces are sorted by group.

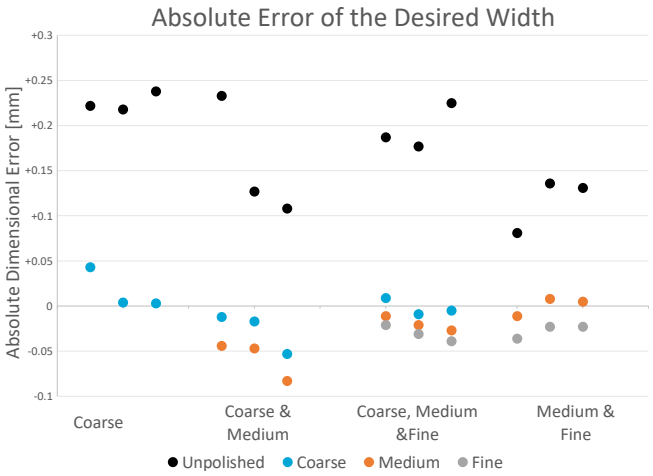

Figure 5.10: Graph of the dimensional error in the width of the test piece base. The test pieces are sorted by group.

5.4.4 Material removal distribution

The measured difference in the width of the square and round extending pillar is presented in Figure 5.11 and Figure 5.11. These have been placed on the same Y-axis scale.

The error between the measured width of the extending pillars and the desired dimension of 2 mm has been put into four graphs (Figure 5.13), all with the same Y-axis. The average error of the extending pillars in the as-built state is listed in Table 5.5.

Table 5.5: Table of average error of the as-built extending pillars.

	Average [mm]	Deviation [mm]
Square Tip	0.03	0.04
Square Bottom	0.04	0.02
Round Tip	0.04	0.03
Round Bottom	0.07	0.02

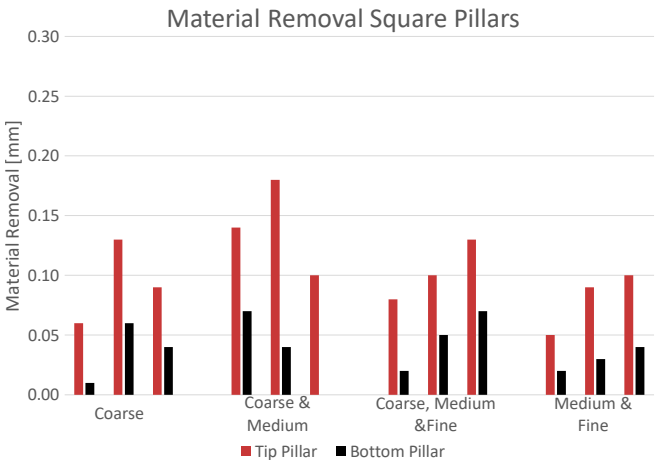

Figure 5.11: Graph of the material removed at the bottom and tip of the extending pillars. The test pieces are sorted by group.

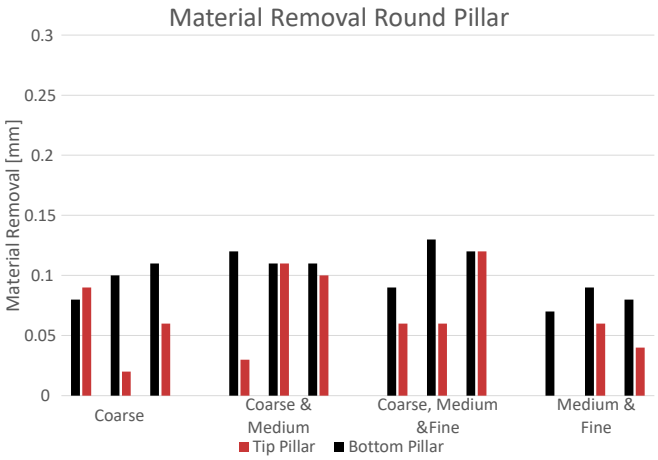

Figure 5.12: Graph of the material removed at the bottom and tip of the extending pillars. The test pieces are sorted by group.

5.4.5 Surface access

Inside corner
Close up photos of the side of the recessed cubes were taken for qualitative observations of the accessibility of MFT. Selection of one of each polishing group is shown in Figure 5.14.

Recessed taper & cone
Close up photos of the recessed taper (Figure 5.15) and cone (Figure 5.16) were taken for qualitative observations of the accessibility of mass finishing polishing.

Cable paths & gear arch
Close up photos of the cable guides and gear arch were taken for qualitative observations of the accessibility of MFT (Figure 5.17).

5.5 Interpretation of Results

5.5.1 Effect of polishing on the geometry

Material removal
Figure 5.9 shows that the coarse polishing step removes the most material, which is unsurprising. What it also shows is that the effect of a medium polishing step removes a lot more material if not preceded by a coarse step, and this effect is also present for the fine polishing step. The surface roughness of the part directly after printing is the highest, and therefore most material will be removed with the initial polishing step.

Figure 5.10 relates the material removal to the aimed part dimensions. The as-built parts were on average 0.17 $\pm$ 0.05 mm wider than desired. However, with the exception of Group 1, all test pieces were polished until below the aimed width. While the width of part can be varied to adjust for the printing inaccuracy, MFT does seem to take care of most of the inherent error.

Although strictly not a result of MFT, the extending pillars have a lower dimensional error than the width of the base prior to polishing of around 0.04 mm. It should be noted that these were measured with calipers, whereas the width of the base was measured with a micrometer. This does not fully explain the discrepancy between the width of base and the extending pillars. It could be possible that the dimensional error is cumulative with printing width, or at least until a certain width.

The dimension of the pillar tips exhibit a larger variance than the bottom of the pillar or the base. This could be a result of a larger heat affected zone, as the small pillar section does not conduct the heat away as easily as the base of the block. This larger heat affected zone causes particles farther away from the laser focus to (partially) fuse to the part. If this is the case, this would also explain why the dimensional error of the base is higher than that of the pillars, as a larger surface area (i.e. more heat required) is fused at once, causing a larger radius around the perimeter to be affected by the heat. Additionally, the particles fused outside the melt pool did not fully melt, making them easier to remove by the MFT steps.

The use of MFT in most cases seems to leave the parts smaller by a small amount ($<$ 0.05 mm). From the view point of parts fitting together, this would be sufficient for surfaces of which both mating faces are polished. For faces where only one or none of the mating faces can receive polishing, a clearance should be implemented accordingly. Although the sample size is small, an initial clearance of 0.15 mm per unpolished face should be adequate. However, the dimensional error of unpolished surfaces is a lot more variable than that of polished surfaces, therefore two polished mating faces are preferred in terms of dimensional consistency.

Material removal distribution
In Table 5.6 the relative removal at the tip is listed, with the amount removed at the tip of the extending features relative to the amount removed at the bottom. The amount of material removed at the tip is higher than that removed at the base, as was expected. The bottom of the pillar is likely shielded from the abrasive stones and therefore the amount of abrasion here is smaller. However, it does not seem that the different polishing steps have a ratio associated with them, which is likely a result of the limited sample size.

The rounding of the edges, as shown in Table 5.3, is comparable among groups 1, 2, and 3, and group 4 being around 20% lower. This is in line with the finding that the coarse step removes most material. The use of a

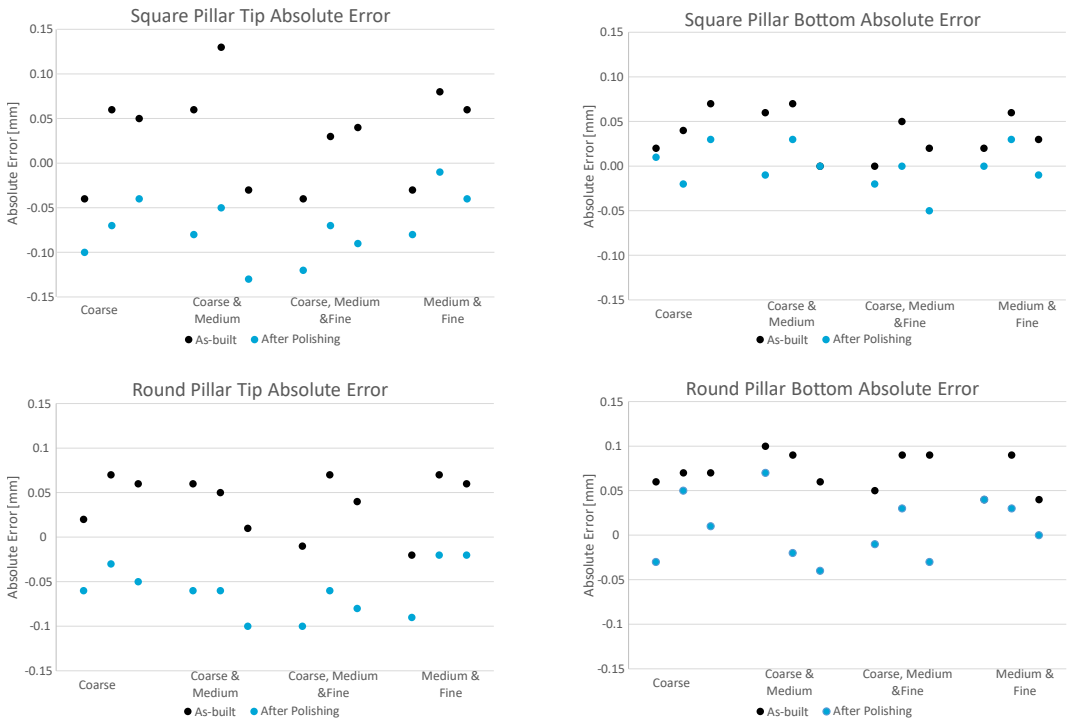

Figure 5.13: Graphs of the dimensional error in the width of the tip of the extending pillars. The test pieces are sorted by group.

coarse first step makes it difficult to end up with a part with sharply defined features, although the difference is small.

A coarse step also leaves a more uneven polishing pattern on recessed features, which is undesirable. However, as previously stated, a coarse step is useful in the removal of satellites.

5.5.2 Polishing accessibility

Recessed corner

The polishing patterns can be seen in Figure 5.14 by the absence of marking lacquer. The biggest difference between the groups is that the test pieces that underwent the coarse polishing step have a pattern that has the most pronounced polishing at the top left corner. This is the corner that is best accessible by the media. The group that only underwent the medium and fine polishing steps has a polishing pattern that is more evenly distributed.

Taking a closer look at the recessed corner after medium and fine polishing steps (group 4), a preliminary dimension for the unpolishable corner region can be set. Using the DinoXscope optical measuring tool, placing a line at 0.4 mm from the side of the recessed cube does mark the start or is already in the polished region. This preliminary dimension can be used to further the design, in particular the area where the protrusion and the gear arch meet.

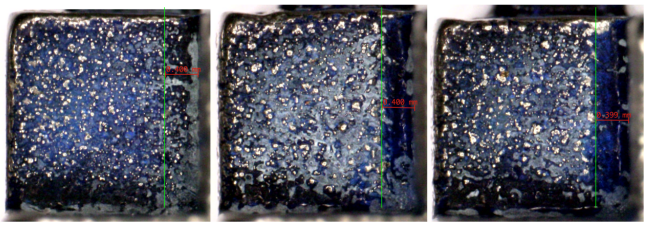

Figure 5.18: Photos of the recessed corner of group 4 (medium & fine) after polishing. Using the DinoXscope measuring tool, a green line has been placed 0.4 mm from the wall. This line is on the edge or in the polished region for all test pieces in this group.

Recessed taper & cone

In the figures showing the recessed tapers and cones (Figure 5.15 & 5.16) it is visible that both geometries do not receive full polishing on the sides. It was expected that at the wider end of these geometries the sides would receive sufficient polishing, but it appears that this is not the case.

On the other side, the bottoms of the taper and cone do receive adequate polishing, more than hypothesised. In hindsight this could have been expected, as these faces are easier for media to run past than the sides.

Particularly interesting is how the polishing pattern occurred on the recessed cone. Here it is visible that the angle of the surface with respect to the open side of the feature is dictating the polishability of a surface and that

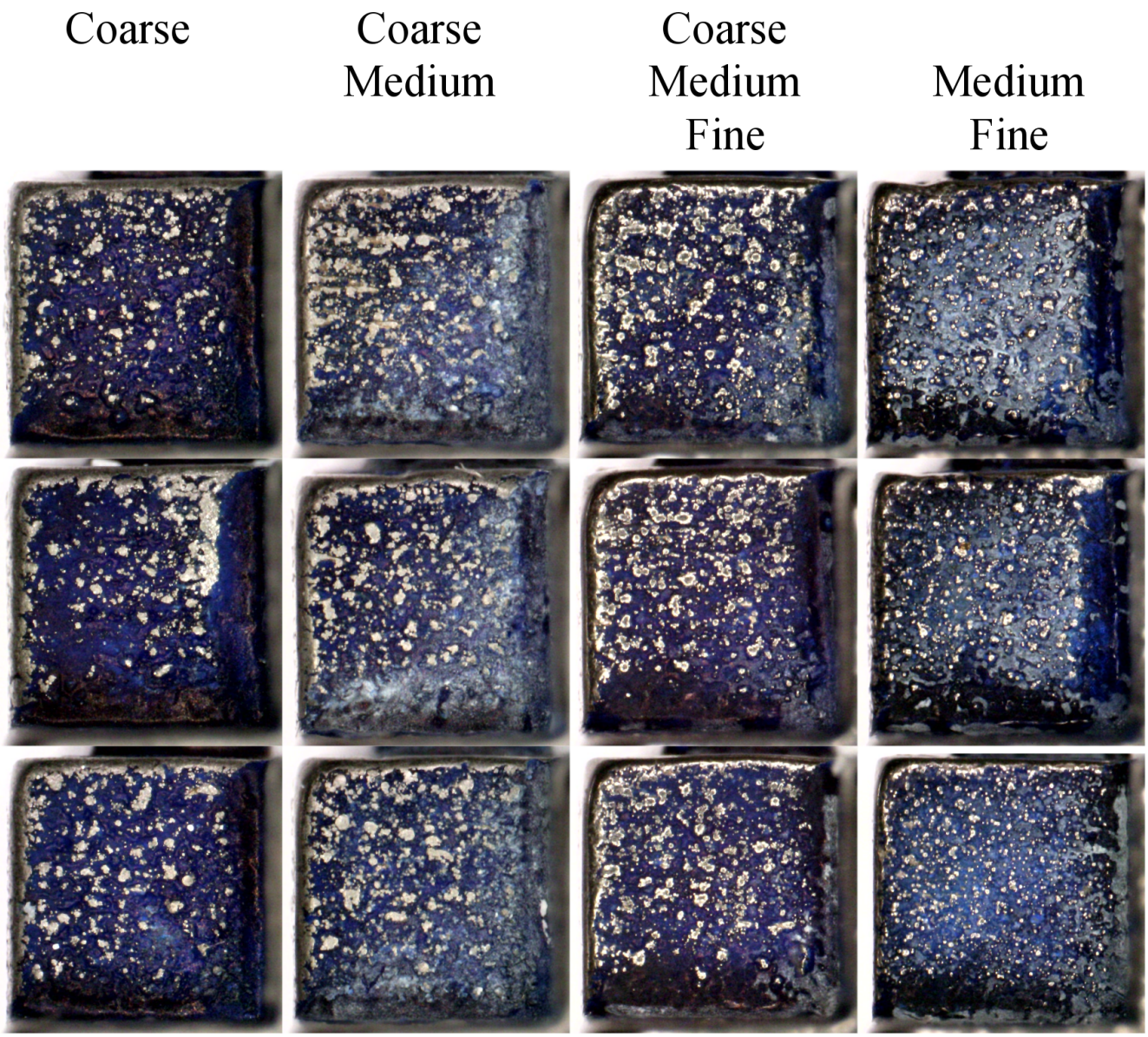

Figure 5.14: Close up photos of the recessed cube taken with a microscope. The photos are grouped by treatment group.

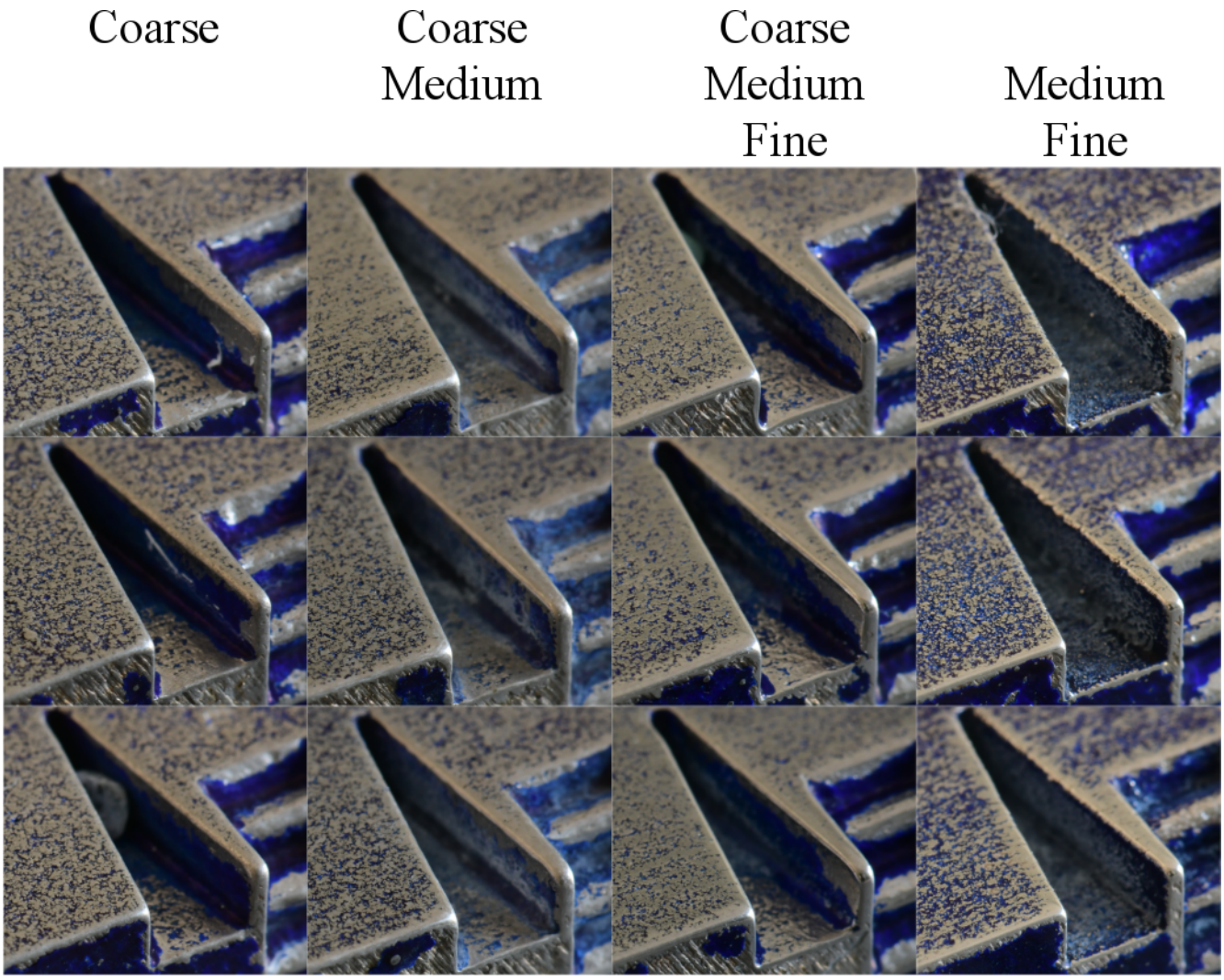

Figure 5.15: Close up photos of the recessed taper taken with a Nikon D850 digital camera. Note that a piece of abrasive media is lodged in one of the coarse photos.

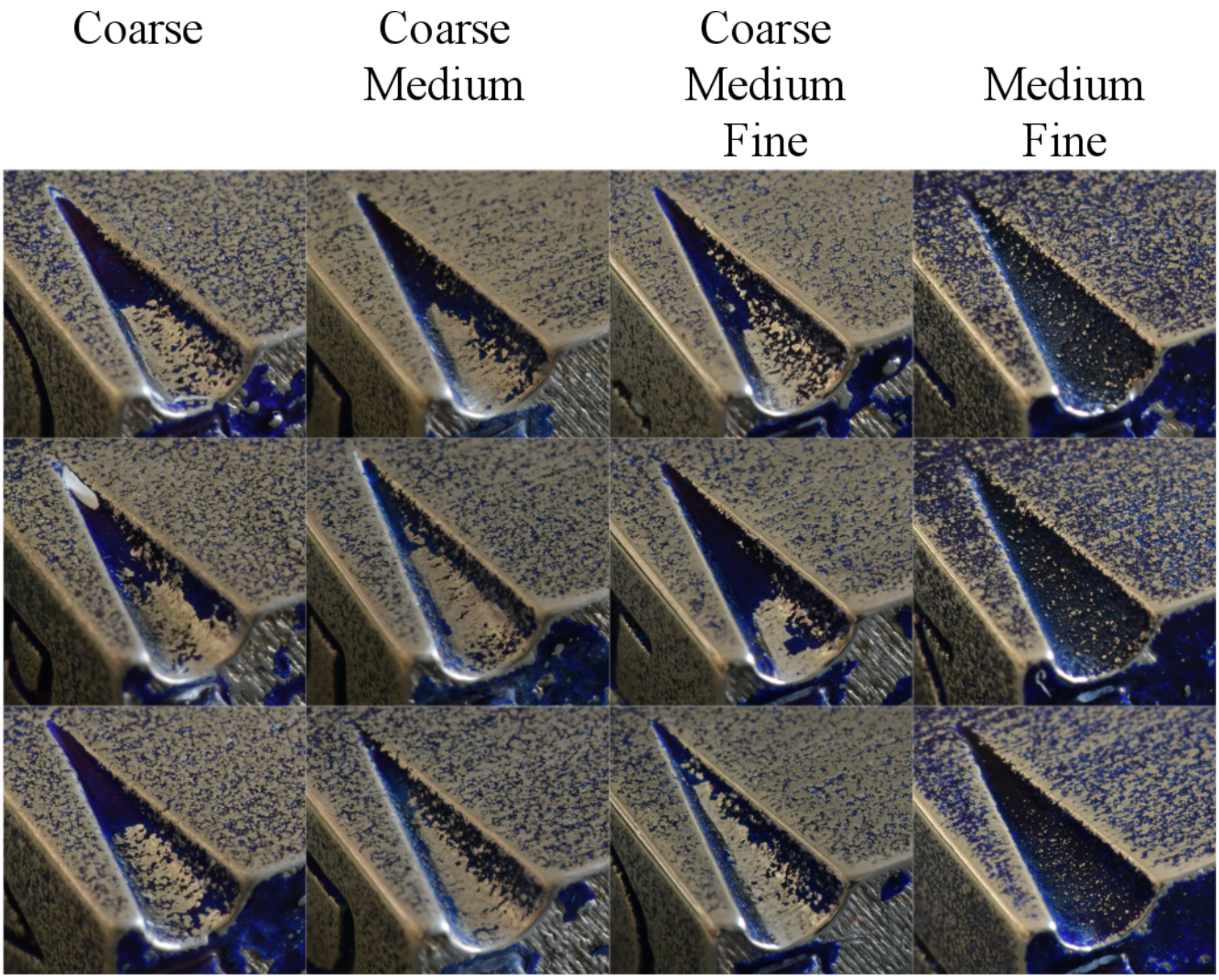

Figure 5.16: Close up photos of the recessed cone taken with a Nikon D850 digital camera. Note that a piece of abrasive media is lodged in one of the coarse photos.

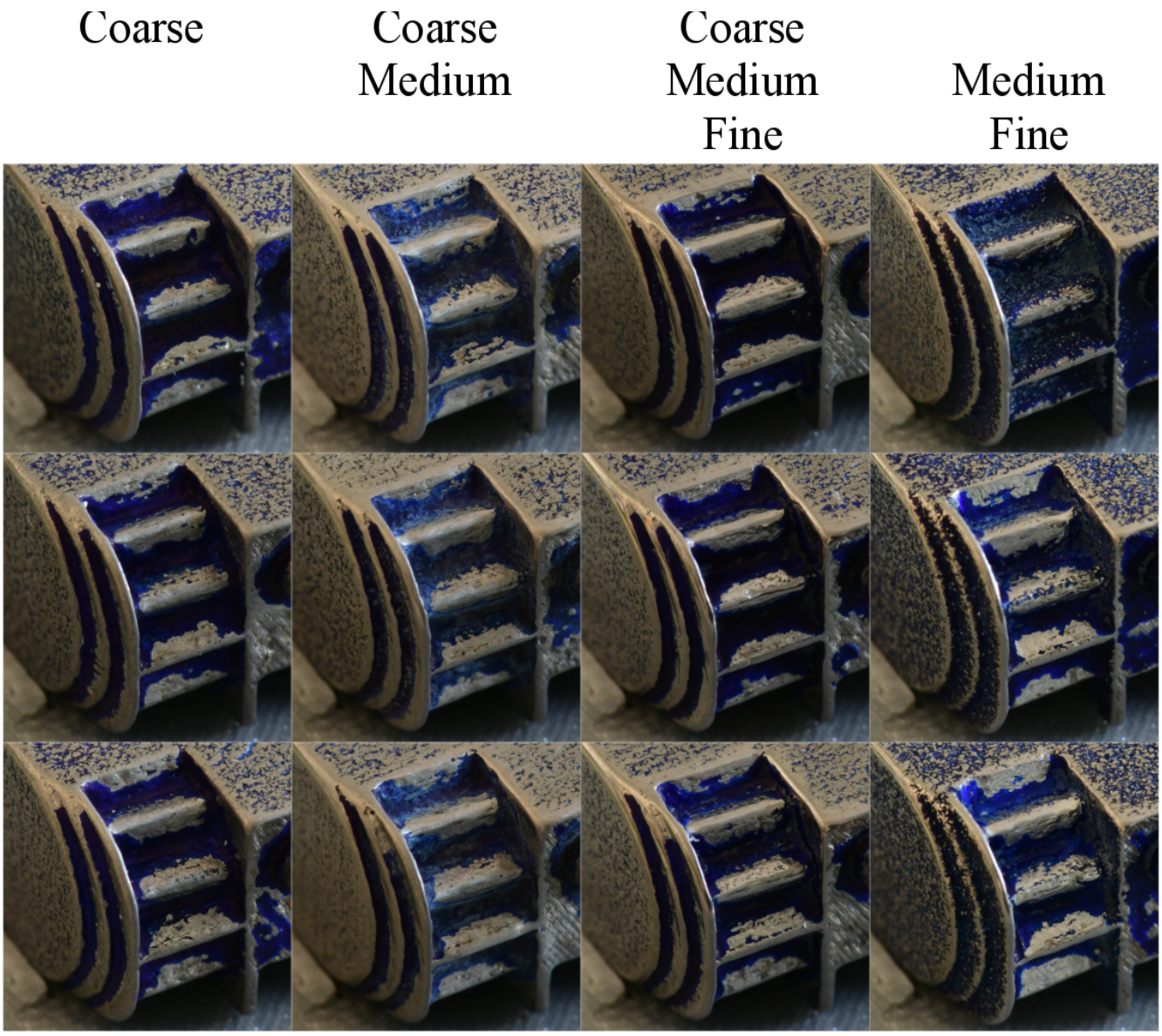

Figure 5.17: Close up photos of the cable guides and gear arch taken with a Nikon D850 digital camera.

Table 5.6: Table listing the average material removal of the tip and the base of the extending square pillar and the round pillar. In the right most column the removal at the tip relative to the removal at the base is listed. The groups are tagged with a C for Coarse, M for Medium, and F for Fine.

Square Pillar			
Group	Average Material Removal [mm]		Decrease at Tip [%]
	Tip	Base	
1 C	0.09	0.04	2.5
2 C-M	0.14	0.04	3.8
3 C-M-F	0.10	0.05	2.2
4 M-F	0.08	0.03	2.7
Round Pillar			
Group	Average Material Removal [mm]		Decrease at Tip [%]
	Tip	Base	
1 C	0.10	0.06	1.7
2 C-M	0.11	0.08	1.4
3 C-M-F	0.11	0.08	1.4
4 M-F	0.08	0.03	2.4

channel walls will receive limited polishing.

Both the recessed taper and cone have one test piece in which a piece of abrasive media has lodged itself into the feature. It does not seem that the lodged media has changed the resulting polishing pattern, possibly because it is a smaller chip from a larger abrasive stone.

Cable guides & gear arch

Zooming in on the two groups that were polished with the fine media (Figure 5.19) shows initially a similar polishing pattern in both groups on the cable guides. However, upon closer inspection the more aggressive coarse step has left group 3 more rounded over at the cable guide edges. Rounded over edges are problematic for cable retention, as it makes the cables more likely to slip out of the cable guide.

In the bottom row of the figure (group 4), a faint polishing pattern can be seen in the both the inside radius of the cable guides as the base of the gear teeth. This does indicate that to a certain degree these surface are being polished. Although top row also underwent a fine polishing step, this pattern is not visible here. This could be a result of the small sample size, or that the coarse step alters the marking lacquer in a way.

Surface satellites

Another observation that came to light is the effect of so-called satellites on surfaces of printed parts on MFT. Satellites are small beads on top of the surface that are a by-product of the SLM process. These beads are created by splatter of the melt pool, and randomly land on the surface.

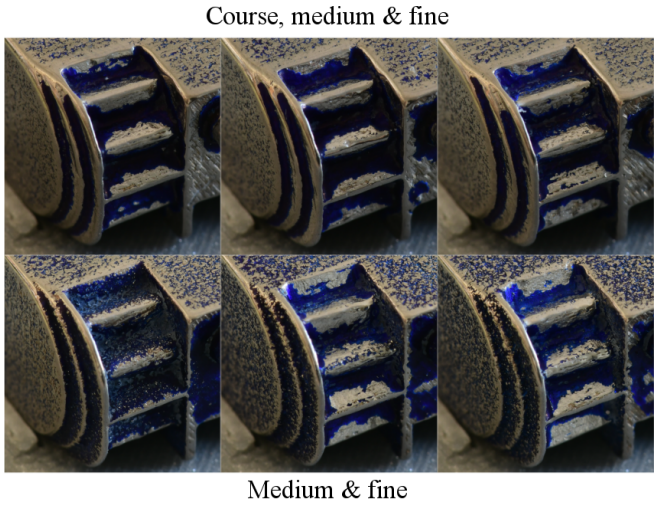

Figure 5.19: Photos of all test pieces in group 3 (coarse, medium & fine) and group 4 (medium & fine).

Figure 5.20 is a close up of the top surface of test piece H. The satellites appear to prevent the abrasive media to access the surface surrounding the satellites.

The satellites are most pronounced on surfaces face upward during printing. Since they are unavoidable, this should be taken into consideration when orienting the part. Alternatively, a coarse MFT step for longer should remove most of the satellites, but this will also be aggressive to the features of the part.

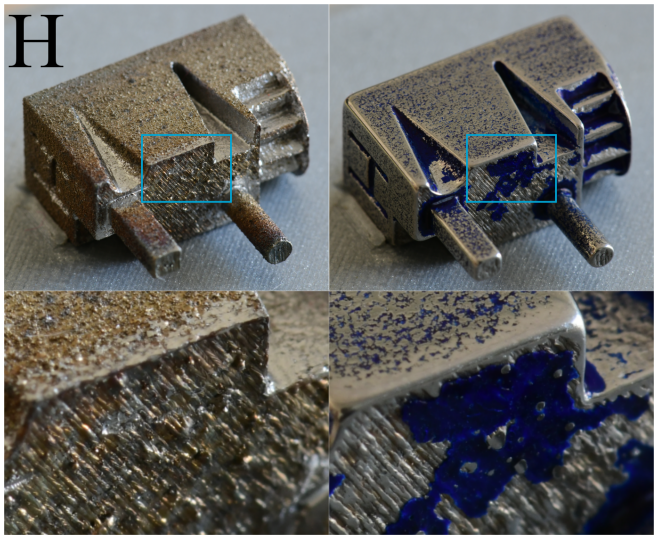

Figure 5.20: Photos of test piece H, before and after coarse, medium, and fine polishing. The zoomed in sections focus on the beads on the surface called satellites, which seem to prevent the abrasive media to access the surrounding surface.

5.5.3 Experiment evaluation

The use of the marking lacquer seems to be an effective method to evaluate MFT behaviour for surfaces. However, the application happens in a wet state, and it appears that the lacquer is drawn to inside corners of features due to surface tension. This makes it hard to distinguish between poor polishing or a thicker marking layer near inside corners. This makes the use of this specific lacquer less viable for sharp inside corners like the base of the gear arch and recessed corner.

5.5.4 Experiment impact for the design

A number of design considerations have come forward with the results of the experiment that can be applied directly to the main design of this report:

- Channels are hard to polish adequately below 3 mm. The use of channels in one piece through which sliding has to occur should be avoided. Larger channels in combination with the chosen abrasives have a greater chance of success, but are not feasible in combination with the current size constraints.
- The tapering of the pillars appears to be negligible in terms of generating a taper angle that could be used for protrusions to hold the centre body together.
- The unpolished region at the inside corner was hard to measure consistently, but the maximum radius for polishing with the fine polishing step is estimated to be around 0.4 mm. The outside corner rounding for the groups with fine polishing were measured to be 0.16 - 0.27 mm. The edge rounding will therefore not provide sufficient clearance for the edge between the gear arch and protrusion/cut-out. A clearance recess should be included here to ensure proper part assembly.
- The process of SLM leaves the parts, at least in the case of the machine used by the supplier, oversized. The use of MFT polishing both brings the dimensions of the part down to slightly under the desired dimensions, but also lowers the spread on the dimensions. This improves the consistency of the parts assembly process, and largely omits the need for additional part size tolerancing.

6 Final Design

6.1 Joint Feature

6.1.1 Overview

The joints are the most complex sections of this instrument, and consequently required the most redesign to be adapted into 3D printable and polishable components. The final design was modelled in SolidWorks (Dassault Systèmes SolidWorks Corp.). In Figure 6.1 a close up of the designed joint can be viewed. The feature dimensioning will be discussed in the following sections.

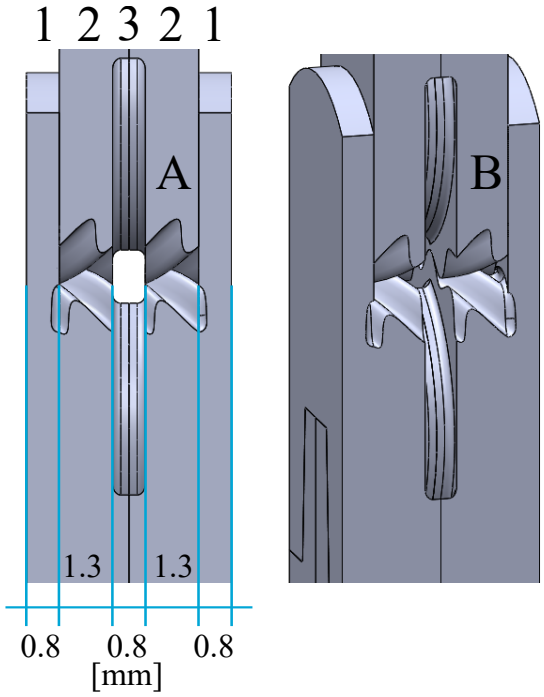

Figure 6.1: Computer 3D model of the final joint concept. A) a side view of the joint with features 1) protrusion/cut-out, 2) gear arch, and 3) cable guides. B) angled view.

6.1.2 Cable guides

The cable guides are mostly unaltered from the original DragonFlex design, with the exception of being placed on the outside of the part and the unnecessary walls removed. The each cable path has a width of 0.4 mm and an inside radius of 0.2 mm. The two cable paths together require 0.8 mm in the joint, leaving 4.2 mm for the remaining features.

The cable guide walls that remain are the walls that are on the inside of the bending cable. The bending of the cable is schematically depicted in Figure 6.2 for the full joint range of motion.

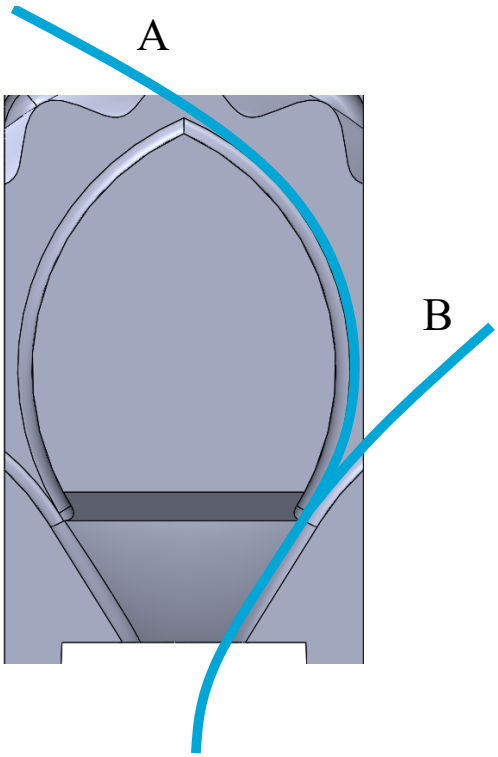

Figure 6.2: Side view of the cable path. The blue line represents the actuation cable and is presented in its two extreme positions. A) the cable when the joint is bending to the left, and B) the cable when the joint is bending to the right.

6.1.3 Protrusion & Cut-out

In Section 3.6 a print with a protrusion of 0.5 mm was found to be insufficiently thick to withstand thermal warpage, whereas a 1 mm protrusion is. The protrusion and cut-out feature occurs twice in this joint design, so the chosen thickness is also effectively doubled. It was chosen that the protrusions will have a thickness of 0.8 mm instead of 1 mm, because of space consideration. The stiffness of plates scales with the third power of the thickness, which would mean that this plate is 4 times stiffer than the 0.5 mm protrusion.

The protrusion inside face is a sliding surface, and for this reason a recess has been added at the base to ensure polishability. In Figure 6.3 a red line marks the start of this recess, which is 0.4 mm wide. This recess' function is to provide clearance for the media, so that no unpolished region remains after MFT. This dimension is chosen based of the measurement of the start of the polishing region in Section 5.5.2.

The material removal analyses showed that the dimensional error became negative after polishing. With the polished surfaces being 0.05 - 0.1 mm below their intended position after MFT, the clearance is possibly enough.

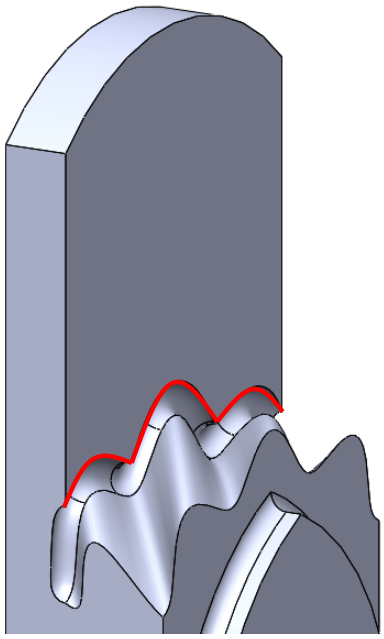

Figure 6.3: Computer 3D model of the protrusion in the centre body. The red line marks the start of the recess which is in place to give clearance during mass finishing polishing.

6.1.4 Gears

The sinusoidal gear arches are designed by wrapping a sine function around the perimeter of a circle. The circle diameter is 7.35 mm and is equal to the gear diameter of the original DragonFlex. This size is fixed due to the cable guide dimensions. The sinusoidal function was, after some iterations, chosen to have an amplitude of 0.3 mm and a frequency that fits 12 teeth on the whole circle. A lower amplitude would decrease the slope of the teeth, making the teeth prone to sliding out of engagement. Iterations with a larger amplitude showed that teeth do not engage properly anymore, as the base of the gear teeth to become too narrow. The equation was inputted parametrically into SolidWorks using the following equations:

$$Gx(t) = cos(t) * (D/2 + a * cos(t * n))$$

$$Gy(t) = sin(t) * (D/2 + a * cos(t * n))$$

These equations use the constants D for the circle diameter, a for amplitude, and n for the number of teeth.

The helical gears are rotated along the circle centre with an angle of 30°. This angle ensures that the end of one teeth coincides with the start of the next one (Figure 6.4). This ensures multiple gears are engaged at once, making the rolling motion smoother. Decreasing the number of teeth would require a steeper helical angle to do the same. This would make the base of the gears harder to polish, as the teeth are brought closer together.

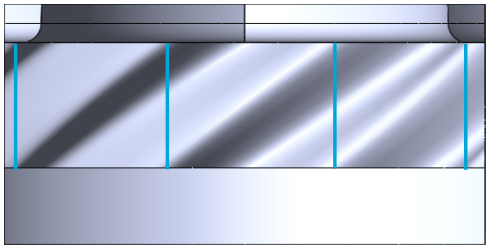

Figure 6.4: Top view of a centre body part. Marked with blue lines on the gear arch are the starts and ends of the gear teeth to illustrate the 30° rotation.

The gear arch, and also the cable guides, have been designed for a 90° joint range of motion, while the design requirements only require 60°. However, it was noticed during prototyping that due to gear teeth being sliced to a fraction the end of the range of motion became unstable. The gear arch was a feature present on a preliminary concept that was printed in metal. This preliminary print was also polished using an MFT cycle that is comparable to the cycle used in Group 4 (medium and fine abrasives) of previous chapter. The gear arch showed to be effective at constraining the tangential forces, and the rolling motion sufficiently smooth.

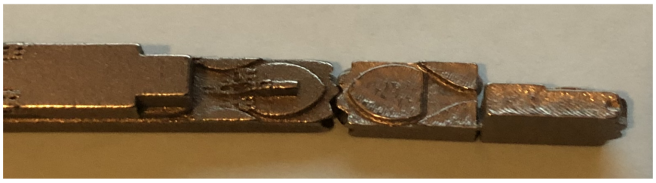

Figure 6.5: Photo of printed parts with the gear arch feature.

6.2 Instrument Components

6.2.1 Gripper

The gripper elements are designed as depicted in Figure 6.6. The elements have a section of cable guide in which the cable should be fixed. For this reason, the polishability of this section is of no consequence.

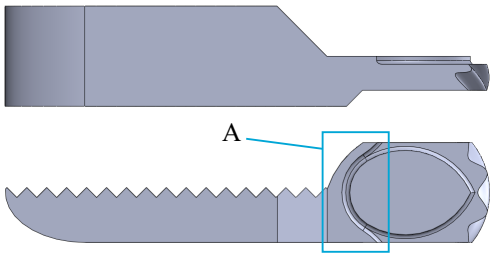

Figure 6.6: Computer 3D image of the gripper element. (A) marks a section of cable guide that is constrained from both sides.

The gripper elements are designed to be oriented at an angle of 20° between the normal vector of the base plate and the longitudinal axis of the part. Using the draft analysis function in SolidWorks areas with an overhang less than 45° are marked red and require support. In Figure 6.7 this function has been applied to a gripper element. Support would be required on the tip of the jaw and a small section of cable guide. The tip of the jaw is non functional, and the section of cable guide constitutes a small section that is likely printable without problems. The draft analysis has the sole function of identifying locations that require structural support, but does not give any information for the need for thermal support.

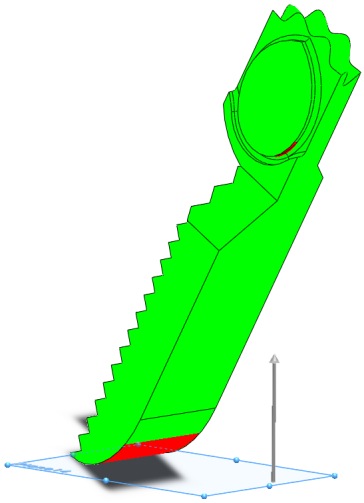

Figure 6.7: Draft analysis of the gripper element, set to 45° overhang. The green surfaces are printable unsupported while the red parts require support. The element is placed at an angle of 60° between the longitudinal axis of the part and the normal vector of the base plate.

6.2.2 Centre body

The centre body of the instrument consists of four identical parts. One of the individual parts is shown in Figure 6.8, and is a component of the centre body at the tip of the instrument. The two prongs and the recess are tapered with a 4° angle to be self-centering with assembly (Figure 6.9). The prongs and recess allow for assembly of the centre body to be in the axial direction. This is advantageous as small dimensional inaccuracies will only have the centre body become shorter or longer, rather than wider or twisted.

The prongs will have more material removed at their tips than at the base, as the extending pillars during the experiment showed. To avoid over-erosion at the tip to become problematic, the prongs are oversized at the tapered faces with the slot by 0.10 mm. This amount is more than the error for either of the pillar types in

most of the polishing groups. Additionally, the width of the recess is below the width of the width of the smallest polishing stone. This means that the sides of the recess will be underpolished, as was seen with the recessed taper. Assuming that the sides of the recess will also be larger than intended as-built, this should leave with enough material for the prongs and the recess to fit together adequately. The rougher surface of the recess walls will likely improve the interference fit of the taper.

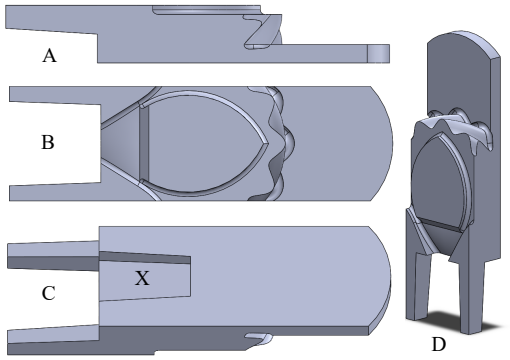

Figure 6.8: Centre body parts of the centre body at the tip. A) a side view of the part. B) front view of the part. C) angled side view with (X) marking the recess to accept and center the prongs. D) an angled view.

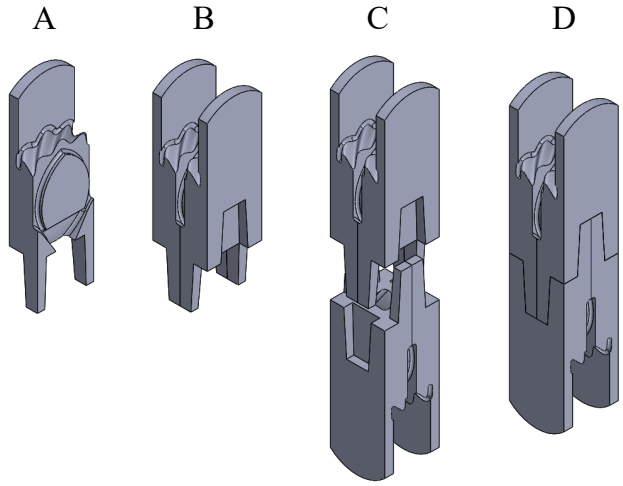

Figure 6.9: Assembly of the tip-side centre body. Two centre body parts make a pair (A to B), and two pairs rotated 90° axially make the full body (C to D).

The centre body at the handle side is similar, albeit with range of motion limiters at the sides (Figure 6.10). The range of motion is limited at 60°.

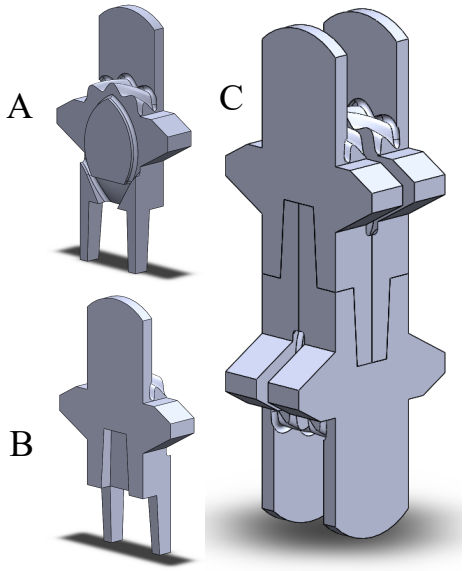

Figure 6.10: Parts of the handle-side centre body (A & B), and the assembly (C).

The centre body parts for both the handle and the tip side are designed to be printed at an angle of 45°. The draft angle analysis of SolidWorks has again been used to determine the need for support (Figure 6.11). The draft angle analysis shows that three surfaces of each body have an overhang of less than 45°. This is due to the taper angle given to the prongs and the recess. These surfaces cross the overhang threshold by 4°, which is unlikely to affect the surface roughness a lot if printed without overhang. Support is required for the edges marked in blue in Figure 6.11.

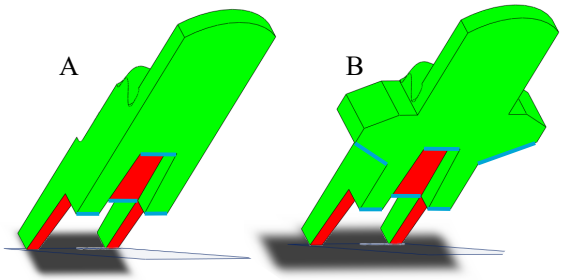

Figure 6.11: Draft analysis of the centre body parts of the tip (A) and handle (B) sides, set to 45° overhang. The green surfaces are printable unsupported while the red parts exceed the 45° threshold. The parts are placed at an angle of 45° between the longitudinal axis of the part and the normal vector of the base plate. The red surfaces exceed the threshold by 4°. Support is required on the edges marked in blue.

6.2.3 Shaft

The shaft consists of five parts; two shaft additions at the tip side, two at the handle side and the middle section

6.12. The shaft additions are similar, with the handle side having range of motion limiters added. The shaft additions fit into the middle section with square tapered pegs 6.13. The cables run along the outside of the middle section.

The shaft middle section can be made at any length, in principle only limited by the build height of the specific SLM printer used. The middle section in the figures below has a length of 30 mm, which is too short for practical use of the instrument.

The connection of the shaft additions on both sides to the shaft is based on an interference taper fit. The tapered hole is unpolishable, and will therefore be more undersized than the MFT process will remove on the tapered pegs. This should fit together without the need for additional clearances. The rough surface of the tapered hole will contribute to a tight fit, as it is will increase friction forces between the parts.

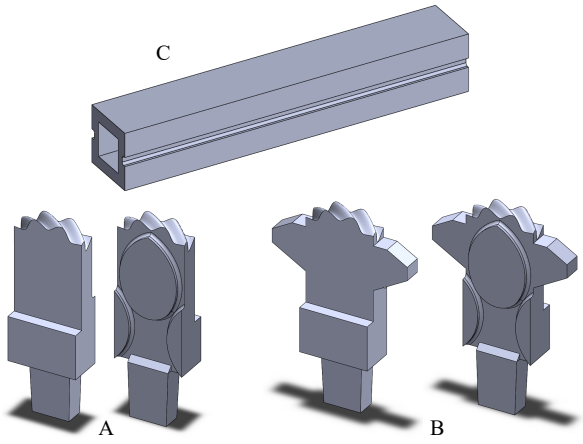

Figure 6.12: Computer 3D models of the shaft components. A) shaft addition tip, B) shaft addition handle, and C) middle section.

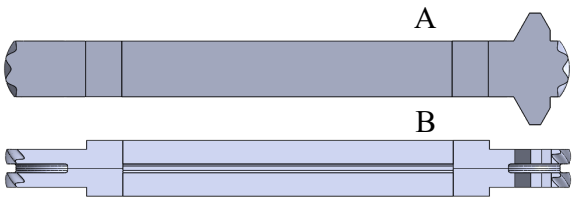

Figure 6.13: Computer 3D models of the shaft sub-assembly. A) side view, and B) front view.

The shaft addition parts should be printed on an angle of 45°, and the middle section standing (Figure 6.14). The draft angle analysis marks the tapered surfaces as being over 45°, which they do by 4°. This overhang is acceptable nonetheless. Support is required on the edges marked in blue.

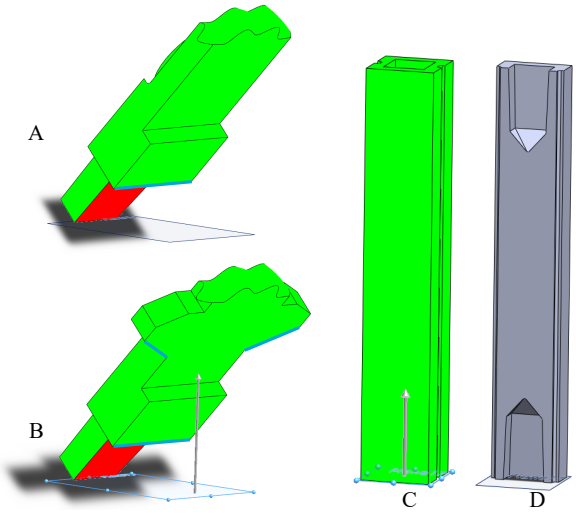

Figure 6.14: Draft analysis of the shaft parts of the shaft addition tip (A), shaft addition handle (B), and middle section (B), set to 45° overhang. The green surfaces are printable unsupported while the red parts exceed the 45° threshold. The shaft addition parts are placed at an angle of 45° between the longitudinal axis of the part and the normal vector of the base plate, the middle section is placed standing up. The red surfaces exceed the threshold by 4°. Support is required on the edges marked in blue. D) shows the middle section cut in half to show the tapered holes, which have a bottom of 50° and do not require support.

6.2.4 Handle

The handle of the instrument can be seen in Figure 6.15. The handle design is relatively straight forward, and the joint used is the same as in the gripper elements.

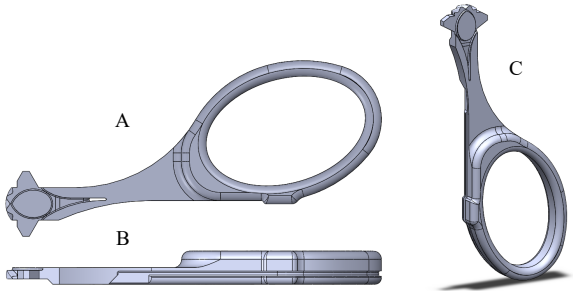

Figure 6.15: Computer 3D model of the handle. A) is a front view, B) a side view, and C) an angled view.

The handle has a cable groove that merges the two cables at the joint, and runs them around the handle (Figure 6.16). The cables are guided into the groove through a hole that is slightly off-set to the plane where the cable enter the joint. This is to ensure the cables are pulled against the cable guides to maintain position. This section is entirely unpolishable, but this is of no consequence, as the cable is stationary at this location.

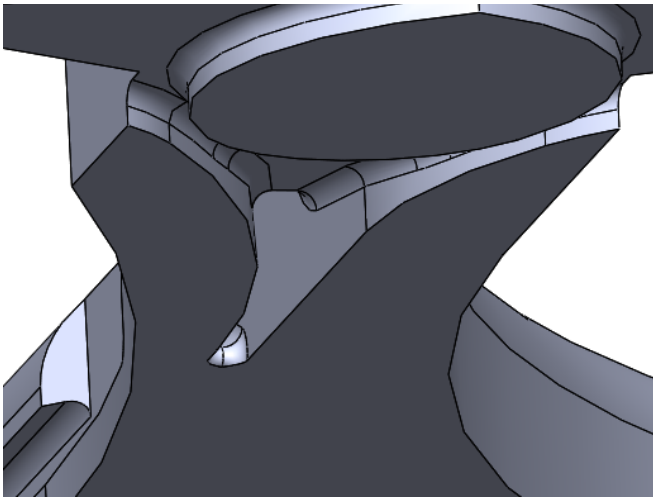

Figure 6.16: Close up of the where the two actuation cables are merged into the cable groove.

The handle is designed to be printed at an angle of 45° (Figure 6.17). The part is more difficult to support than the other parts, in part due to the double curved surfaces of the finger grips. Support on these surfaces is hard to remove, but fortunately, these surfaces are not crucial for the working of the instrument.

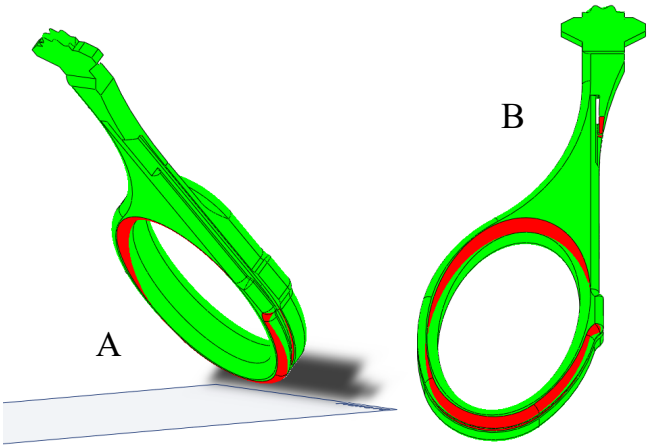

Figure 6.17: Draft analysis of the shaft parts of the handle. A) shows the handle in the printing orientation, and (B) shows the draft analysis in the building direction.The draft analysis is set to 45° overhang. The green surfaces are printable unsupported while the red parts exceed the 45° threshold. The handle is placed at an angle of 45° between the longitudinal axis of the part and the normal vector of the base plate. Support is required on the red surfaces.

6.2.5 Cables

The actuation cables are off-the-shelf 19 strand wire cables of 0.25 mm diameter. One manufacturer of these cables is Engelmann (DE).

As of now, no cable tensioning mechanism has been included in the design. Any cable tensioning mechanism should be placed in the handle, but was left outside the scope of this thesis. The actuation cables are to be glued in place onto the gripper elements.

6.3 Total Assembly

The instrument in its entirety is depicted in Figure 6.18 as a SolidWorks model. Figure 6.19 is a photo of the instrument printed on a 3:1 scale. The internal degrees of freedom of the 3D printed scale model are shown in Figure 6.20. The only part that has been modified are the handle hole sizes, as these would otherwise become comically large in the scaled version.

The scaled prototype has been assembled without using glue to hold the parts, with the exception of the cables, which demonstrates the effectiveness of the tapered interference fits. Due to the absence of a polishing step, clearance of 0.1 mm was added to all mating faces.

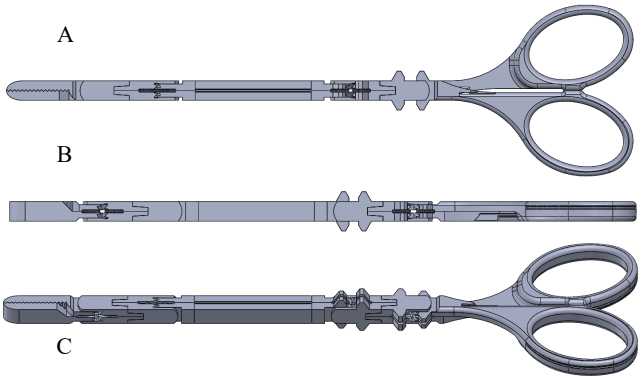

Figure 6.18: Computer 3D model of the instrument assembly. A) is a front view, B) is a side view, and C) is an angled view.

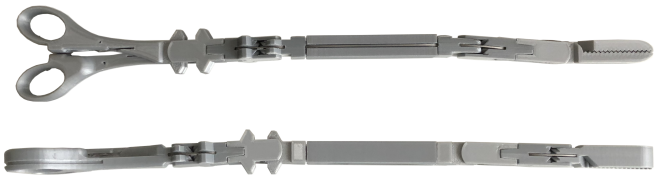

Figure 6.19: 3D printed scale model of the instrument. Printed using FDM in PLA plastic, scale 3:1. Positioned in the front (top) and side (bottom) views.

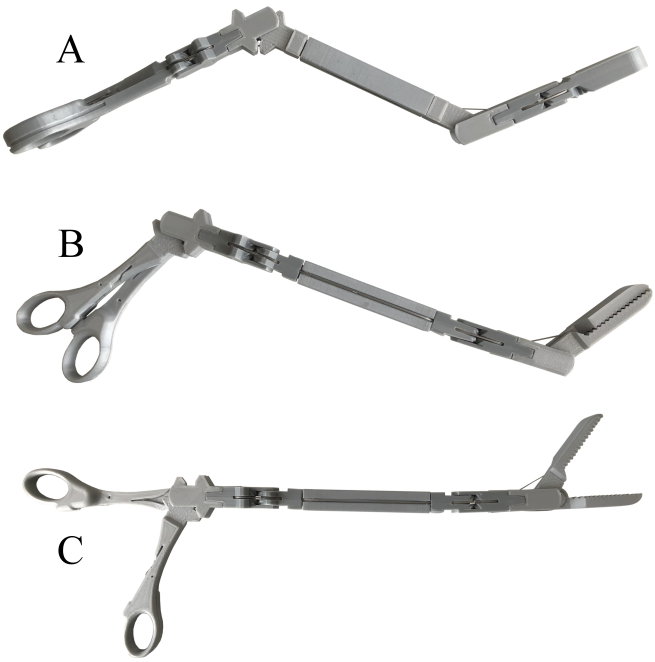

Figure 6.20: 3D printed scale model of the instrument. Printed using FDM in PLA plastic, scale 3:1. Positioned in the three degrees of freedom. A) is the proximal joint rotation, B) is the distal joint rotation, and C) is the gripper actuation.

The way the cables are looped through the instrument is visualised in Figure 6.21. The cables follow the same path on the handle and the gripper side. The instrument uses two cables, which both run up and down the instrument. Because the cables are glued to the gripper jaws, the force is transferred into the gripper jaw, effectively splitting the cable in half.

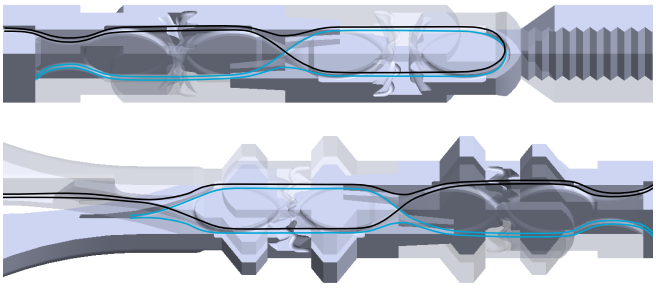

Figure 6.21: Computer 3D model of the gripper side (top) and handle side (bottom) joints of the instrument. Some components have been made transparent to show the internal cable guides. The two cables that the instrument used are the blue and black lines. The cables are glued in place in the gripper jaws and in the handle parts.

7 Discussion

7.1 Evaluation of the Design

7.1.1 Design approach

The starting point for this project was an existing 3D printable gripper. This removed much of the uncertainty of the functionality of the base design, as this was already validated. With that as a starting point, the steps taken in the design process were the following:

1. Determining general outline for the part. This includes the shape, size, and required features.
2. Eliminating recessed & internal features. This was achieved by placing these on the part's perimeter, and splitting the part along one of these features.
3. Finalising the feature dimensions, while respecting the minimal dimensions for printing and polishing.
    - No feature can be thinner than 0.5 mm.
    - The smallest polishable internal radius is 0.4 mm.
    - Channels & crevices smaller than the smallest available media will hardly be polished.
4. Determine which faces require low surface roughness. These include sliding and wear surfaces.
5. Choose printing orientation.
    - Surfaces facing up do not require support material, this is favourable for low roughness surfaces
    - Surfaces facing down that do require a low surface roughness should have an angle with the building direction lower than 45°
6. Allocate vertices and flat surfaces for support locations. Apply chamfers to eliminate overhang if necessary.

During the design of the structure and components, the result of going back and forth between step 1 and 2 was conscious placement of features and the consequence for the manufacturing process. The application of specific design dimensions is only worthwhile after that. The addition of a subsequent step in this process often required the previous steps to be reconsidered as to allow the next step to be added. This is not in any way new for a design process, but with a focus on the combination of SLM and MFT.

The benefit of 3D printing to produce parts that house many features without the associated additional machining costs has been used to counteract the short-comings

of MFT. In particular the poor accessibility of the polishing media into internal features by splitting components, while also providing the features to combine the components again after polishing.

This design has an intrinsic benefit compared to other laparoscopic grippers when it comes to being produced with SLM and MFT. The size of the parts and components is of the same order of magnitude. In particular the absence of small fastener rings or pins, or standalone axles is advantageous for both printing and polishing. The components in this design have a higher shape-complexity than most machined parts, due to having both their functional features and connecting features in one part.

7.1.2 Component splitting

One component of the design process for designing an instrument suitable for both printing and polishing was to find the largest producible part component by splitting the parts. Splitting along the cable guides removed the need for printing holes, which are both hard to print accurately and impossible to polish. This also opened up the option to orientate each component individually during printing, gaining control over which surfaces were facing up and support location. This is advantageous for the surface quality, as surfaces facing down have a much poorer surface quality.

Although 3D printing has the potential to produce a part as one, the part splitting had many advantages for both the printability and the polishability of the parts. In this design, it was opted to split parts into equally sized components. This was chosen so any production inaccuracies were divided over the components in form of lengthening or shortening of the part, as described in Section 6.2.

The component splitting is a tool that can be used for other designs, too. As described, its effective at eliminating small internal structures. However, it is limited by only creating two additional outside surfaces per split. As the parts need to be rejoined into the final part, increasing the number of splits also increases the required number of aligning and retaining features.

7.1.3 Reconnecting the cable guides

Aside from increasing the number of parts, splitting the components did bring one potential new issue to the table. Having split the parts along the cable guides requires the cable guides to be made whole again during assembly. Because the MFT process leaves the cable guide edges rounded over, there is a possibility of cables wedging themselves into the space between the mating faces. This will only become apparent after producing the instrument in its entirety, but two solutions if this is the case are theorised.

The first revolves around counteracting the effect of MFT on that specific edge, by creating artificial burrs. MFT are suited for polishing a wide variety of shapes, but are also used to deburr and round off edges left from other production techniques. While this is often desirable, it possibly rounds off the small features. In the handbook by Gillespie, a figure is presented which relates the burr thickness and height, and edge radius (Figure 7.1). With this graph an artificial burr or ridge can be designed to counteract the chamfering effect of a mass finishing technique. The exact burr dimensions will depend on the MFT process settings and material, but the graph offers quantitative insight into the relation between the available parameters. The rate at which material is removed is depending on many factors and can best be experimentally quantified [41].

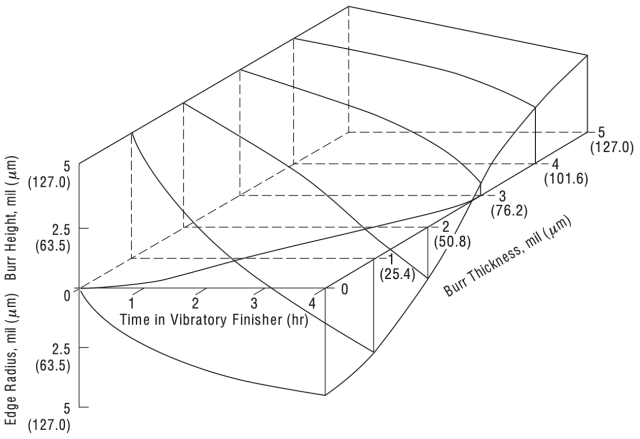

Figure 7.1: Relation between burr thickness, burr height, and edge radius. Taken from [41].

The measured edge rounding in Section 5.4.2 were between 0.20 mm and 0.24 mm on average. This is beyond what the graph in Figure 7.1 shows, which suggests that the effect of the polishing in the experiments is beyond the limit of the X-axis marking time in hours. The total polishing time during the experiments is 6 hours, which does indeed exceed this table. This would mark the base line for the rounding of an unburred edge. Estimating an extrapolation would indicate a burr thickness of around 0.08 - 0.10 mm and around 0.10 mm high. These dimensions would seem as a reasonable starting point for this approach. Figure 7.2 shows two illustrations of burr directions, both with different rationales. It has to be noted that the curves of Figure 7.1 are likely measured with different abrasives and machine settings, but the curves as a whole do offer a reasonable starting point for this approach.

The artificial burrs will not result in a sharp right angle

corner, but are meant to offset and decrease the rounding that results from MFT. Sharp corners are not the end goal in this case, but ensuring cable retainment in the cable guide.

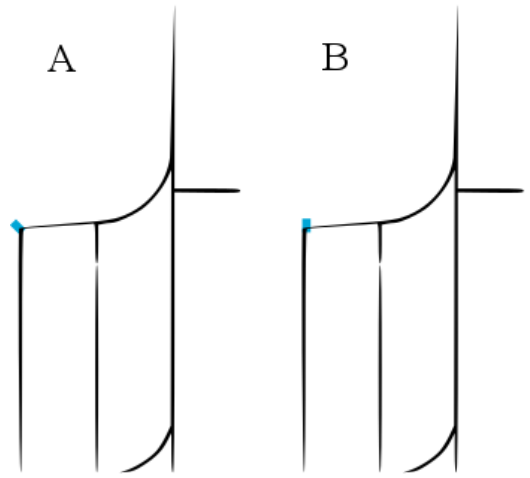

Figure 7.2: Two suggestions for the location of the burr. A) here the burr is angled at 45°, which would be the direction that is abraded most heavily. B) is a burr that is in line with the mating face, this would limit the possible interference the burr has with creating a smooth mating face. Both burrs would run along the cable guide and are sacrificed during the mass finishing polishing process.

The second option would be splitting the part not in the centre of the cable guide, but at the side of the guide or in a zigzag pattern. At the side of the cable guide, against the wall, the cables would be prevented from slipping into crevice by the wall. This could be further supported by a recess in the wall at that side. Splitting the cable guide in a zigzag pattern stops the cable and the crevice from lining up, eliminating the chance of the cable slipping.

7.1.4 Choosing a polishing cycle

The polishing patterns showed that the combination of a medium and fine step had a more even distribution of polishing than when a coarse step was included. It would seem that excluding the use of large ($>$ 6 mm) coarse polishing stones is advisable for the polishing of fine mechanical instruments. The range of available media for this research was limited by the available media at DEMO and what their machine could accept. OTEC, the supplier of the media, has a wider range of media sizes available. For a smoother surface, additional polishing steps are required. Whether just adding subsequent, finer steps to the chosen polishing steps of this project is sufficient is unlikely. In particular the surfaces in line with the building direction have a pitted texture, which for a mirror polish have to be ground away. The depth of these pits after polishing is unknown, but a preceding, coarser polishing cycle has to be added to remove enough material to obtain a smooth surface.

The combination of SLM and MFT has shown good promise to work in tandem. In Section 5.4.3 it is reported that MFT brought the dimensional error from well above (0.17 ± 0.05 mm) the desired width to just under (<0.05 mm). The final dimensions for the Group 4 (medium & fine) were 0.01 - 0.04 mm below the dimension as drawn. For the sliding surfaces of the protrusions and cut-outs this would be equivalent to an H7/f8 engineering fit [11]. This engineering fit is meant for rotating axles in holes, where this specific engineering fit is a close running fit. A close running fit is used when dealing small mechanical loads and moderate speeds.

Consistency between polishing batches is hard to predict, because the instrument components and the smallest available polishing media are comparable in size. The state of the polishing media is of importance for the material removal rate and media accessibility. Both are lower for dull media compared to new. Research into ceramic abrasives wear by Uhlman & Eulitz [53] showed that the strongest decline of media roughness occurred in the first 30 hours, and cutting performance decreasing over the first 90 hours. After 90 hours a steady state was reached. This makes consistent polishing between batches before 90 hours difficult. It would seem sensible to evaluate the polishing of the instrument by reasonably worn media, as new media for each batch is not realistic. Reasonably worn media could be 30 hours old or even 90 hours. The media used in this project was fresh from the supplier, as to reduce the number of variables.

The surface roughness of 3D printed parts after an MFT treatment has been extensively discussed in literature. The focus of this work is in the interaction between polishing and geometry. The final surface roughness of the work pieces has not been measured in this experiment.

7.2 Instrument Finalisation & Optimisation

7.2.1 Cable fixation in the handle

Cable fixation has been left unaddressed in the handle design. In the DragonFlex a tensioning system is employed to grant continuous access to change the length of the cable. This system is shown in Figure 7.3, and could be copied into the new design.

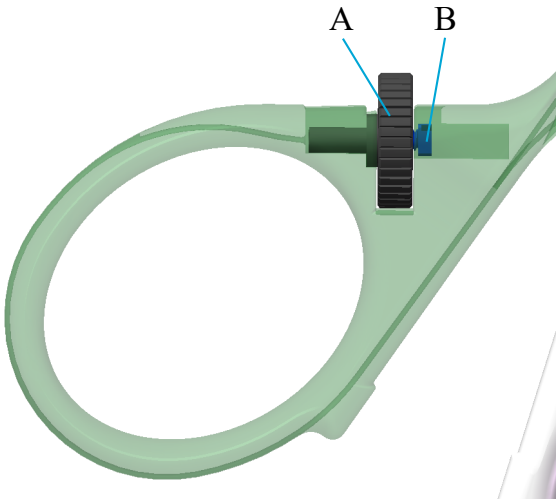

Figure 7.3: Computer 3D model of a version of the DragonFlex' tensioning system. It consist of two machined parts embedded in the handle: a nut with a gnurled adjustment wheel (A) and a bolt with a square head (B) in which the cable is glued into. The cable wraps around the handle hole into the tensioning system.

A tensioning system like Figure 7.3 in the new design would allow allow for partial disassembly. The cable would be glued to the tensioning bolts and gripper jaw, but all other components could be disassembled. These components are custom made for this instrument, but a plethora of off-the-shelf cable tensioners exist and can be incorporated into the design.

However, from the perspective of designing a surgical instrument, the question can be asked whether disassembly is necessary if a further developed instrument would be single use. If that is the case, a simpler solution would be to glue the cable directly to the handle, possibly in the cable groove. The cables can be tensioned by an external jig, glued in position, and then trimmed to length. The jig can be reused to assemble other instruments, which would lower the complexity of actual instrument.

7.2.2 Optimisation for the range of motion

In Section 6.1.4 it is explained that the gear radius is designed for ±90° range of motion, but limited at ±60°. The reason for this is such that at the limits of the range of motion whole gear teeth are engaged, and not a fractional gear tooth. The original DragonFlex design avoids this by not slicing the last gear tooth, but this does conflict with the design requirement of 5 x 5 mm cross sectional area. The width is exceeded by 0.65 mm in the DragonFlex design (Figure 7.4). It can be argued for that this relative small amount would still be acceptable. However, for the sinusoidal gear profile, which uses fewer teeth and thus larger teeth, an extending tooth would exceed the requirement by an unacceptable amount.

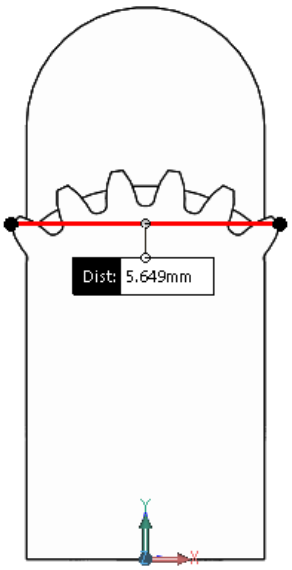

Figure 7.4: Measured width of the extending gear teeth of the DragonFlex design. The teeth distance between the extreme points is 5.65 mm.

The possible range of motion of ±90° for the gear arch can be lowered in the future. This would increase the necessary bending radius of the cables. A larger bending radius increases the lifespan of the cables. Designing the gear arch and cable guides for ±60° range of motion would not be feasible, as this requires a fractional gear tooth again to obtain the ±60° joint range of motion. The possible range of motion of the gear arch should be larger than that of the joint, so that no fractional teeth have to engage.

7.3 Evaluation of Polishing Experiment

7.3.1 Use of marking lacquer

Visualisation of polishing patterns using marking lacquer is a novel approach to further understanding the details of MFT processes. It is a simple and inexpensive method to observe differences in polishing compatibility for different geometries. The MFT literature has been primarily focused on the effectiveness of MFT to reduce surface roughness, which has been well-documented for many printable alloys. However, due to the stochastic nature of the process, these surface roughness values can not be applied to the all surfaces of a part. This is where this different test fills a gap.

As already touched upon in Section 5.5.3, the marking lacquer did leave a thicker layer in inside corners and the base of the gear teeth. A different marking material can be used for a more even marking layer. An alternative to the sprayable marking lacquer used in the experiment can be machinist layout fluid, which is applied by brush

or submersion. If the surface tension is the cause of the lacquer pulling into the corners, machinist layout fluid can perhaps be diluted with a solvent.

7.3.2 Quantification of results

The method of marking lacquer to visualise the polishing patterns is qualitative in nature. If these results could be quantified, it would improve the usefulness of experiments like these. Ideally, the results could be coupled to material removal or surface roughness to provide direct values for designing instruments manufactured with PBF.

The marking lacquer seemed to have seeped into surface roughness left by PBF on the sides of the test pieces. After polishing the blue marking lacquer only remained in the crevices on the surface. MFT removes the peaks of the surface first, and then gradually removes more material until no crevices remain. If the aim of polishing is not a fully smooth surface, these crevices will be present after polishing, still filled with marking lacquer. The fraction of blue surface area of a surface can possibly be related to an amount of material removed from that surface. This would make visual evaluation of the material removal distribution possible, revealing which areas have material removed above nominal, and more importantly, an estimation of how much more. A similar approach could be applied to the surface roughness.

This would require a large sample size of surfaces, in many different surface orientations. However, if a model like that could be built, it would allow to fine-tune the MFT production process for small mechanical instruments of varying geometries. Visual measuring in this way would make inspection of normally unreachable surfaces possible.

7.3.3 Impact on design process

The use of generalised geometries to investigate the interaction of the polishing with the geometry allowed to start designing the instrument components from a known order of magnitude for dimensions. This reduced how much had to be relied on educated guesses about the polishing accessibility based on the smallest available media. For example, the dimensions of the relief where the protrusion plate and the gear arch meet is a direct result of experimental results.

Due to logistical issues prompted by a global event, an iterative approach to finalise the specific feature dimensions was unfeasible. The MFT experiment results in the form of polishing patterns and geometrical changes did allow to design the parts with a good starting point for the features' dimensions. The final validation of these dimensions has not yet been performed for the same reason that an iterative approach was problematic.

8 Conclusion & Recommendations

This project's main goal was to design laparoscopic grippers that can be manufactured using SLM and MFT. This was approached by formulating and validating design considerations for both techniques and applying these to the DragonFlex laparoscopic gripper.

The subsequent step to this project is printing and polishing the instrument in its entirety. This would validate the design as a whole, which unfortunately has not been possible to include. Now, a set of partial validations, in the form of experiments, lay as the foundation for the design of a 3D printable, metal laparoscopic gripper that can be polished using MFT. A novel method of visualising the polishing patterns using marking lacquer was developed. This method was used to quantify the polishing media accessibility to inside corners, channels and gear teeth.

The instrument design consists of 17 components, which is six more than the DragonFlex design. Parts were split to eliminate the holes for actuation cables, and accommodate cut-outs, as both of are both unprintable or unpolishable. These features were placed on the outside of a part, as to enable polishing access. Each of the 17 components has been designed to be 3D printable with minimal support, and all geometries that require polishing abide by the guidelines experimentally validated. A new gear tooth profile based on the sine function was implemented to replace the involute profile that proved hard to print and polish. The sinusoidal gear arch has a shallow tooth profile, which makes the base of the teeth accessible for polishing abrasives. To ensure a smooth rolling trajectory, the teeth were designed to be helical, so to have multiple gear teeth engaged at all time.

Each of the components that permanently mate with other components are linked by tapered interference fits. The choice for the tapered approach limits the need for high dimensional precision. Because of the taper connection, any misalignment exhibits itself by slightly longer or shorter parts, as opposed to twist or gaps.

The mechanical stability of the design has been validated by a 3:1 scale model. The polishability of the features is partially verified with the observed polishing patterns during the experiment. The experiment showed a poor polishability for channels, which were removed from the design. The unpolished area around inside corners was estimated to be around 0.4 mm, which has been absorbed into the design in a form of a recess at the interface between the gears and protrusions. This ensures that the gears can engage fully. Altogether leaves that to conclude that the proposed design is suitable to be manufactured by SLM and MFT.

For future research an elaboration on the visualisa-

tion technique used in this research could progress this technique into a helpful tool in a designer's toolbox. This elaboration can be in the form of matching the remaining fraction of marking lacquer on a surface area to quantitative surface roughness or material removal values. Being able to correlate the fraction of marking lacquer to these values would be a relatively quick and inexpensive method to obtain an initial reading on the effect of the mechanical polishing. This would be particularly beneficial for recessed or curved surfaces, from which obtaining the surface roughness value is difficult.

The polishing cycle duration and abrasive media used in this research were based off a previous polishing experiment. The use of coarse abrasive media (DZS 6/6) showed to be ineffective at polishing the finer geometries, while contributing to the edge rounding and feature definition loss. Variation of the smaller abrasive media (ZSP 3/5 and DZP 3/3) with other finer media, or increasing the polishing duration of these steps was not included in this research. In future research it would be advisable to explore the limits of mass finishing techniques in terms of small geometry access.

References

[1] A. A.F.A. Veenhof, M. S. Vlug, M. H.G.M. Van Der Pas, C. Sietses, D. L. Van Der Peet, E. S.M. De Lange-De Klerk, H. J. Bonjer, W. A. Bemelman, and M. A. Cuesta. Surgical stress response and postoperative immune function after laparoscopy or open surgery with fast track or standard perioperative care: A randomized trial. *Annals of Surgery*, 255(2):216–221, 2012. ISSN 00034932. doi: 10.1097/SLA.0b013e31824336e2.

[2] William E Jr Kelley. The Evolution of Laparoscopy and the Revolution in Surgery in the Decade of the 1990s. *JSLS*, 12(4):351–357, 2008.

[3] Armin Schneider and Hubertus Feussner. Operative (Surgical) Laparoscopy. *Biomedical Engineering in Gastrointestinal Surgery*, pages 269–327, 2017. doi: 10.1016/b978-0-12-803230-5.00007-5.

[4] Filip Jelínek and Paul Breedveld. Design for Additive Manufacture of Fine Medical Instrumentation-DragonFlex Case Study. *Journal of Mechanical Design, Transactions of the ASME*, 137(11):1–7, 2015. ISSN 10500472. doi: 10.1115/1.4030997.

[5] ASTM International. StandardTerminology for Additive Manufacturing Technologies. *Standard Terminology for Additive Manufacturing – General Principles – Terminology*, ISO/ASTM 5:2–4, 2015. ISSN 1882-675X. doi: 10.1520/F2792-12A.2. URL `http://compass.astm.org/EDIT/html_annot.cgi?ISOASTM52900+15`.

[6] Andreas Kirchheim, Hans-jörg Dennig, and Livia Zumofen. Industrializing Additive Manufacturing - Proceedings of Additive Manufacturing in Products and Applications - AMPA2017. *Industrializing Additive Manufacturing - Proceedings of Additive Manufacturing in Products and Applications - AMPA2017*, (January), 2018. doi: 10.1007/978-3-319-66866-6.

[7] Carl Schubert, Mark C. Van Langeveld, and Larry A. Donoso. Innovations in 3D printing: A 3D overview from optics to organs. *British Journal of Ophthalmology*, 98(2):159–161, 2014. ISSN 00071161. doi: 10.1136/bjophthalmol-2013-304446.

[8] Helena Dodziuk. Applications of 3D printing in healthcare. *Kardiochirurgia i Torakochirurgia Polska*, 13(3):283–293, 2016. ISSN 17315530. doi: 10.5114/kitp.2016.62625.

[9] Costanza Culmone, Gerwin Smit, and Paul Breedveld. Additive manufacturing of medical instruments: A state-of-the-art review. *Additive Manufacturing*, 27(March):461–473, 2019. ISSN 22148604. doi: 10.1016/j.addma.2019.03.015. URL `https://doi.org/10.1016/j.addma.2019.03.015`.

[10] Ian Gibson, David Rosen, and Brent Stucker. *Additive Manufacturing Technologies*, volume 9. Springer US, 2nd edition, 2014. ISBN 9781493921126. doi: 10.2495/SDP-V9-N5-658-668.

[11] H Wittel, D Muhs, D Jannasch, and J Vossiek. *Roloff/Matek Machineonderdelen Tabellenboek*. SDU Uitgevers, 5th edition, 2013.

[12] Formlabs. Material Data Sheet Grey Pro, 2018. URL `https://formlabs.com/media/upload/Technical_Data_Sheet_EN_-_Grey_Pro.pdf`.

[13] Tuan D. Ngo, Alireza Kashani, Gabriele Imbalzano, Kate T.Q. Nguyen, and David Hui. Additive manufacturing (3D printing): A review of materials, methods, applications and challenges. *Composites Part B: Engineering*, 143(December 2017):172–196, 2018. ISSN 13598368. doi: 10.1016/j.compositesb.2018.02.012. URL `https://doi.org/10.1016/j.compositesb.2018.02.012`.

[14] M. Hanief and M. F. Wani. Effect of surface roughness on wear rate during running-in of En31-steel: Model and experimental validation. *Materials Letters*, 176:91–93, 2016. ISSN 18734979. doi: 10.1016/j.matlet.2016.04.087. URL `http://dx.doi.org/10.1016/j.matlet.2016.04.087`.

[15] Filip Jelínek, Giada Gerboni, Paul W.J. Henselmans, Rob Pessers, and Paul Breedveld. Attaining high bending stiffness by full actuation in steerable minimally invasive surgical instruments. *Minimally Invasive Therapy and Allied Technologies*, 24(2):77–85, 2015. ISSN 13652931. doi: 10.3109/13645706.2014.953961.

[16] Rob Pessers. Steerability and Stiffness Applied in minimally invasive instruments. (1207), 2011.

[17] Filip Jelínek, Rob Pessers, and Paul Breedveld. DragonFlex smart steerable laparoscopic instrument. *Journal of Medical Devices, Transactions of the ASME*, 8(1):27–28, 2014. ISSN 1932619X. doi: 10.1115/1.4026153.

[18] Filip Jelínek, Tom Diepens, Sander Dobbenga, Geert Van Der Jagt, Davey Kreeft, Annemijn Smid, Rob Pessers, and Paul Breedveld. Method for minimising rolling joint play in the steerable laparoscopic instrument prototype DragonFlex. *Minimally Invasive Therapy and Allied Technologies*, 24

(3):181–188, 2015. ISSN 13652931. doi: 10.3109/13645706.2014.968170.

[19] A. Townsend, N. Senin, L. Blunt, R. K. Leach, and J. S. Taylor. Surface texture metrology for metal additive manufacturing: a review. *Precision Engineering*, 46:34–47, 2016. ISSN 01416359. doi: 10.1016/j.precisioneng.2016.06.001. URL http://dx.doi.org/10.1016/j.precisioneng.2016.06.001.

[20] Dario Croccolo, Massimiliano De Agostinis, Stefano Fini, Giorgio Olmi, Francesco Robusto, Snežana Ćirić Kostić, Aleksandar Vranić, and Nebojša Bogojević. Fatigue Response of As-Built DMLS Maraging Steel and Effects of Aging, Machining, and Peening Treatments. *Metals*, 8(7):505, 2018. ISSN 2075-4701. doi: 10.3390/met8070505. URL http://www.mdpi.com/2075-4701/8/7/505.

[21] S Bruschi, G Tristo, Z Rysava, P F Bariani, D Umbrello, and L De Chiffre. Environmentally clean micromilling of electron beam melted Ti6Al4V. *Journal of Cleaner Production*, 133:932–941, 2016. doi: 10.1016/j.jclepro.2016.06.035. URL https://www.scopus.com/inward/record.uri?eid=2-s2.0-84988851058&doi=10.1016%2Fj.jclepro.2016.06.035&partnerID=40&md5=1a1dae4fb7b6f99af5ab75adb44c97d6.

[22] N Worts, J Jones, and J Squier. Surface structure modification of additively manufactured titanium components via femtosecond laser micromachining. *Optics Communications*, 430:352–357, 2019. doi: 10.1016/j.optcom.2018.08.055. URL https://www.scopus.com/inward/record.uri?eid=2-s2.0-85052966761&doi=10.1016%2Fj.optcom.2018.08.055&partnerID=40&md5=0e1658b7d843ecddcb3e2bfb8de149be.

[23] Hany Hassanin, Francesco Modica, Mahmoud Ahmed El-Sayed, Jian Liu, and Khamis Essa. Manufacturing of Ti-6Al-4V Micro-Implantable Parts Using Hybrid Selective Laser Melting and Micro-Electrical Discharge Machining. *Advanced Engineering Materials*, 18(9):1544–1549, 2016. doi: 10.1002/adem.201600172.

[24] Naor Elad Uzan, Shlomo Ramati, Roni Shneck, Nachum Frage, and Ori Yeheskel. On the effect of shot-peening on fatigue resistance of AlSi10Mg specimens fabricated by additive manufacturing using selective laser melting (AM- SLM). *Additive Manufacturing*, 21(September 2017):458–464, 2018. ISSN 2214-8604. doi: 10.1016/j.addma.2018.03.030. URL https://doi.org/10.1016/j.addma.2018.03.030.

[25] Pawan Tyagi, Tobias Goulet, Christopher Riso, and Francisco Garcia-Moreno. Reducing surface roughness by chemical polishing of additively manufactured 3D printed 316 stainless steel components. *International Journal of Advanced Manufacturing Technology*, 100(9-12):2895–2900, 2019. ISSN 14333015. doi: 10.1007/s00170-018-2890-0.

[26] R Coelho, R Azevedo, and C Assis. An investigation of anisotropy on AISI 316L obtained by additive manufacturing (AM) measuring surface roughness after micro-endmilling operations. In *European Society for Precision Engineering and Nanotechnology, Conference Proceedings - 18th International Conference and Exhibition, EUSPEN 2018*, pages 357–358, 2018. URL https://www.scopus.com/inward/record.uri?eid=2-s2.0-85054489907&partnerID=40&md5=ef5deffa341e9c3dc60dc6a03481d985.

[27] K L Tan and S H Yeo. Surface modification of additive manufactured components by ultrasonic cavitation abrasive finishing. *Wear*, 378-379:90–95, 2017. doi: 10.1016/j.wear.2017.02.030. URL https://www.scopus.com/inward/record.uri?eid=2-s2.0-85013119796&doi=10.1016%2Fj.wear.2017.02.030&partnerID=40&md5=7ef2131ad9fd16f89cc00b9dea0536ae.

[28] A G Demir and B Previtali. Additive manufacturing of cardiovascular CoCr stents by selective laser melting. *Materials and Design*, 119:338–350, 2017. doi: 10.1016/j.matdes.2017.01.091. URL https://www.scopus.com/inward/record.uri?eid=2-s2.0-85011278254&doi=10.1016%2Fj.matdes.2017.01.091&partnerID=40&md5=c1148061c415943a4ae4dfe4ab1d982d.

[29] Anthony T. Beaucamp, Yoshiharu Namba, Phillip Charlton, Samyak Jain, and Arthur A. Graziano. Finishing of additively manufactured titanium alloy by shape adaptive grinding (SAG). *Surface Topography: Metrology and Properties*, 3(2), 2015. ISSN 2051672X. doi: 10.1088/2051-672X/3/2/024001.

[30] T Pereira, J Potgieter, J V Kennedy, A Mukhtar, and M Fry. The effect of reheating layers in Metal Additive Manufacturing on the external surface finish of a printed part. In *Proceedings of the 2018 25th International Conference on Mechatronics and Machine Vision in Practice, M2VIP 2018*, 2019. doi: 10.1109/M2VIP.2018.8600902. URL https://www.scopus.com/inward/record.uri?eid=2-s2.0-85061770217&doi=10.1109%2FM2VIP.2018.8600902&partnerID=40&md5=ca6168dd6797f456b57bf54a3a5343cc.

[31] V. A. Aleksandrov, S. K. Sundukov, D. S. Fatyukhin, and A. A. Filatova. Ultrasonic Methods for Improving Object Surface Quality Prepared by Corrosion-Resistant Steel Powder Selective Laser Melting. *Metal Science and Heat Treatment*, 60(5-6):381–386, 2018. ISSN 15738973. doi: 10.1007/s11041-018-0287-1.

[32] S Bagehorn, J Wehr, and H J Maier. Application of mechanical surface finishing processes for roughness reduction and fatigue improvement of additively manufactured Ti-6Al-4V parts. *International Journal of Fatigue*, 102:135–142, 2017. doi: 10.1016/j.ijfatigue.2017.05.008. URL https://www.scopus.com/inward/record.uri?eid=2-s2.0-85019237794&doi=10.1016%2Fj.ijfatigue.2017.05.008&partnerID=40&md5=84c3355f71b16c2afceff95a2b2cd9bc.

[33] Z Rysava and S Bruschi. Comparison between EBM and DMLS Ti6Al4V machinability characteristics under dry micro-milling conditions, 2016. URL https://www.scopus.com/inward/record.uri?eid=2-s2.0-84958064330&doi=10.4028%2Fwww.scientific.net%2FMSF.836-837.177&partnerID=40&md5=d1e0c390c608641d40c2d34880fb104b.

[34] W S Gora, Y Tian, A P Cabo, M Ardron, R R J Maier, P Prangnell, N J Weston, and D P Hand. Enhancing surface finish of additively manufactured titanium and cobalt chrome elements using laser based finishing. In *9th International Conference on Photonic Technologies*, volume 83, pages 258–263, 2016. doi: 10.1016/j.phpro.2016.08.021.

[35] A P Nagalingam and S H Yeo. Controlled hydrodynamic cavitation erosion with abrasive particles for internal surface modification of additive manufactured components. *Wear*, 414-415:89–100, 2018. doi: 10.1016/j.wear.2018.08.006. URL https://www.scopus.com/inward/record.uri?eid=2-s2.0-85051654989&doi=10.1016%2Fj.wear.2018.08.006&partnerID=40&md5=69fd398727e5d8290822f481afefb98a.

[36] C G Klingaa, T Dahmen, S Baier, S Mohanty, and J H Hattel. Build orientation effects on the roughness of SLM channels. *Proceedings of the Joint Special Interest Group meeting between euspen and ASPE Advancing Precision in Additive Manufacturing (2019).*, (November), 2019. URL www.euspen.eu.

[37] U Tradowsky, J White, R M Ward, N Read, W Reimers, and M M Attallah. Selective laser melting of AlSi10Mg : Influence of post-processing on the microstructural and tensile properties development. *Materials and Design*, 105:212–222, 2016. ISSN 0264-1275. doi: 10.1016/j.matdes.2016.05.066. URL http://dx.doi.org/10.1016/j.matdes.2016.05.066.

[38] Materialise. Metal 3D Printing, 2020. URL https://www.materialise.com/en/manufacturing/3d-printing-technology/metal-3d-printing.

[39] Jingchao Jiang and Xun Xu. Support Structures for Additive Manufacturing : A Review. 2018. doi: 10.3390/jmmp2040064.

[40] Martin Leary. *Design for Additive Manufacturing*. Elsevier, 2020. ISBN 9780128167212. doi: 10.1016/B978-0-12-816721-2.00011-7.

[41] LaRoux Gillespie. *Mass Finishing Handbook*. Industrial Press, New York, NY, USA, 1st edition, 2007. ISBN 978-0-8311-3257-6. URL https://app.knovel.com/web/toc.v/cid:kpMFH00002/viewerType:toc//root_slug:mass-finishing-handbook/url_slug:surface-requirements?issue_id=kpMFH00002.

[42] Mikdam Jamal and Michael N. Morgan. Design process control for improved surface finish of metal additive manufactured parts of complex build geometry. *Inventions*, 2(4):1–18, 2017. ISSN 24115134. doi: 10.3390/inventions2040036.

[43] OTEC Präzisionsfinish GmbH. OTEC Ceramic Abrasives. URL https://www.otec.de/en/products/media/wet-finishing/ceramic-abrasives/.

[44] LaRoux K. Gillespie. Edge Requirements. *Mass Finishing Handbook*, pages 31–49, 2007.

[45] G. M. Yang, J. C. Coquille, J. F. Fontaine, and M. Lambertin. Influence of roughness on characteristics of tight interface fit of a shaft and a hub. *International Journal of Solids and Structures*, 38(42-43):7691–7701, 2001. ISSN 00207683. doi: 10.1016/S0020-7683(01)00035-X.

[46] Jaydeep H. Palep. Robotic assisted minimally invasive surgery. *Journal of Minimal Access Surgery*, 5(1):1–7, 2009. ISSN 09729941. doi: 10.4103/0972-9941.51313.

[47] Intuitive Inc. EndoWrist products, 2020. URL https://www.intuitive.com/en-us.

[48] Paul Breedveld, Henk G. Stassen, Dirk W. Meijer, and Jac J. Jakimowicz. Manipulation in laparoscopic surgery: Overview of impeding effects and supporting aids. *Journal of Laparoendoscopic and Advanced Surgical Techniques - Part A*, 9(6):469–480, 1999. ISSN 10926429. doi: 10.1089/lap.1999.9.469.

[49] A Gatto, L Iuliano, F Calignano, and E Bassoli. Electrodischarge drilling performance on parts produced by DMLS. *International Journal of Advanced Manufacturing Technology*, 58(9-12): 1003–1018, 2012. doi: 10.1007/s00170-011-3446-8. URL `https://www.scopus.com/inward/record.uri?eid=2-s2.0-84857457195&doi=10.1007%2Fs00170-011-3446-8&partnerID=40&md5=7ede8d3a484581009ae90b9ab61b228b`.

[50] F.J. Siers. *Methodisch Ontwerpen*. Noordhoff Uitgevers, Groningen/Houten, 3rd edition, 2004. ISBN 978-90-01-50901-9.

[51] S. Manasnayakorn, A. Cuschieri, and G. B. Hanna. Ideal manipulation angle and instrument length in hand-assisted laparoscopic surgery. *Surgical Endoscopy and Other Interventional Techniques*, 22 (4):924–929, 2008. ISSN 09302794. doi: 10.1007/s00464-007-9520-5.

[52] Filip Jelínek, Ewout A. Arkenbout, Paul W.J. Henselmans, Rob Pessers, and Paul Breedveld. Classification of joints used in steerable instruments for minimally invasive surgery: A review of the state of the art. *Journal of Medical Devices, Transactions of the ASME*, 9(1), 2015. ISSN 1932619X. doi: 10.1115/1.4028649.

[53] Eckart Uhlmann and Alexander Eulitz. Wear Mechanisms of Ceramic Vibratory Finishing Media. *Nanomanufacturing and Metrology*, 1(2):96–104, 2018. ISSN 2520811X. doi: 10.1007/s41871-018-0010-2. URL `https://doi.org/10.1007/s41871-018-0010-2`.

A Surface Roughness of Polished 3D Printed Metal

In this appendix the measured Ra values are tabulated (Table A.1) of four surfaces, each with a different normal vector angle with respect to the building direction. In Figure A.1 a model of the test piece and measured surfaces is shown. Two test pieces (A & B) were used to gain a preliminary understanding of the surface roughness reduction. A polishing cycle of fine and medium abrasives, both for 1.5 hours was applied. The average surface roughness reduction is 0.35 %.

Table A.1: Table of measured surface roughness (Ra) of 3D printed test pieces. The surface measurements were taken on four different surfaces of different normal vector angles with respect to the building direction.

Angle	NO MFT	A	B	MFT	A	B
0°	Ra [µm]	8.23	7.55	Ra [µm]	5.43	5.07
90°	Ra [µm]	9.49	5.63	Ra [µm]	4.51	4.59
45°	Ra [µm]	11.86	9.68	Ra [µm]	8.34	7.74
60°	Ra [µm]	12.91	8.81	Ra [µm]	8.72	6.61

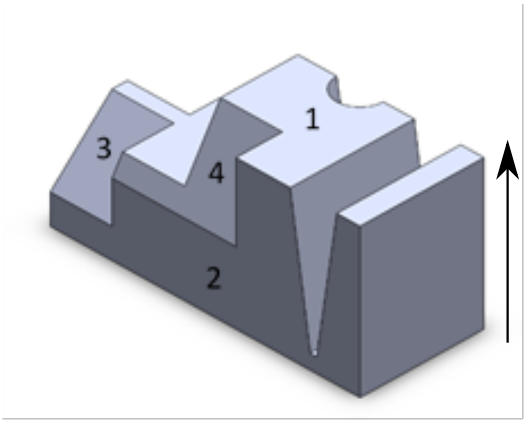

Figure A.1: The four surfaces on which the surface roughness values were measured. Surface 1 is at 0°, surface 2 at 90°, surface 3 at 45°, and surface 4 at 60°, respectively. The arrow marks the building direction.

B Polishing Test Plan

Goal

Investigation of the polishability of specific geometries, and the effect of polishing on these geometries. The following geometries were added:

- Two types of pillars; one square and one round, both 6 mm high and 2 mm in diameter. A double curved surface, comparable with the desired gear arch.
- A double curved suface, comparable with the desired gear arch.
- Recessed features; an internal cube of 3 x 3 x 3 mm, a 2 mm deep channel that runs from 3 mm to 0.4 mm over 8mm, and a cone that runs from 3 mm to 0 mm over 8 mm.
- Cable guide of 0.4 mm deep with an internal corner radius of 0.2 mm, which matches the cable guides of the original DragonFlex design.

These geometries, with the exception of the cable guides, were taken from a previous literature review on post-processing techniques for 3D printed metal structures. With these geometries the following aspects are investigated;

- The tapering of the pillars, which is expected to happen due to the tips of the pillars experiencing more abrasion than the base.
- The degree to which a double curved surface can be polished it is expected that mass finishing polishing has little to no issue with double curved surfaces.
- The depth to which a corner or channel can be polished with mass finishing polishing; it is expected that an unpolished zone remains in a region close to the inside corner. For the taper and cone it is expected that below a certain width, polishing will not be possible. This threshold value is desired information.

In addition to these geometries, two other dimensions will be taken. The first being the amount of corner rounding that will occur at right outside corners. Second is the dimensional width decrease during polishing. These two values will help towards estimate the initial part sizes.

Not all test pieces will receive the same polishing treatment. Test pieces will be sorted in groups of three and four different polishing schemes will be used.

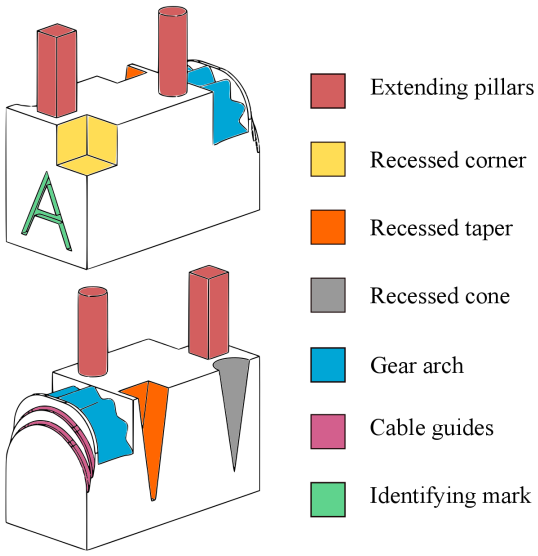

Figure B.1: Illustration of the test piece used to investigate the effect and accessibility of mass finishing polishing. The colours mark different features used.

Procedure

There are twelve test pieces, each marked witha a letter (A to L). These twelve are split up into four groups of three test pieces.

1. A B C
2. D E F
3. G H I
4. J k L

Step	Polishing media	Duration	Test piece groups	Test piece letters
1 Coarse	DZS 6/6 - SC 15	2 hours	1 2 3	A t/m I
2 Medium	KM 10 + PM 10 - SC 15	2 hours	2 3 4	D t/m L
3 Fine	ZSP 3/5 + DZP 3/3 - SC5	2 hours	3 4	G t/m L

All test pieces are to be degreased and coated in marking lacquer prior to polishing. This lacquer has to be applied in a thin, even coating on all surfaces, with the exception of the bottom. Whether lacquer is applied to the bottom does not matter to this experiment. The lacquer has to be fully dried as per the instructions of the packaging. Between polishing steps no new lacquer may be applied. The lacquer has the purpose of visualising where no polishing has occured. Aside from coating, all test pieces have to be measured across their width with a micrometer, as illustrated in the figure below. The measurement of the width is around 8 mm. This measurement has to be repeated after each polishing step.

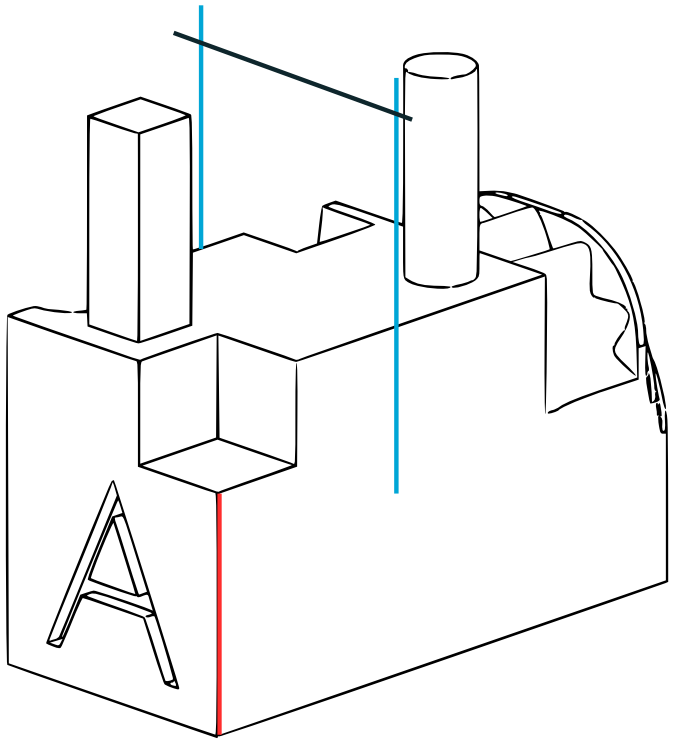

Figure B.2: Test piece with the measurement locations of the edge rounding (red edge) and the base width (blue and black lines).

C Experiment Data

The measured dimensions of the test pieces of the polishing experiment. The width measurements were taken with screw gauge, and the round and square pillar measurements with digital calipers.

pre-polishing [mm]					
test piece	width	round top	round bottom	square top	square bottom
A	8.222	2.02	2.06	1.96	2.02
B	8.218	2.07	2.07	2.06	2.04
C	8.238	2.06	2.07	2.05	2.07
D	8.233	2.06	2.10	2.06	2.06
E	8.127	2.05	2.09	2.13	2.07
F	8.108	2.01	2.06	1.97	2.00
G	8.187	1.99	2.05	1.96	2.00
H	8.177	2.07	2.09	2.03	2.05
I	8.225	2.04	2.09	2.04	2.02
J	8.081	1.98	2.04	1.97	2.02
K	8.136	2.07	2.09	2.08	2.06
L	8.131	2.06	2.04	2.06	2.03

coarse [mm]					
test piece	width	round top	round bottom	square top	square bottom
A	8.043	1.94	1.97	1.90	2.01
B	8.004	1.97	2.05	1.93	1.98
C	8.003	1.95	2.01	1.96	2.03
D	7.988				
E	7.983				
F	7.947				
G	8.009				
H	7.991				
I	7.995				

medium [mm]					
test piece	width	round top	round bottom	square top	square bottom
D	7.956	1.94	2.07	1.92	1.99
E	7.953	1.94	1.98	1.95	2.03
F	7.917	1.90	1.96	1.87	2.00
G	7.989				
H	7.979				
I	7.973				
J	7.989				
K	8.008				
L	8.005				

fine [mm]					
test piece	width	round top	round bottom	square top	square bottom
G	7.979	1.90	1.99	1.88	1.98
H	7.969	1.94	2.03	1.93	2.00
I	7.961	1.92	1.97	1.91	1.95
J	7.964	1.91	2.04	1.92	2.00
K	7.977	1.98	2.03	1.99	2.03
L	7.977	1.98	2.00	1.96	1.99

D Photos Test Pieces

In this section shows the photos of the test pieces in three different positions. The photos were taken with a Nikon D850 digital camera, with a positioning plate to insure consistency between photos. The test pieces are grouped per polishing group.

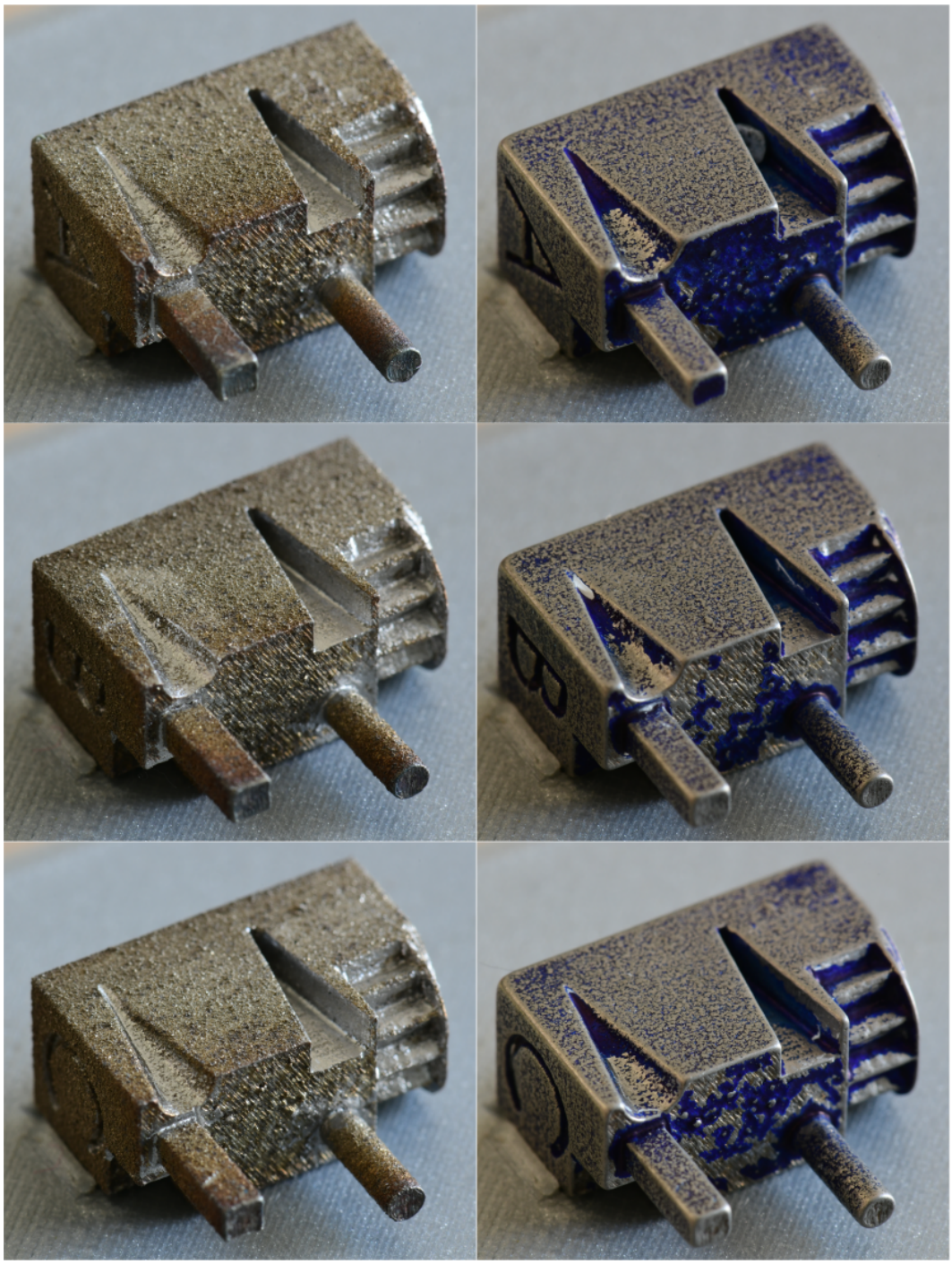

Figure D.1: Photos of test pieces A, B and C before and after polishing. These test pieces underwent a coarse polishing.

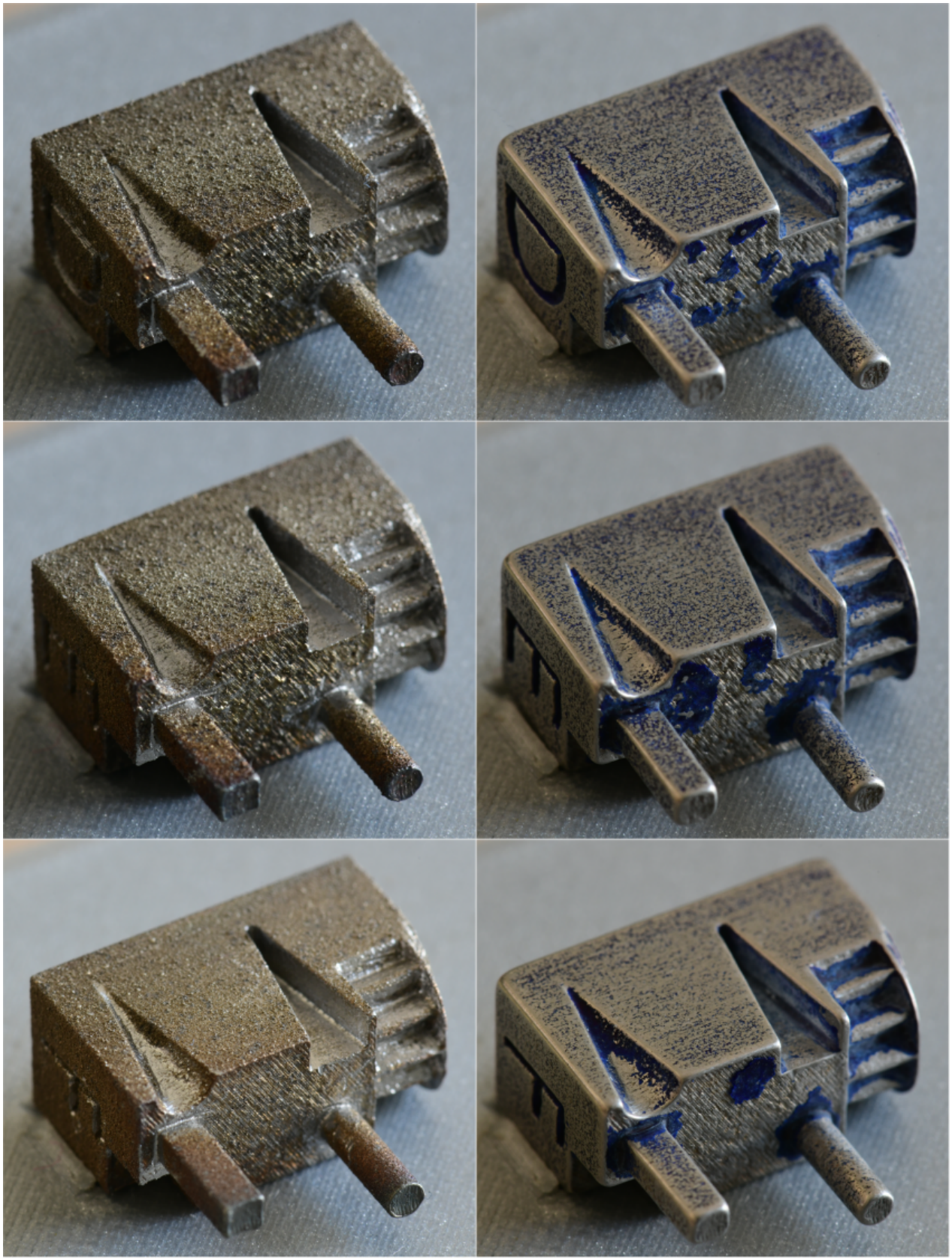

Figure D.2: Photos of test pieces D, E and F before and after polishing. These test pieces underwent a coarse and medium polishing.

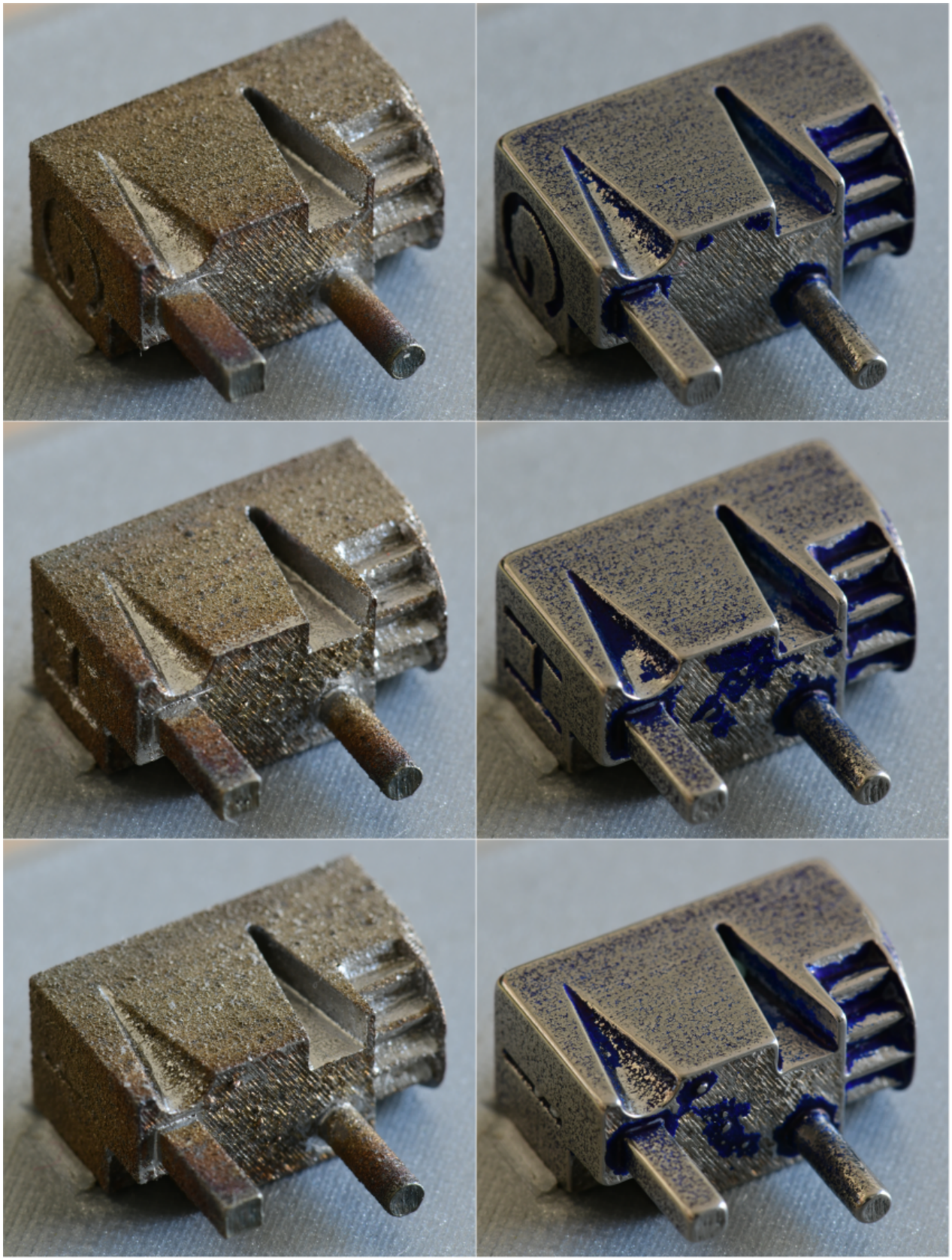

Figure D.3: Photos of test pieces G, H and I before and after polishing. These test pieces underwent a coarse, medium and fine polishing.

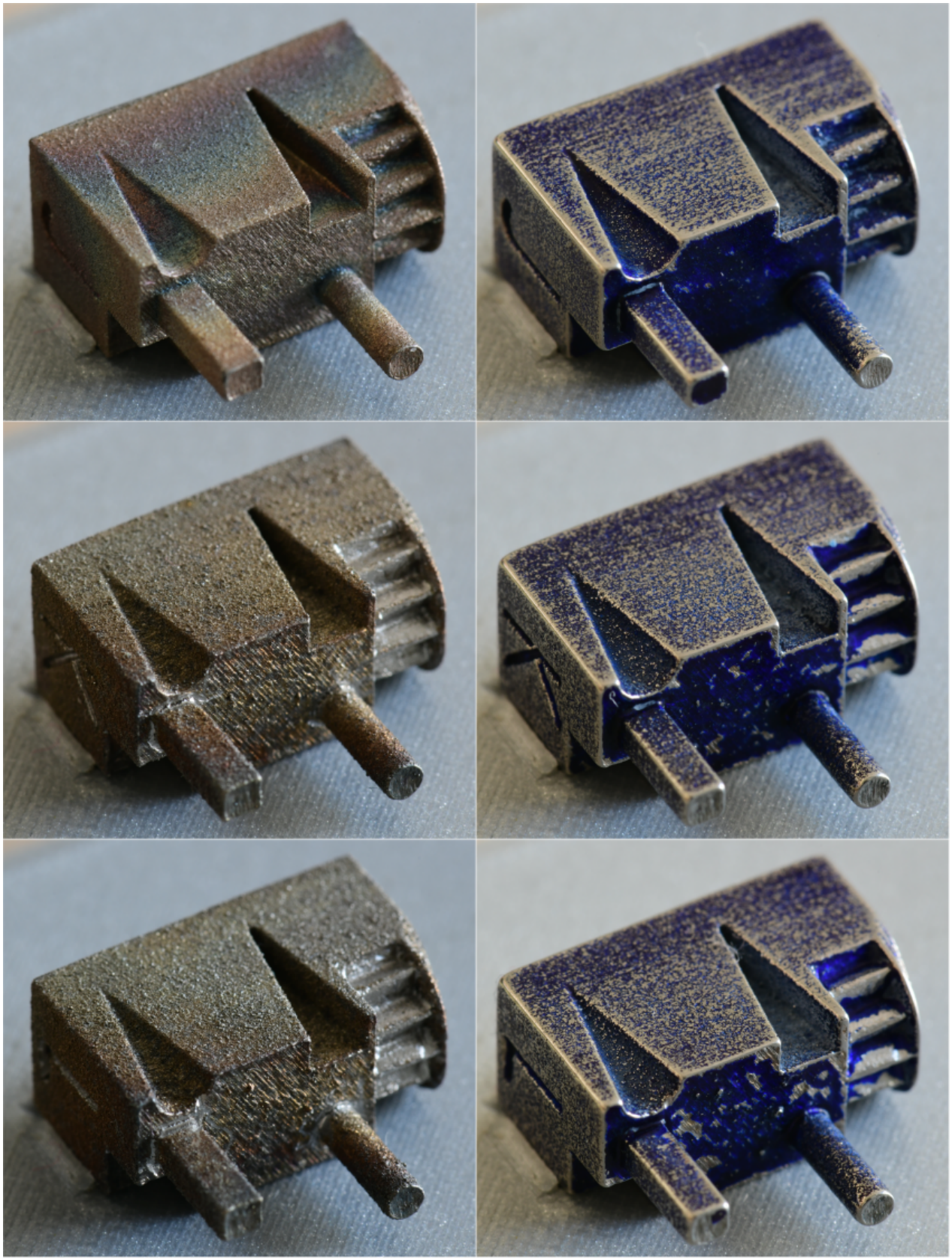

Figure D.4: Photos of test pieces J, K and L before and after polishing. These test pieces underwent a medium and fine polishing.

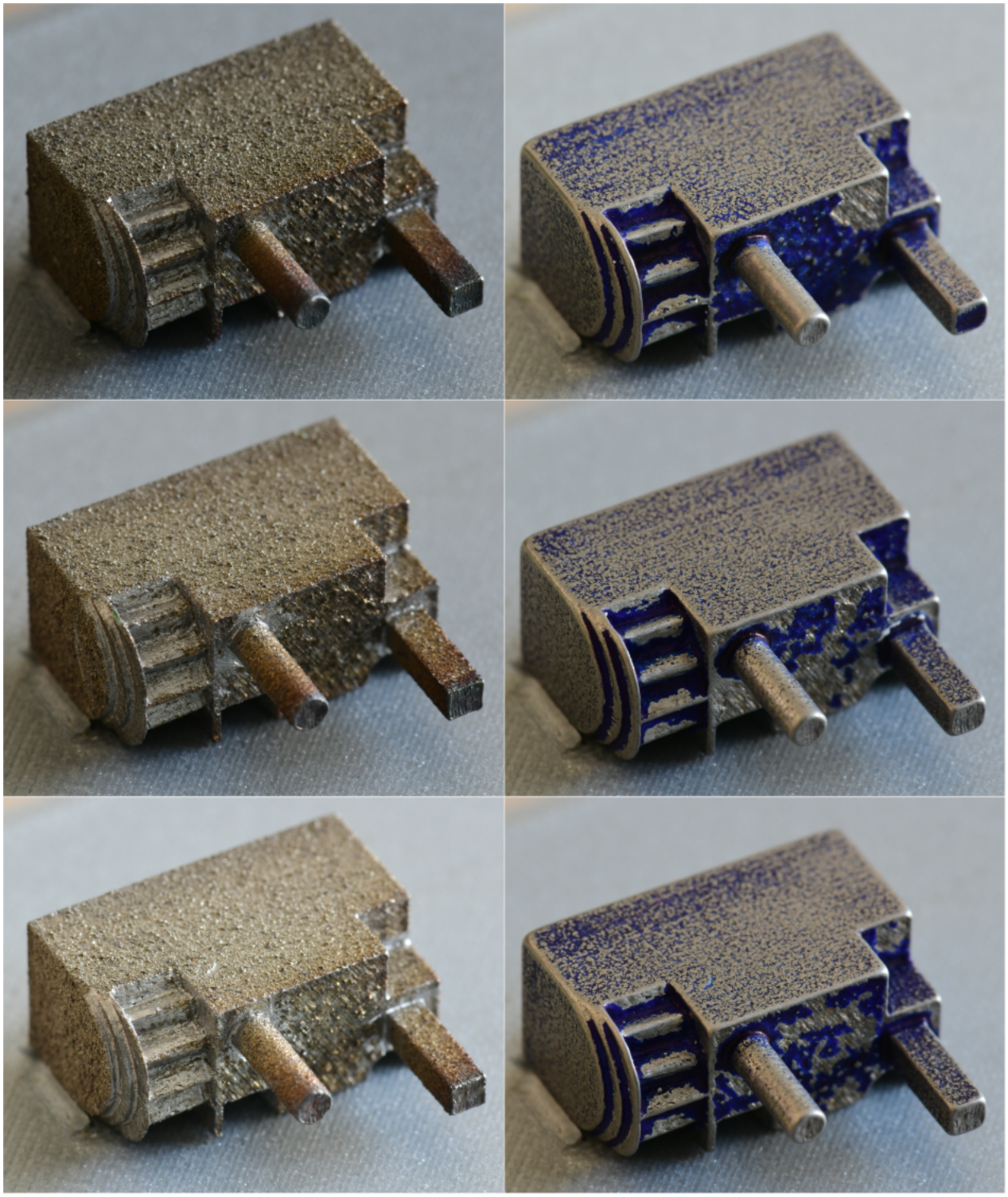

Figure D.5: Photos of test pieces A, B and C before and after polishing. These test pieces underwent a coarse polishing.

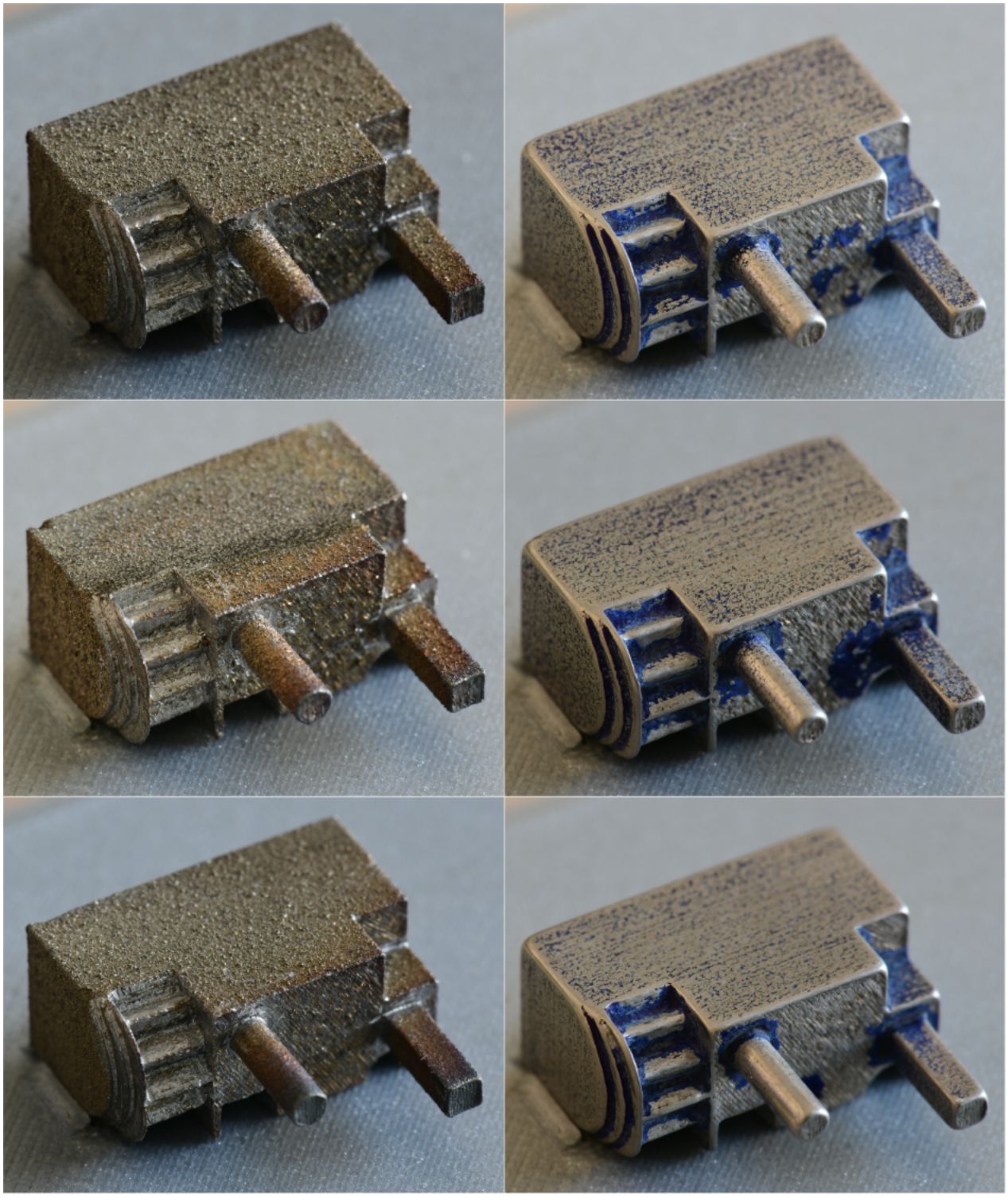

Figure D.6: Photos of test pieces D, E and F before and after polishing. These test pieces underwent a coarse and medium polishing.

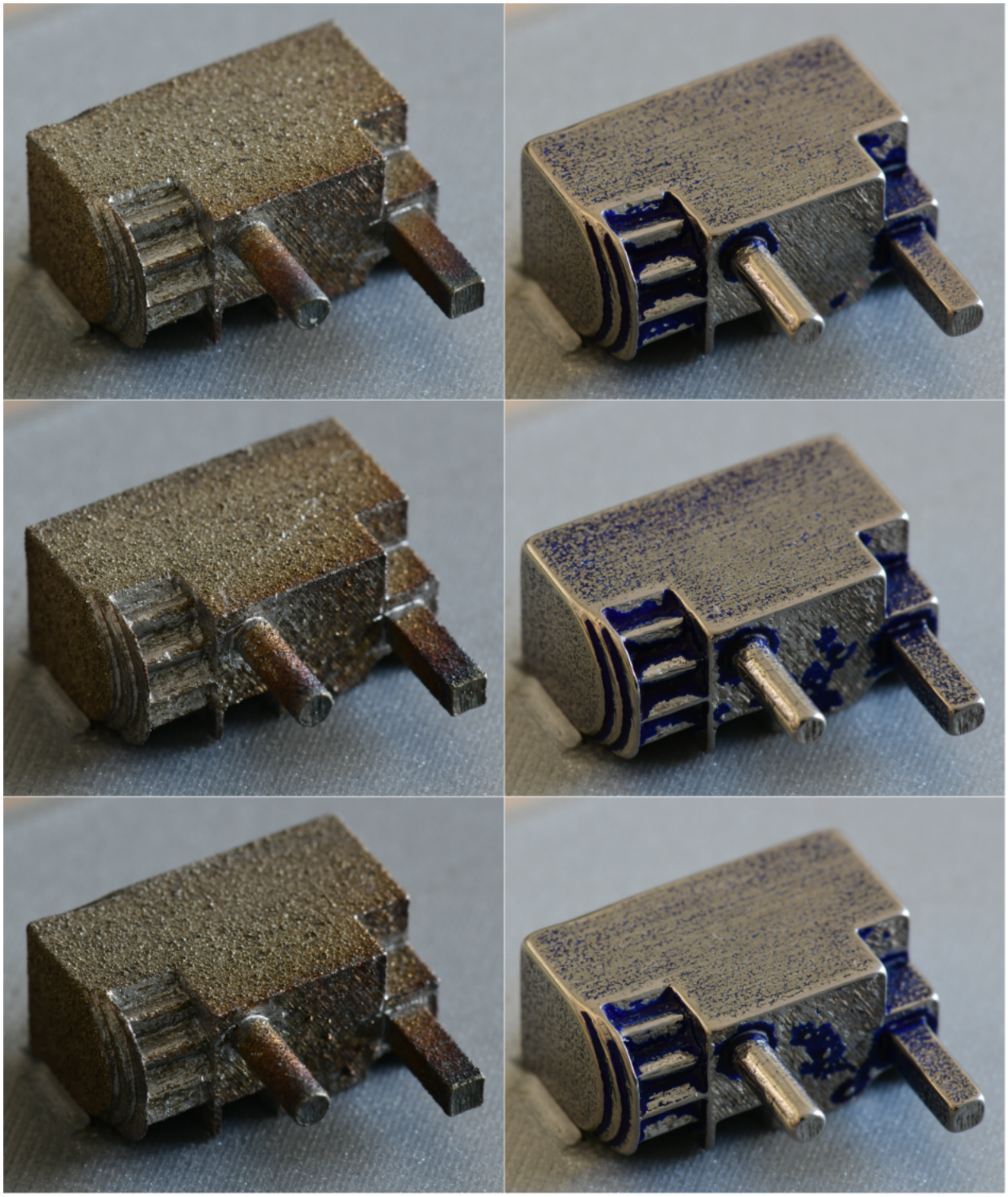

Figure D.7: Photos of test pieces G, H and I before and after polishing. These test pieces underwent a coarse, medium and fine polishing.

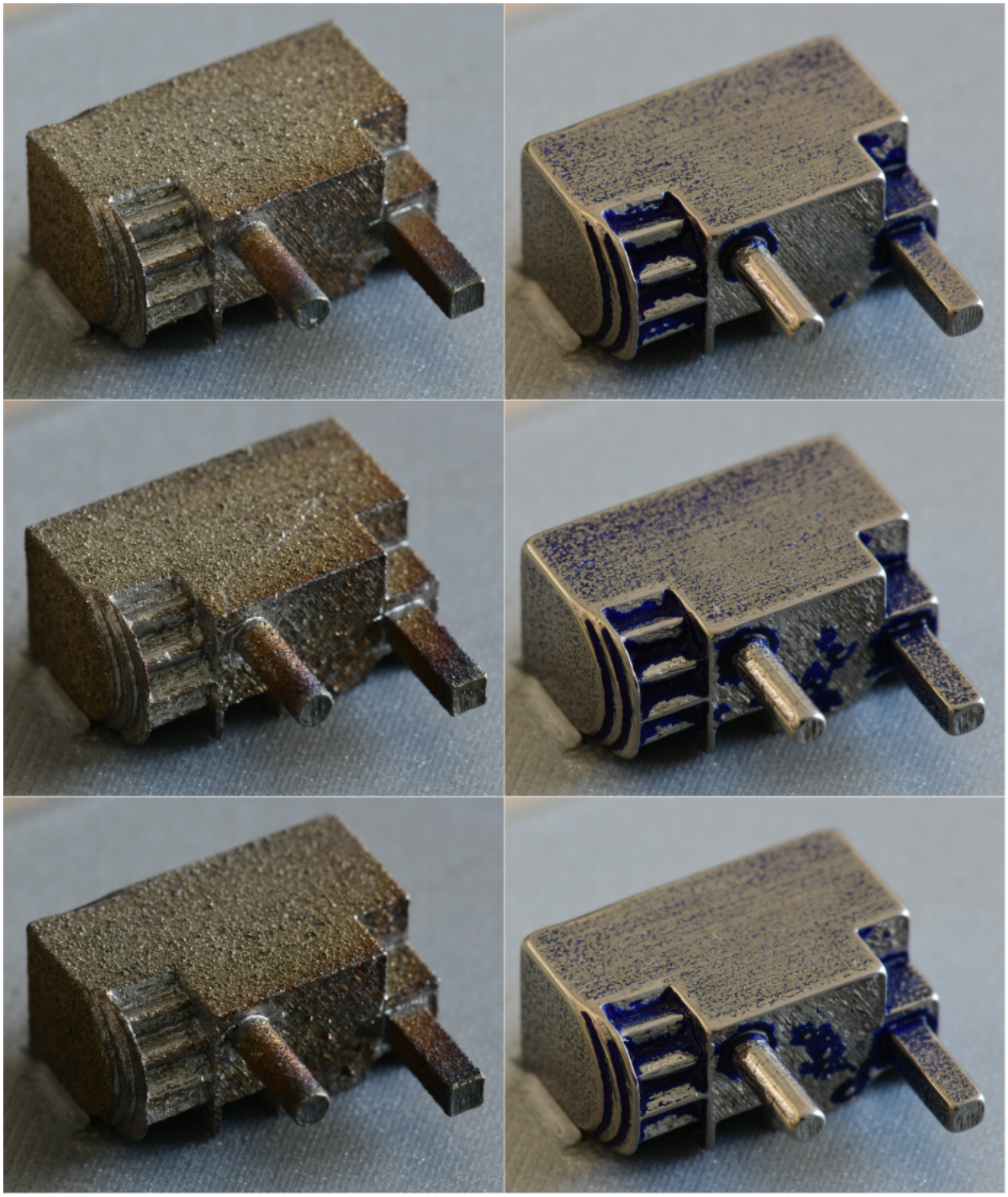

Figure D.8: Photos of test pieces J, K and L before and after polishing. These test pieces underwent a medium and fine polishing.

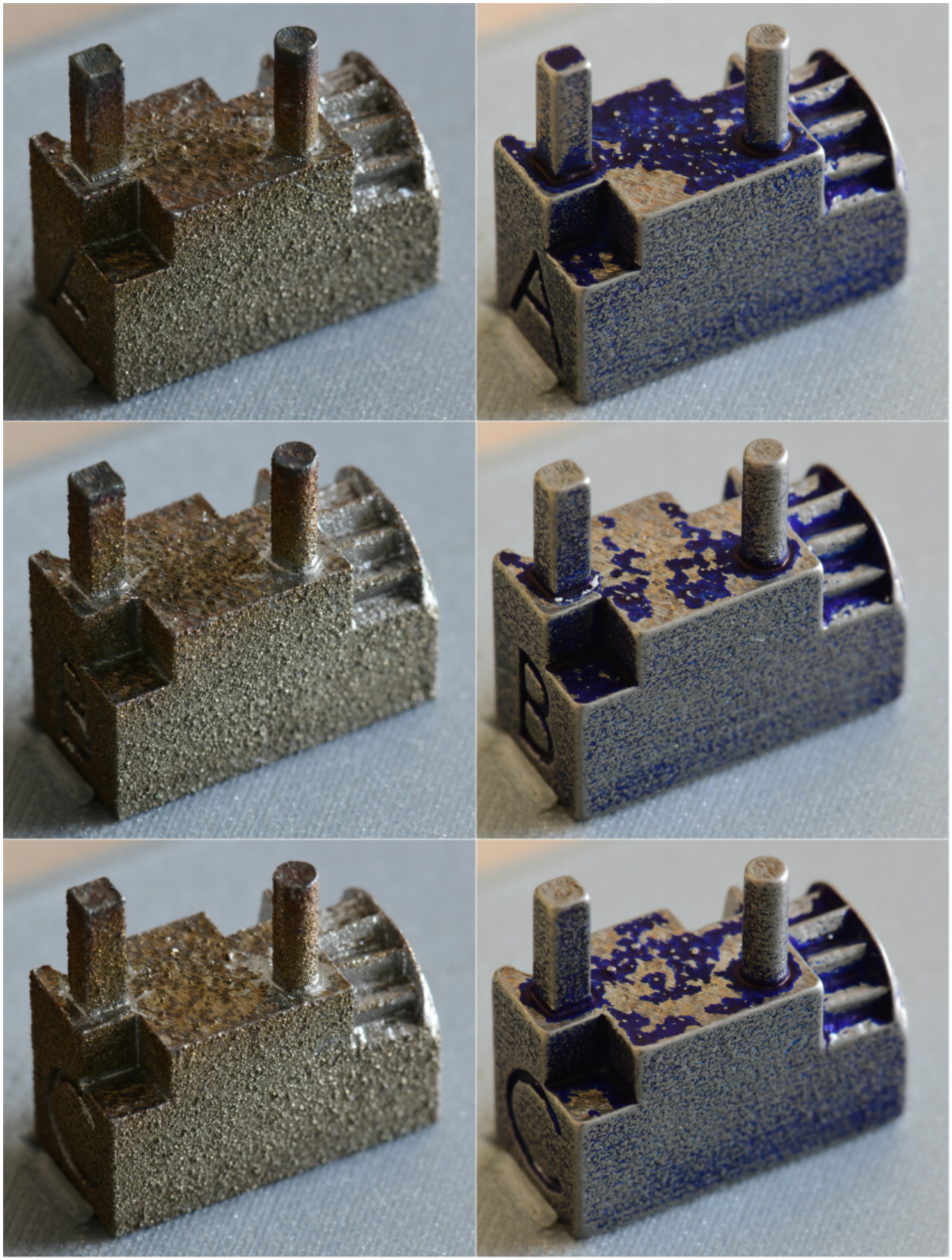

Figure D.9: Photos of test pieces A, B and C before and after polishing. These test pieces underwent a coarse polishing.

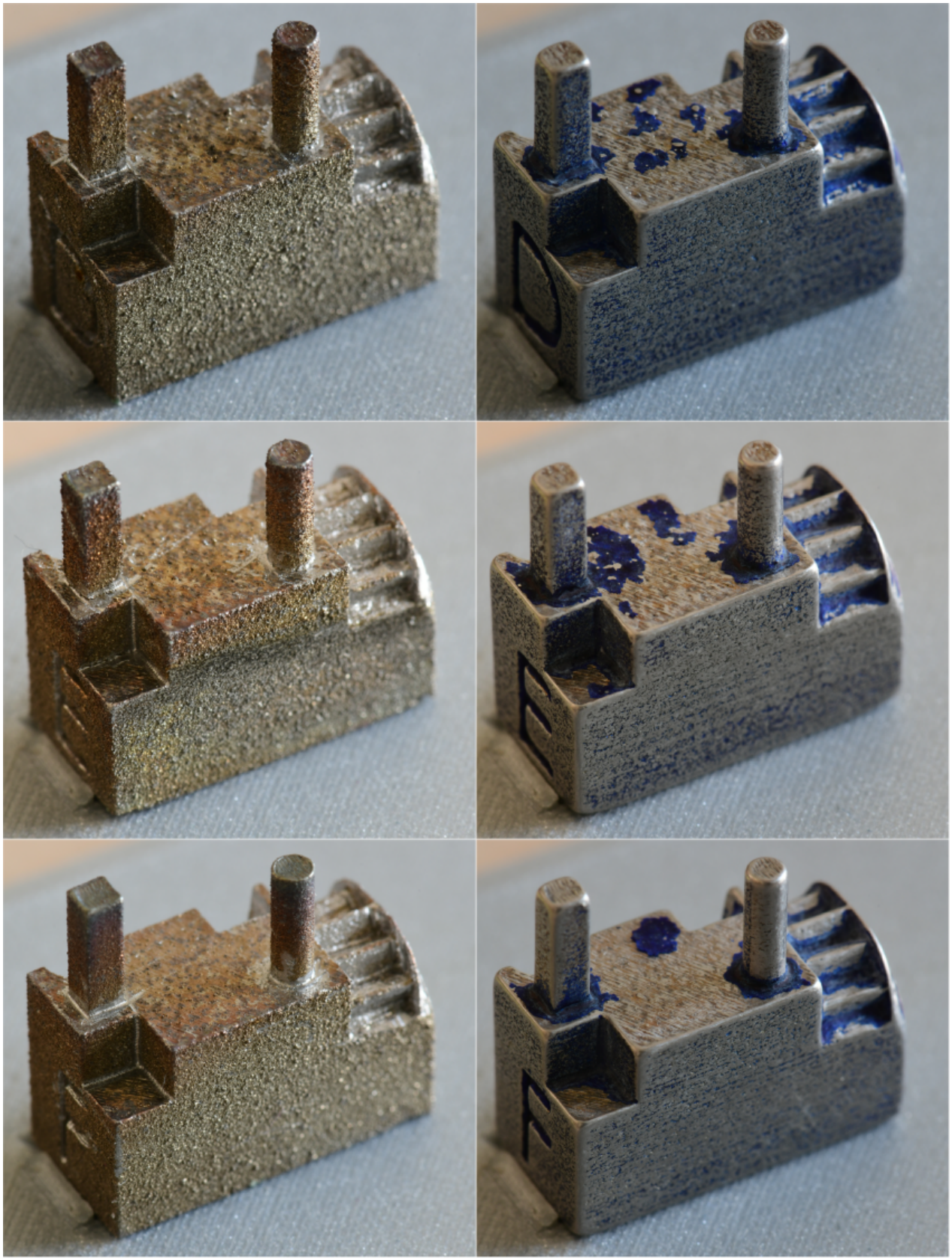

Figure D.10: Photos of test pieces D, E and F before and after polishing. These test pieces underwent a coarse and medium polishing.

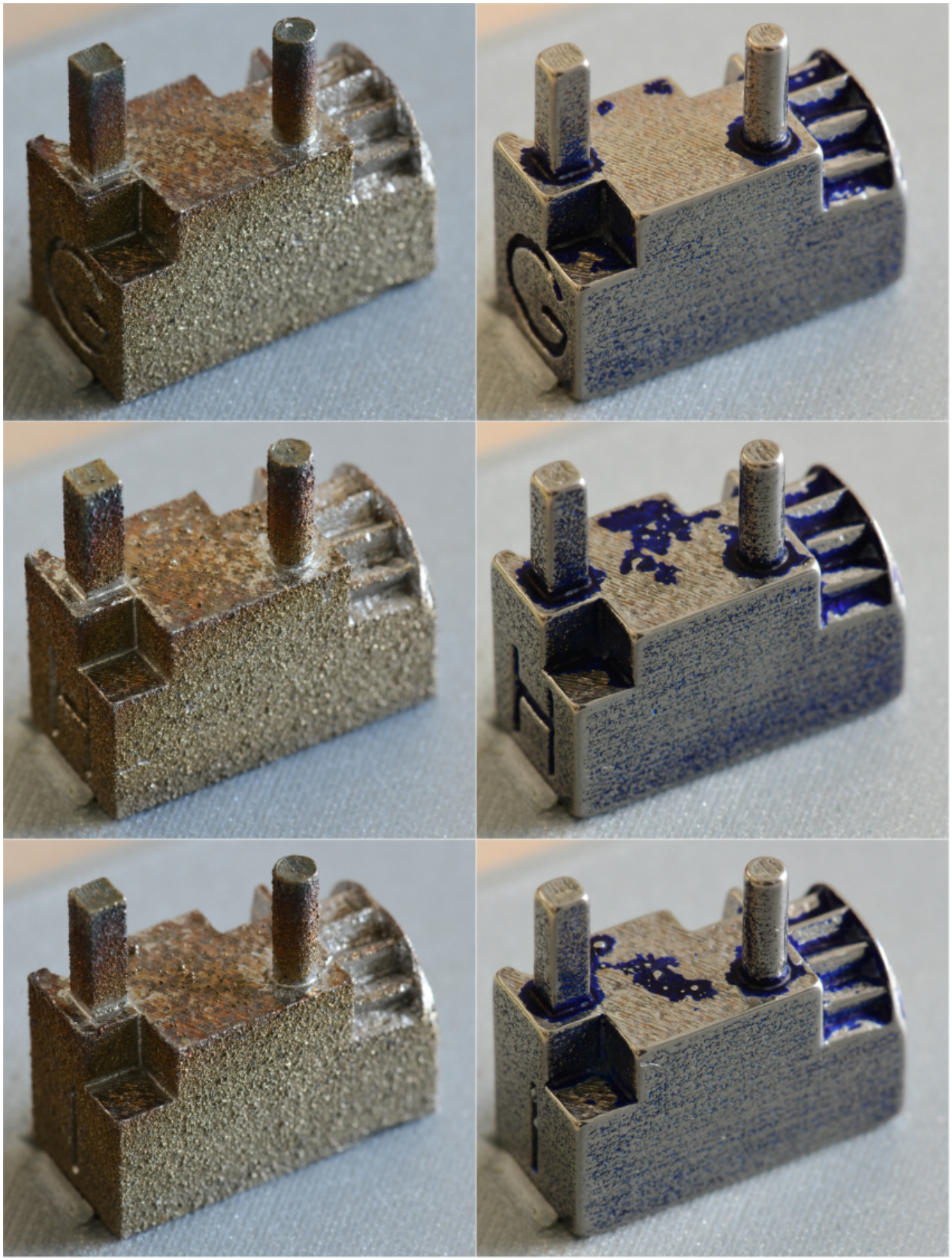

Figure D.11: Photos of test pieces G, H and I before and after polishing. These test pieces underwent a coarse, medium and fine polishing.

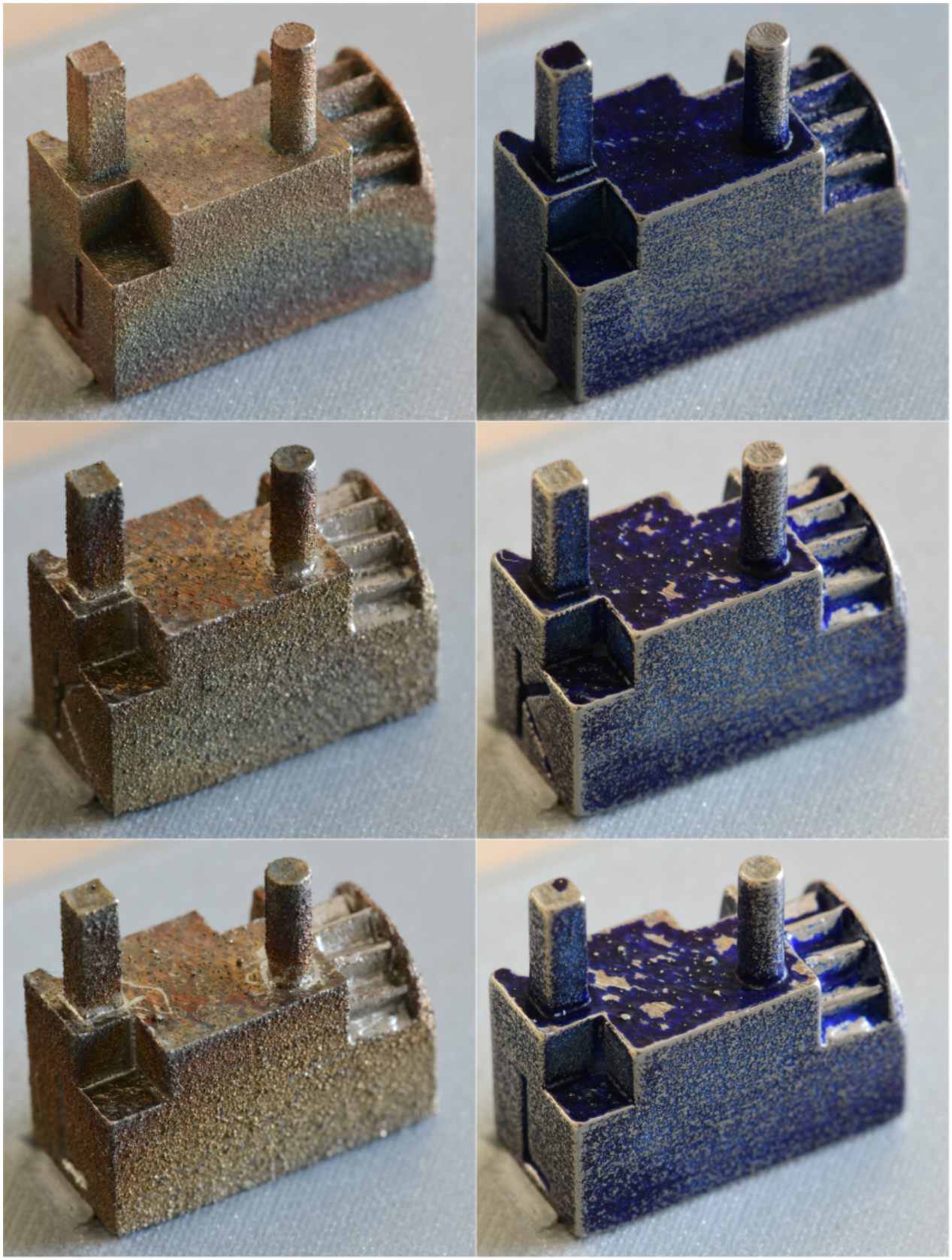

Figure D.12: Photos of test pieces J, K and L before and after polishing. These test pieces underwent a medium and fine polishing.

E Technical Drawings of the Instrument

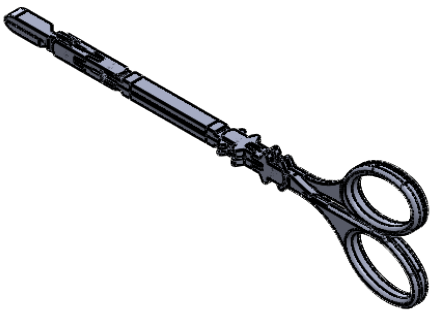

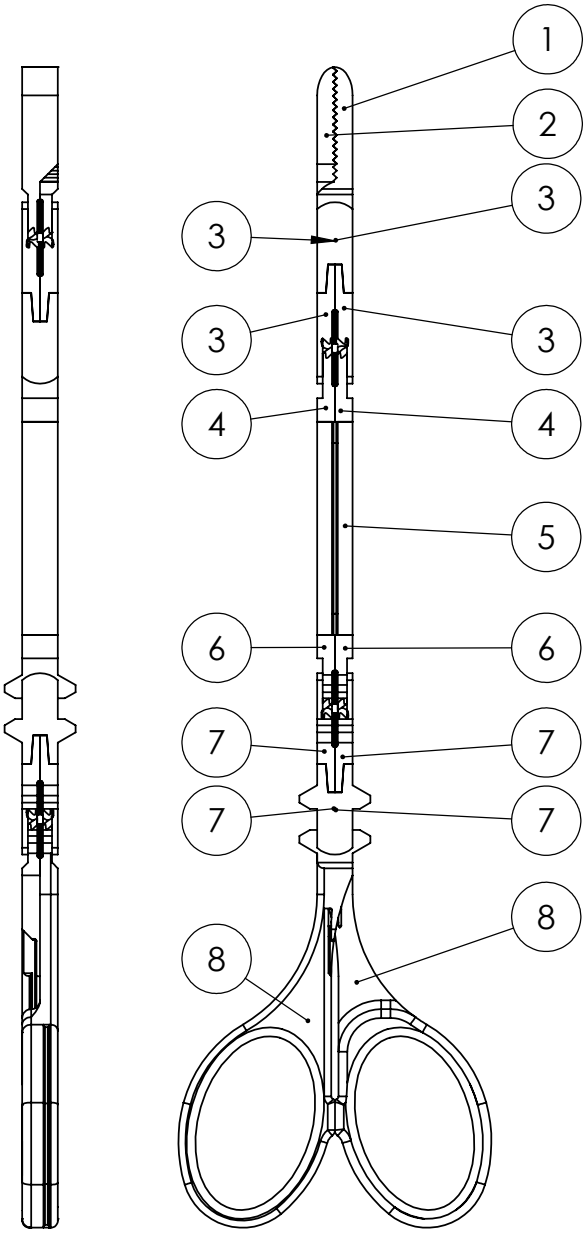

1	Gripper 1
2	Gripper 2
3	Centre body tip
4	Shaft addition tip
5	Shaft
6	Shaft addition handle
7	Centre body handle
8	Handle

UNLESS OTHERWISE SPECIFIED: DIMENSIONS ARE IN MILLIMETERS SURFACE FINISH: TOLERANCES: LINEAR: ANGULAR:		FINISH:		DEBURR AND BREAK SHARP EDGES		DO NOT SCALE DRAWING	REVISION
	NAME	SIGNATURE	DATE				TITLE:
DRAWN							
CHK'D							
APPV'D							
MFG							
Q.A				MATERIAL:		DWG NO.	A4
						assembly	
				WEIGHT:		SCALE 1:1	SHEET 1 OF 1

GEAR TYPES 1 & 2

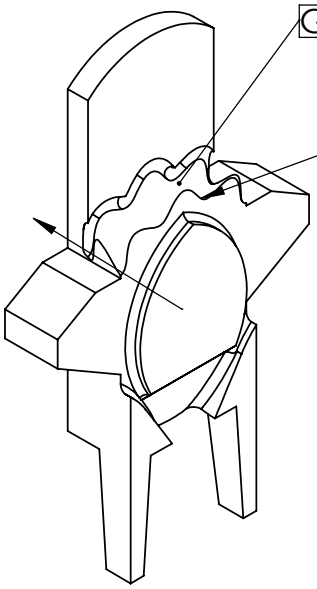

Gear type 1

Line equation:
X(t) = cos(t)*(3.675+0.3*cos(t*12))
Y(t) = sin(t)*(3.675+0.3*cos(t*12))
Centered on the origin of the cable guide

Rotated 30deg cw over the width (1.3 mm) following the arrow from the origin

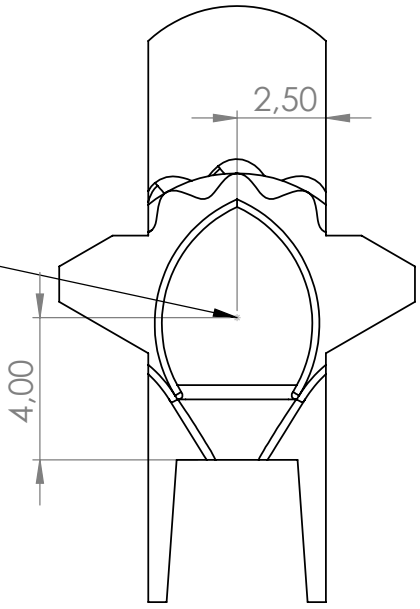

Cable guide origin

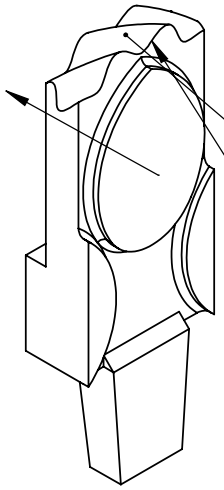

Gear type 2

Line equation:
X(t) = cos(t)*(3.675-0.3*cos(t*12))
Y(t) = sin(t)*(3.675-0.3*cos(t*12))
Centered on the origin of the cable guide

Roted 30deg ccw over the width (1.3 mm) following the arrow from the origin

UNLESS OTHERWISE SPECIFIED: DIMENSIONS ARE IN MILLIMETERS SURFACE FINISH: TOLERANCES: LINEAR: ANGULAR:		FINISH:			DEBURR AND BREAK SHARP EDGES		DO NOT SCALE DRAWING	REVISION
	NAME	SIGNATURE	DATE				TITLE:	
DRAWN								
CHK'D								
APPV'D								
MFG								
Q.A				MATERIAL:			DWG NO.	A4
							gear types	
				WEIGHT:			SCALE:5:1	SHEET 1 OF 1

CABLE GUIDE TYPE A

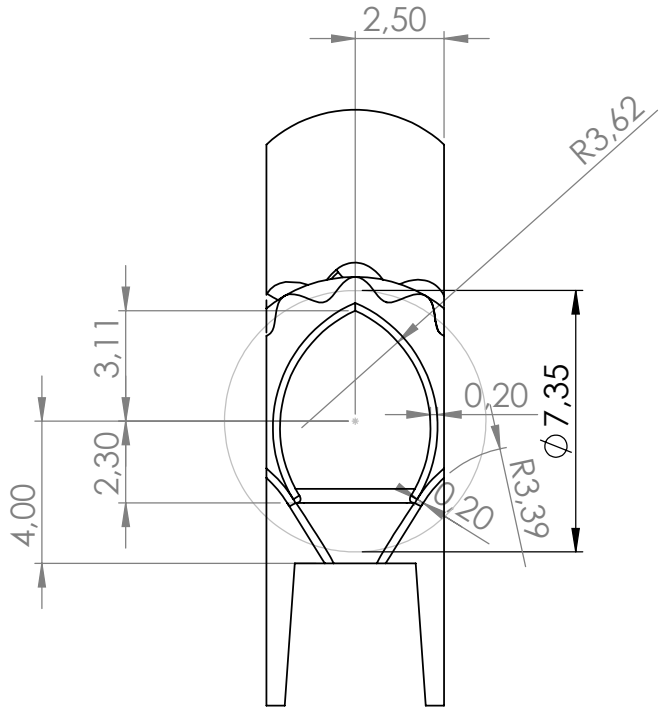

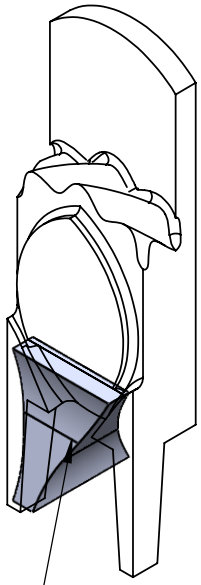

Construction of the cable guides by constructing the negative space.

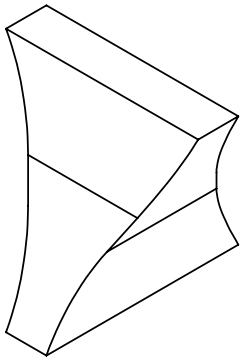

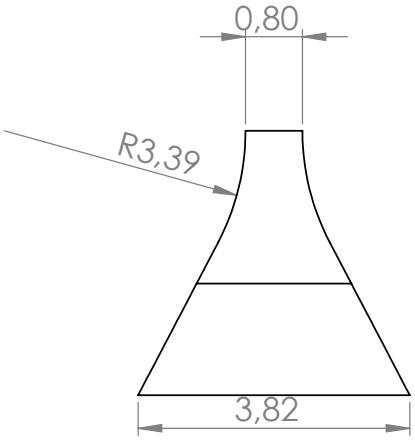

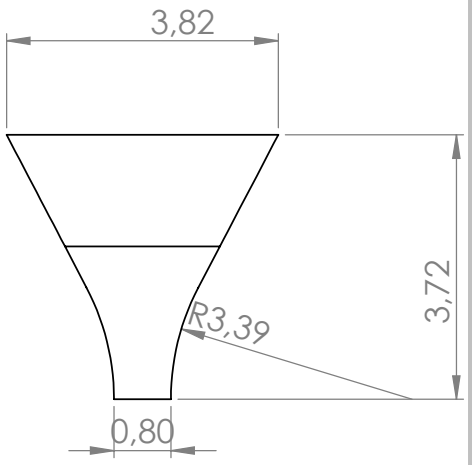

UNLESS OTHERWISE SPECIFIED: DIMENSIONS ARE IN MILLIMETERS SURFACE FINISH: TOLERANCES: LINEAR: ANGULAR:	FINISH:	DEBURR AND BREAK SHARP EDGES	DO NOT SCALE DRAWING / REVISION

	NAME	SIGNATURE	DATE
DRAWN			
CHK'D			
APPV'D			
MFG			
Q.A			

TITLE:

MATERIAL:

DWG NO. cable guide a

A4

WEIGHT:

SCALE:5:1

SHEET 1 OF 1

CABLE GUIDE TYPE B

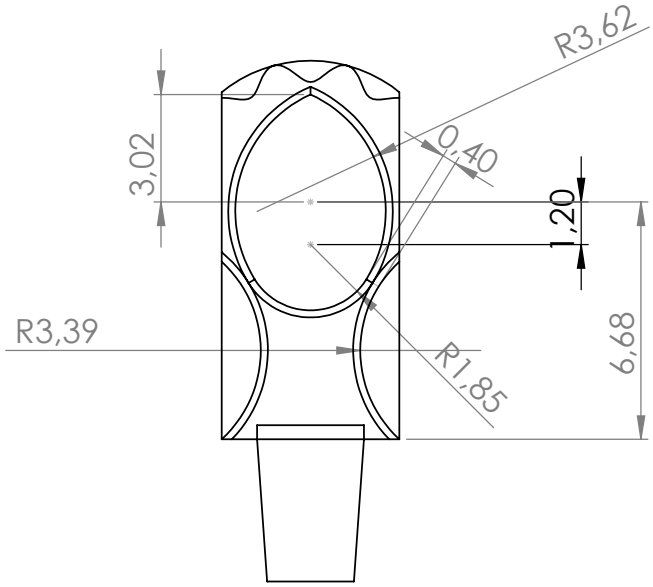

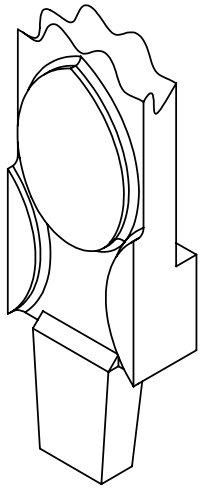

UNLESS OTHERWISE SPECIFIED: DIMENSIONS ARE IN MILLIMETERS SURFACE FINISH: TOLERANCES: LINEAR: ANGULAR:		FINISH:		DEBURR AND BREAK SHARP EDGES		DO NOT SCALE DRAWING	REVISION
	NAME	SIGNATURE	DATE			TITLE:	
DRAWN							
CHK'D							
APPV'D							
MFG							
Q.A				MATERIAL:		DWG NO. cable guide b	A4
				WEIGHT:		SCALE:5:1	SHEET 1 OF 1

CABLE GUIDE TYPE C

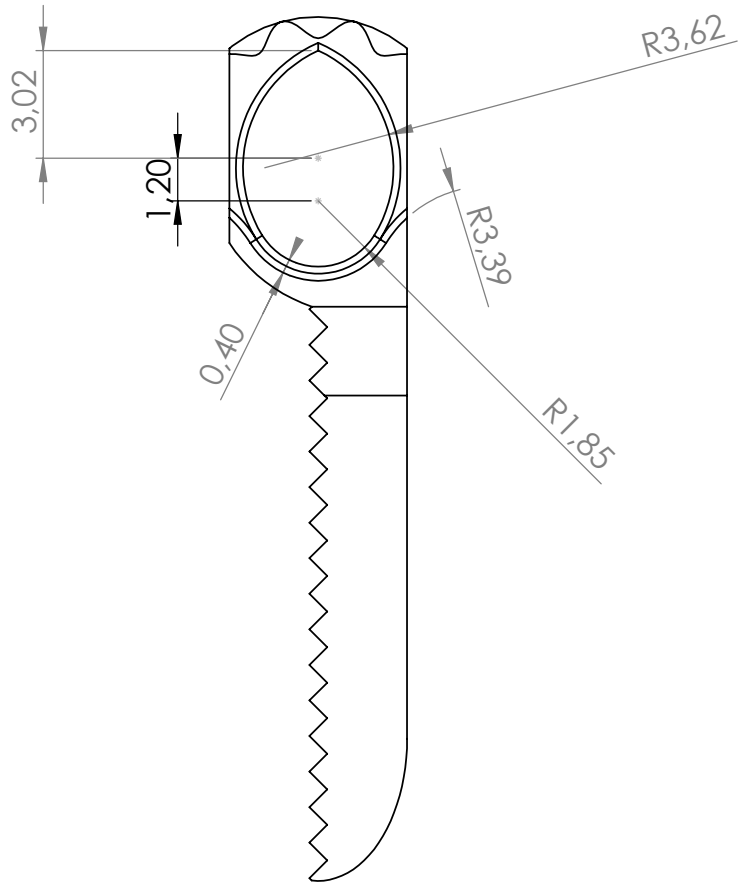

UNLESS OTHERWISE SPECIFIED: DIMENSIONS ARE IN MILLIMETERS SURFACE FINISH: TOLERANCES: LINEAR: ANGULAR:	FINISH:	DEBURR AND BREAK SHARP EDGES	DO NOT SCALE DRAWING / REVISION

	NAME	SIGNATURE	DATE
DRAWN			
CHK'D			
APPV'D			
MFG			
Q.A			

TITLE:

MATERIAL:

DWG NO. cable guide c

A4

WEIGHT:

SCALE:5:1

SHEET 1 OF 1

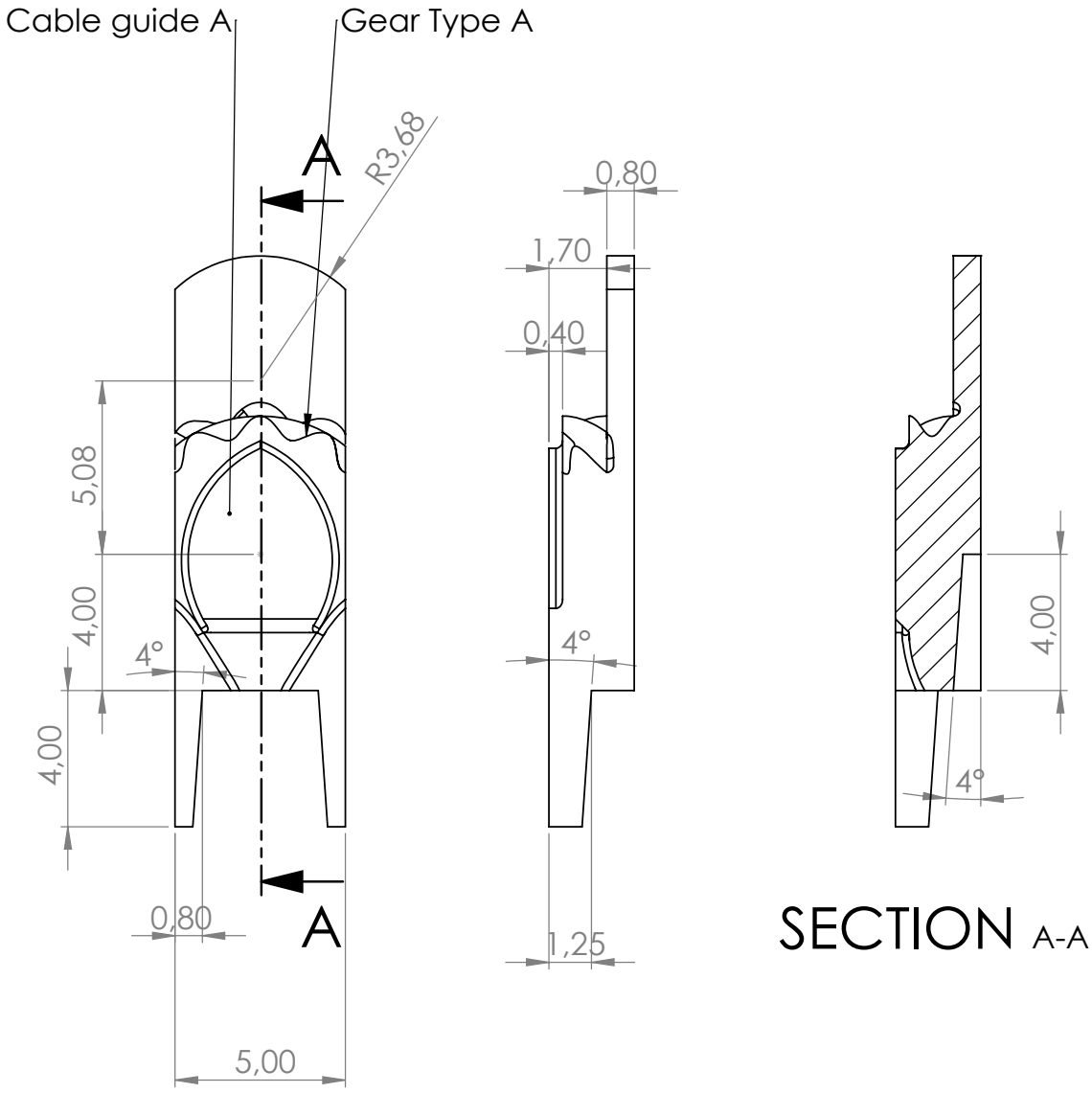

SECTION A-A

UNLESS OTHERWISE SPECIFIED: DIMENSIONS ARE IN MILLIMETERS SURFACE FINISH: TOLERANCES: LINEAR: ANGULAR:		FINISH:		DEBURR AND BREAK SHARP EDGES		DO NOT SCALE DRAWING		REVISION
	NAME	SIGNATURE	DATE				TITLE:	
DRAWN								
CHK'D								
APPV'D								
MFG								
Q.A				MATERIAL:			DWG NO. centre body tip	A4
				WEIGHT:			SCALE:5:1	SHEET 1 OF 1

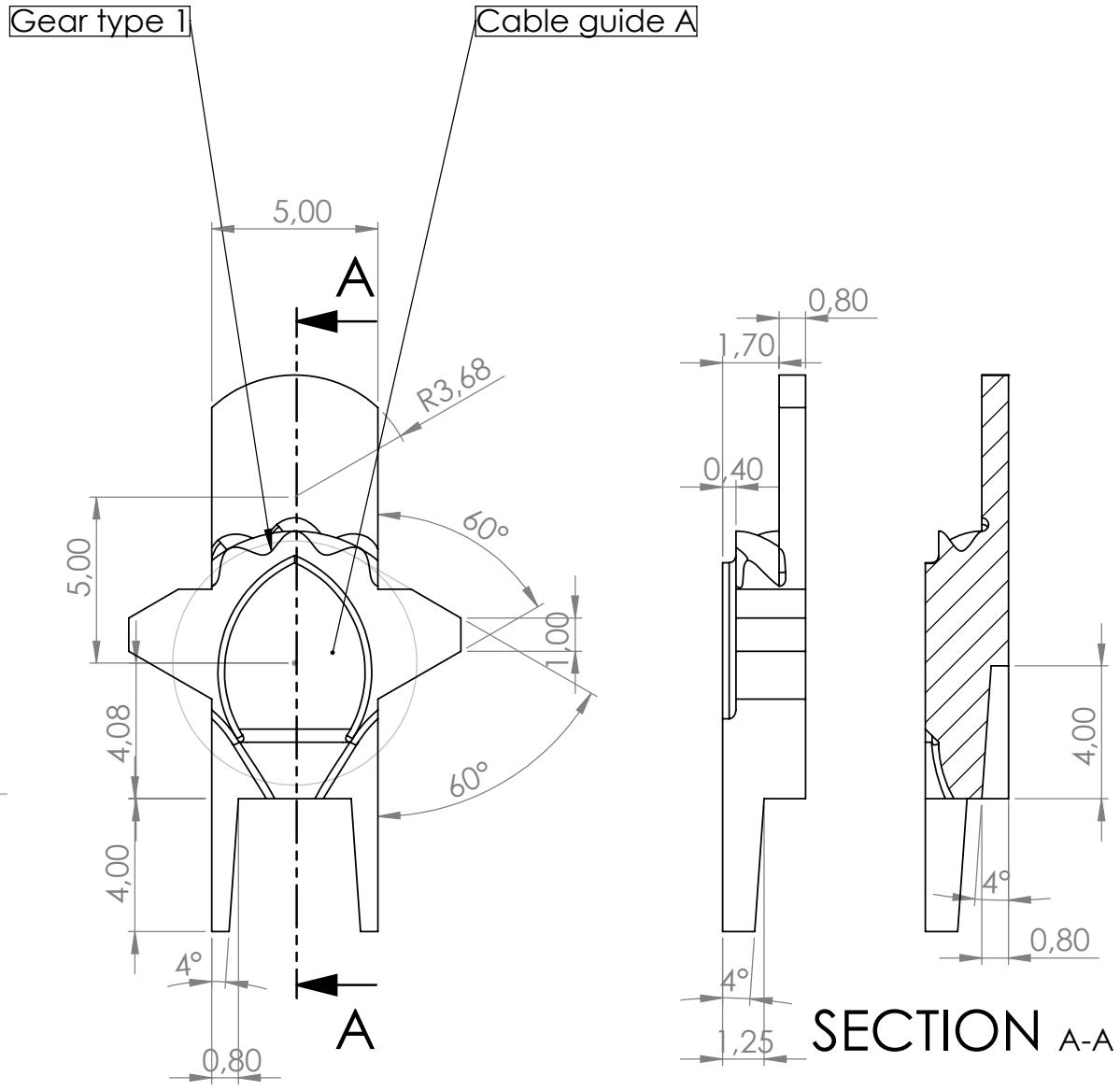

SECTION A-A

UNLESS OTHERWISE SPECIFIED: DIMENSIONS ARE IN MILLIMETERS SURFACE FINISH: TOLERANCES: LINEAR: ANGULAR:		FINISH:		DEBURR AND BREAK SHARP EDGES		DO NOT SCALE DRAWING	REVISION
	NAME	SIGNATURE	DATE				TITLE:
DRAWN							
CHK'D							
APPV'D							
MFG							
Q.A				MATERIAL:		DWG NO.	A4
						centre body handle	
				WEIGHT:		SCALE:5:1	SHEET 1 OF 1

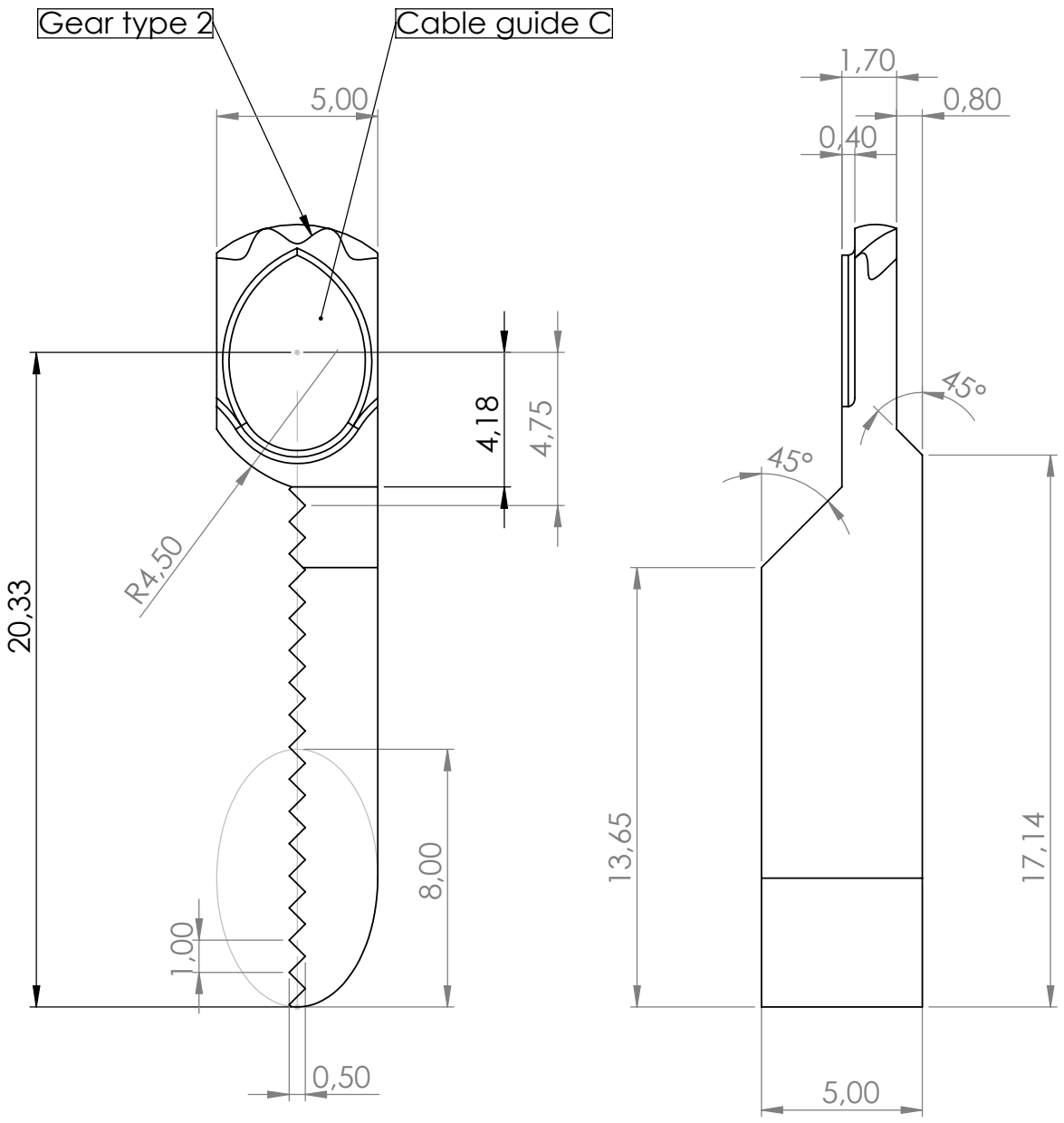

UNLESS OTHERWISE SPECIFIED: DIMENSIONS ARE IN MILLIMETERS SURFACE FINISH: TOLERANCES: LINEAR: ANGULAR:	FINISH:	DEBURR AND BREAK SHARP EDGES	DO NOT SCALE DRAWING / REVISION

	NAME	SIGNATURE	DATE
DRAWN			
CHK'D			
APPV'D			
MFG			
Q.A			

TITLE:

MATERIAL:

DWG NO. gripper 1

A4

WEIGHT:

SCALE:5:1

SHEET 1 OF 1

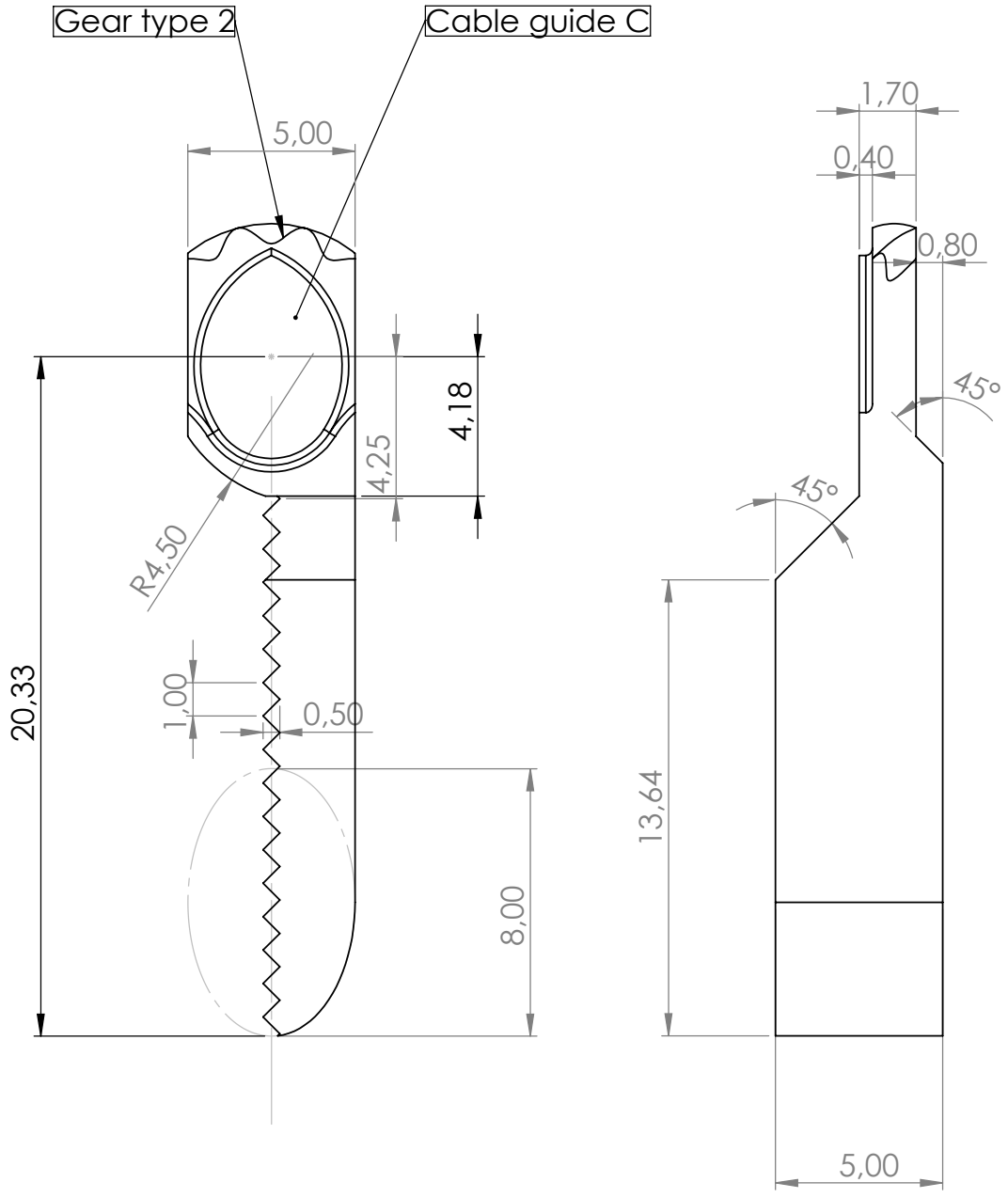

UNLESS OTHERWISE SPECIFIED: DIMENSIONS ARE IN MILLIMETERS SURFACE FINISH: TOLERANCES: LINEAR: ANGULAR:		FINISH:		DEBURR AND BREAK SHARP EDGES		DO NOT SCALE DRAWING	REVISION
	NAME	SIGNATURE	DATE				TITLE:
DRAWN							
CHK'D							
APPV'D							
MFG							
Q.A				MATERIAL:		DWG NO.	A4
						gripper 2	
				WEIGHT:		SCALE:5:1	SHEET 1 OF 1

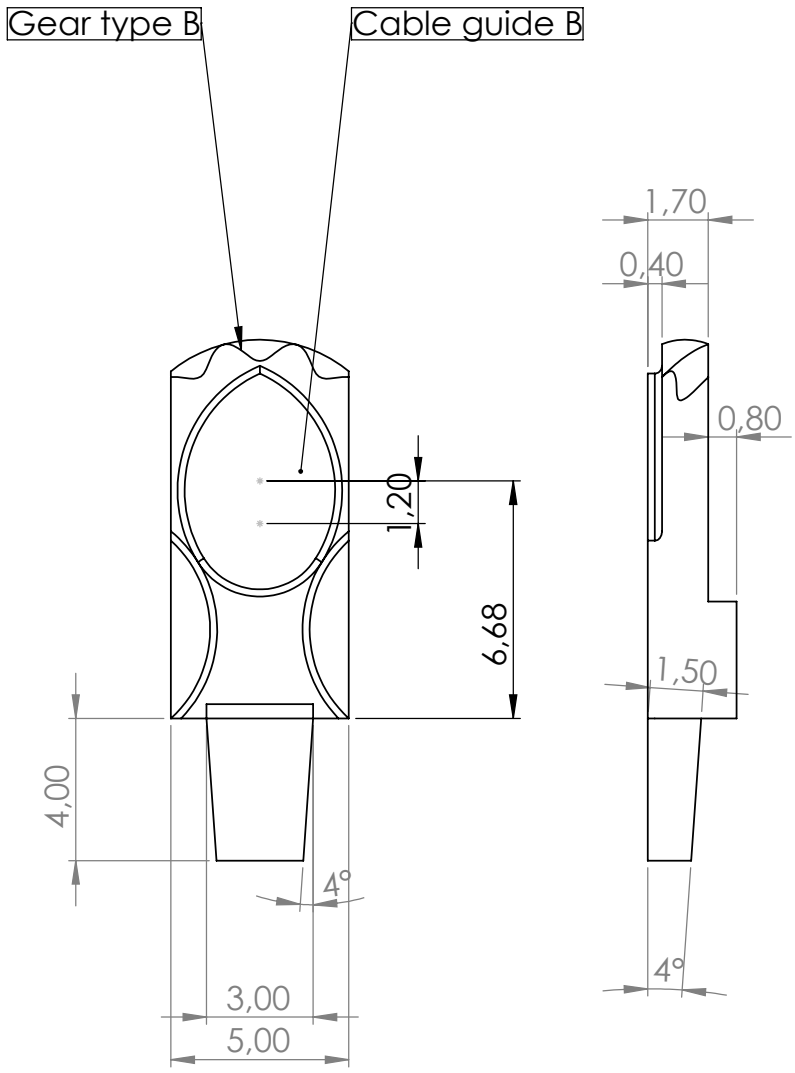

UNLESS OTHERWISE SPECIFIED: DIMENSIONS ARE IN MILLIMETERS SURFACE FINISH: TOLERANCES: LINEAR: ANGULAR:	FINISH:	DEBURR AND BREAK SHARP EDGES	DO NOT SCALE DRAWING / REVISION

	NAME	SIGNATURE	DATE
DRAWN			
CHK'D			
APPV'D			
MFG			
Q.A			

TITLE:

MATERIAL:

DWG NO. shaft add. tip

A4

WEIGHT:

SCALE:5:1

SHEET 1 OF 1

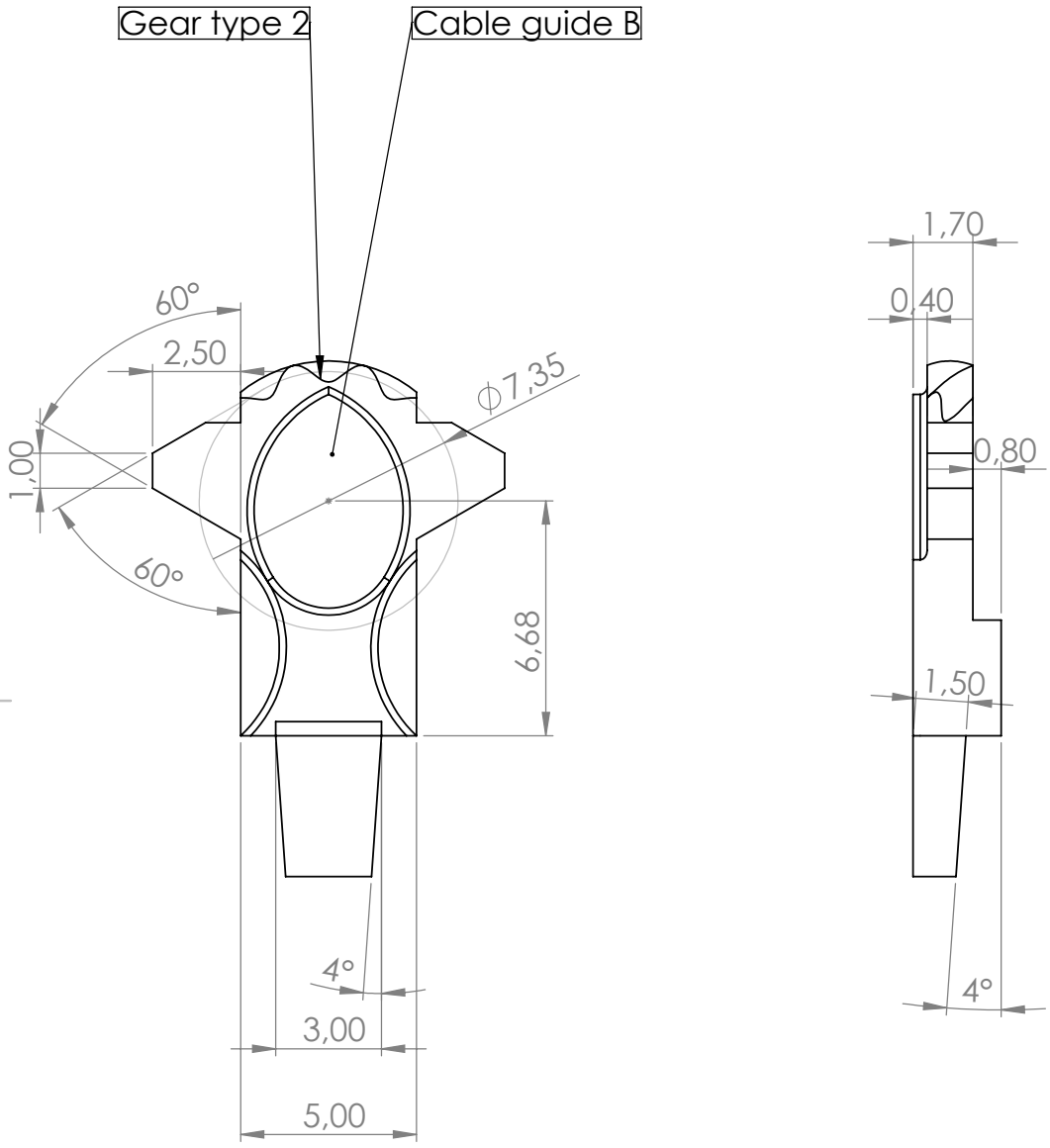

UNLESS OTHERWISE SPECIFIED: DIMENSIONS ARE IN MILLIMETERS SURFACE FINISH: TOLERANCES: LINEAR: ANGULAR:	FINISH:	DEBURR AND BREAK SHARP EDGES	DO NOT SCALE DRAWING / REVISION

	NAME	SIGNATURE	DATE
DRAWN			
CHK'D			
APPV'D			
MFG			
Q.A			

TITLE:

MATERIAL:

DWG NO. shaft add. handle A4

WEIGHT:

SCALE:5:1

SHEET 1 OF 1

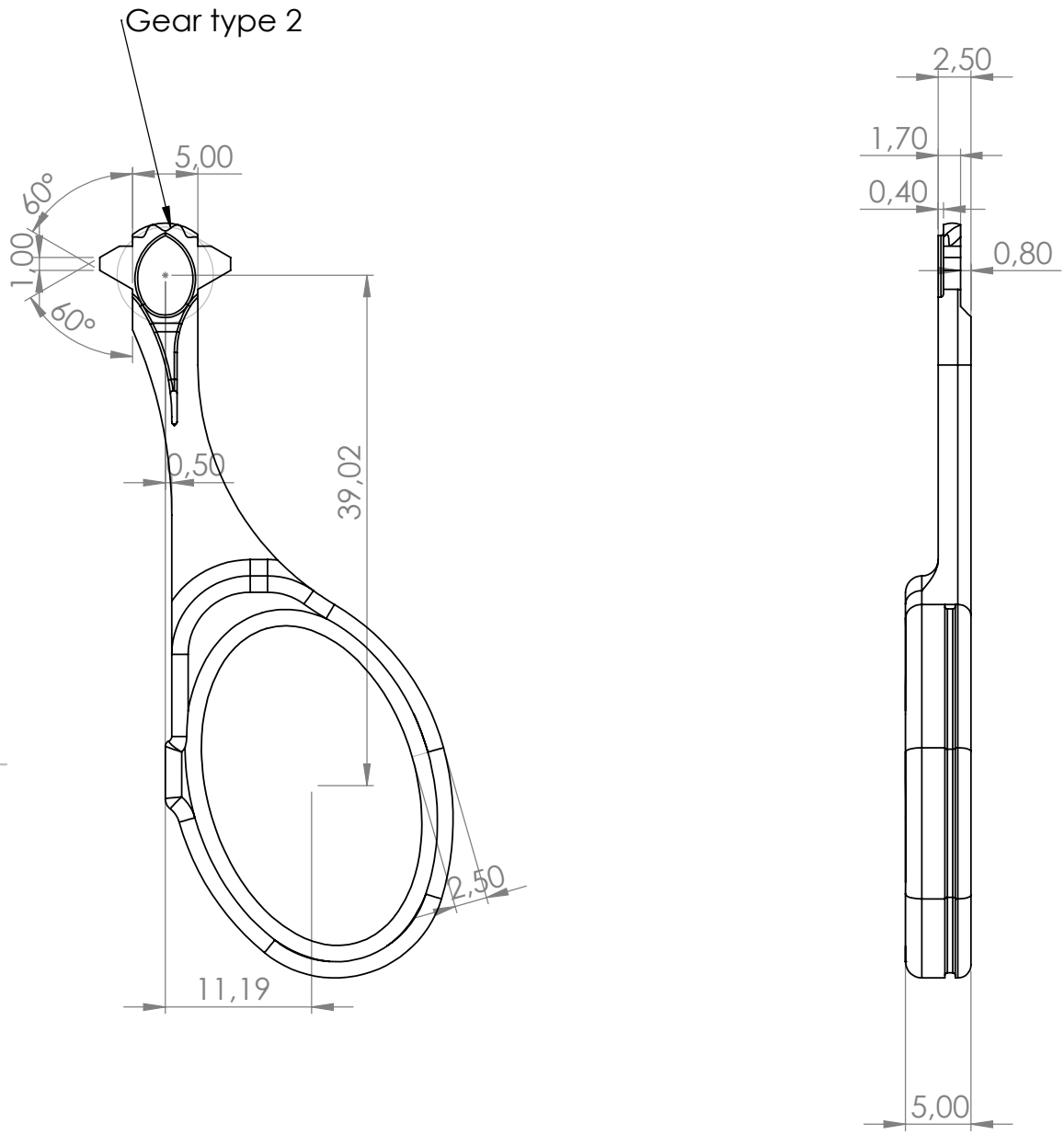

UNLESS OTHERWISE SPECIFIED: DIMENSIONS ARE IN MILLIMETERS SURFACE FINISH: TOLERANCES: LINEAR: ANGULAR:	FINISH:		DEBURR AND BREAK SHARP EDGES	DO NOT SCALE DRAWING	REVISION	
	NAME	SIGNATURE	DATE	TITLE:		
DRAWN						
CHK'D						
APPV'D						
MFG						
Q.A				MATERIAL:	DWG NO. handle	A4
				WEIGHT:	SCALE:5:1	SHEET 1 OF 1

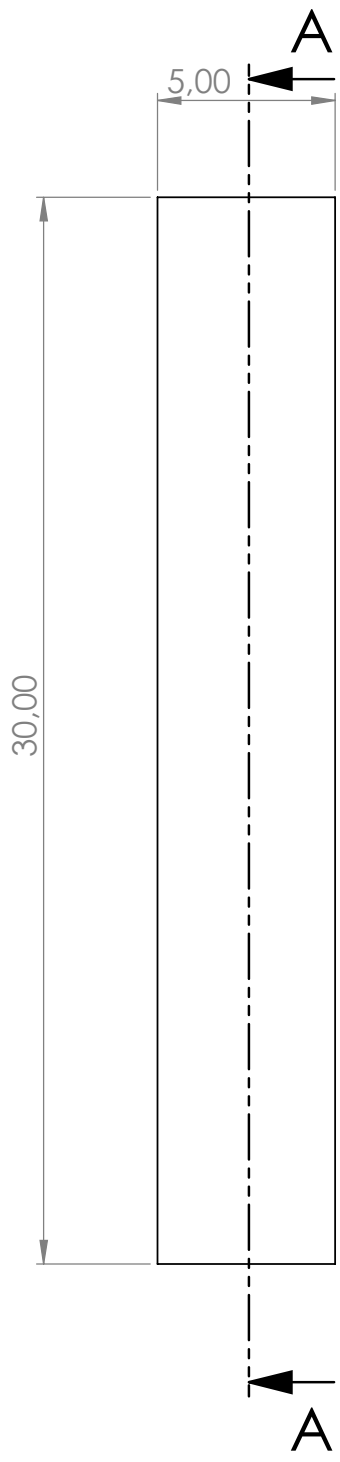

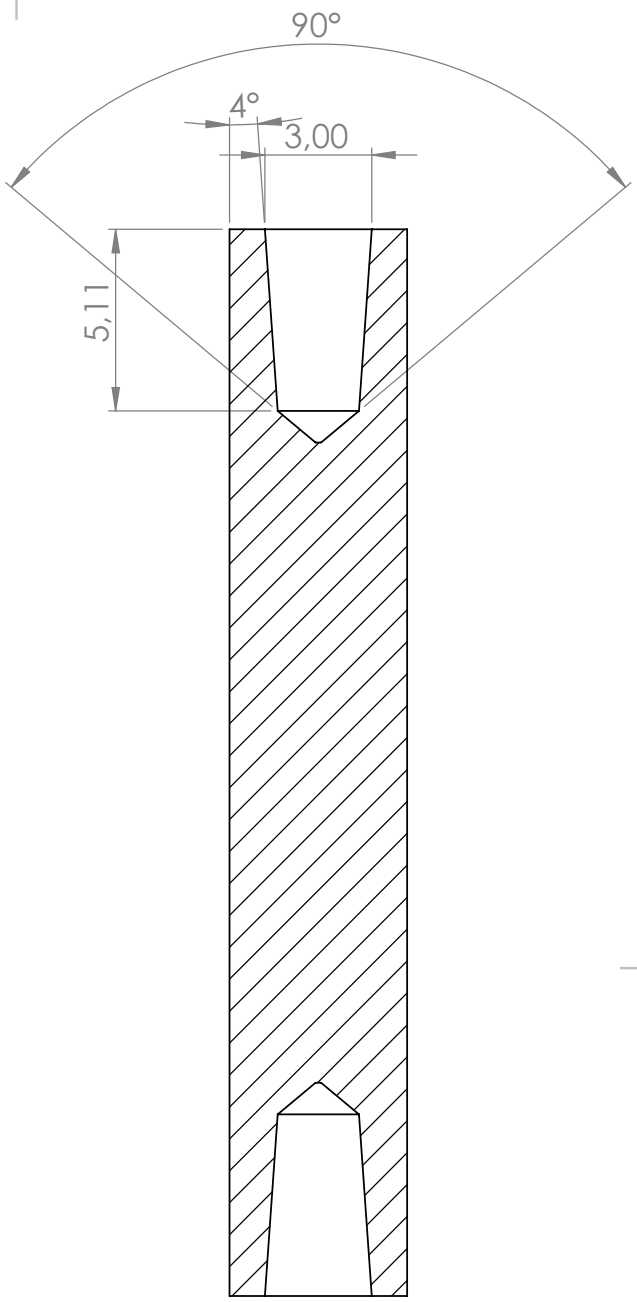

SECTION A-A

UNLESS OTHERWISE SPECIFIED: DIMENSIONS ARE IN MILLIMETERS SURFACE FINISH: TOLERANCES: LINEAR: ANGULAR:	FINISH:	DEBURR AND BREAK SHARP EDGES	DO NOT SCALE DRAWING / REVISION

	NAME	SIGNATURE	DATE				
DRAWN							TITLE:
CHK'D							
APPV'D							
MFG							
Q.A				MATERIAL:			DWG NO. shaft / A4
				WEIGHT:			SCALE:5:1 / SHEET 1 OF 1